MAX-PLANCK-INSTITUT FÜR MOLEKULARE PHYSIOLOGIE

IMPRS for Living Matter
INTERNATIONAL MAX PLANCK RESEARCH SCHOOL

technische universität dortmund

The relationship between oncogenic KRas and wild-type Ras activity and signaling

Dissertation

zur Erlangung des akademischen Grades eines

Doktors der Naturwissenschaften

(Dr. rer. Nat.)

Der Fakultät Chemie und Chemische Biologie

Der Technischen Universität Dortmund

Angefertigt am Max-Planck-Institut für molekulare Physiologie, Dortmund

Vorgelegt von

Kitso Ata Kewagamang

geboren in Gaborone, Botsuana

Oktober 2024

Declaration

Tag der Abgabe der Dissertation: 11 Oktober 2024

Von Kitso Ata Kewagamang

Gutachter:

Prof. Dr. Philippe I. H. Bastiaens

Prof. Dr. Jan Hengstler

1st Examiner:

Prof. Dr. Philippe I. H. Bastiaens

Department of Systemic Cell Biology

Max Planck Institute of Molecular Physiology, Dortmund

Faculty of Chemistry and Chemical Biology, TU Dortmund

2nd Examiner:

Prof. Dr. Jan Hengstler

Department of Toxicology

Leibniz Research Centre for Working Environment and Human Factors (IfADo), Dortmund

The work presented in this thesis was performed under the supervision of Prof. Dr. Philippe I. H. Bastiaens in his laboratory group in the Department of Systemic Cell Biology, Max Planck Institute of Molecular Physiology in Dortmund, Germany.

Kitso Ata Kewagamang was affiliated with the International Max Planck Research School for Living Matter, Dortmund, Germany.

Eidesstattliche Versicherung (Affidavit)

Name, Vorname
(Surname, first name)

Matrikel-Nr.
(Enrolment number)

Belehrung:

Wer vorsätzlich gegen eine die Täuschung über Prüfungsleistungen betreffende Regelung einer Hochschulprüfungsordnung verstößt, handelt ordnungswidrig. Die Ordnungswidrigkeit kann mit einer Geldbuße von bis zu 50.000,00 € geahndet werden. Zuständige Verwaltungsbehörde für die Verfolgung und Ahndung von Ordnungswidrigkeiten ist der Kanzler/die Kanzlerin der Technischen Universität Dortmund. Im Falle eines mehrfachen oder sonstigen schwerwiegenden Täuschungsversuches kann der Prüfling zudem exmatrikuliert werden, § 63 Abs. 5 Hochschulgesetz NRW.

Die Abgabe einer falschen Versicherung an Eides statt ist strafbar.

Wer vorsätzlich eine falsche Versicherung an Eides statt abgibt, kann mit einer Freiheitsstrafe bis zu drei Jahren oder mit Geldstrafe bestraft werden, § 156 StGB. Die fahrlässige Abgabe einer falschen Versicherung an Eides statt kann mit einer Freiheitsstrafe bis zu einem Jahr oder Geldstrafe bestraft werden, § 161 StGB.

Die oben stehende Belehrung habe ich zur Kenntnis genommen:

Official notification:

Any person who intentionally breaches any regulation of university examination regulations relating to deception in examination performance is acting improperly. This offence can be punished with a fine of up to EUR 50,000.00. The competent administrative authority for the pursuit and prosecution of offences of this type is the chancellor of the TU Dortmund University. In the case of multiple or other serious attempts at deception, the candidate can also be unenrolled, Section 63, paragraph 5 of the Universities Act of North Rhine-Westphalia.

The submission of a false affidavit is punishable.

Any person who intentionally submits a false affidavit can be punished with a prison sentence of up to three years or a fine, Section 156 of the Criminal Code. The negligent submission of a false affidavit can be punished with a prison sentence of up to one year or a fine, Section 161 of the Criminal Code.

I have taken note of the above official notification.

Ort, Datum
(Place, date)

Unterschrift
(Signature)

Titel der Dissertation:
(Title of the thesis):

Ich versichere hiermit an Eides statt, dass ich die vorliegende Dissertation mit dem Titel selbstständig und ohne unzulässige fremde Hilfe angefertigt habe. Ich habe keine anderen als die angegebenen Quellen und Hilfsmittel benutzt sowie wörtliche und sinngemäße Zitate kenntlich gemacht.
Die Arbeit hat in gegenwärtiger oder in einer anderen Fassung weder der TU Dortmund noch einer anderen Hochschule im Zusammenhang mit einer staatlichen oder akademischen Prüfung vorgelegen.

I hereby swear that I have completed the present dissertation independently and without inadmissible external support. I have not used any sources or tools other than those indicated and have identified literal and analogous quotations.

The thesis in its current version or another version has not been presented to the TU Dortmund University or another university in connection with a state or academic examination.*

*Please be aware that solely the German version of the affidavit ("Eidesstattliche Versicherung") for the PhD thesis is the official and legally binding version.

Ort, Datum
(Place, date)

Unterschrift
(Signature)

Table of Contents

List of Figures

List of Tables

List of Equations

List of Supplementary Figures

Abbreviations

β	beta
ΔHVR	deleted Hypervariable Region
δ	delta
γ or $\boldsymbol{\gamma}$	gamma
µg	microgram
µL	microlitre
µM	micromolar
AKT	Ak strain transforming, also known as Protein Kinase B
ANOVA	analysis of variance
Arl	Arf-like GTPase
APS	ammonium persulfate
BCA	bicinchoninic acid assay
BFP	monomeric Blue Fluorescent Protein generated by site-specific and random mutagenesis of TagRFP
BRaf	serine/threonine-protein kinase
BSA	bovine serum albumin
Caco2/TC7	(cancer coli) human colon adenocarcinoma cell line, TC7 clone
CID	chemically-Induced dimerization
CO_2	carbon dioxide
CRC	colorectal cancer
DH	Dbl homology
DMEM	Dulbecco's Modified Eagle Medium
DMSO	dimethyl sulfoxide
DNA	deoxyribonucleic acid
DTT	dithiothreitol
DUSP	dual-specificity MAP kinase phosphatase
eDHFR	Escherichia Coli dihydrofolate reductase enzyme
EDTA	ethylenediaminetetraacetic acid
EGF	epidermal growth factor
EGFR	epidermal growth factor receptor
eNOS	endothelial nitric oxide synthase
ER	endoplasmic reticulum
eRas	endogenous pan Ras
ERK	extracellular signal-regulated kinase
FBS	fetal bovine serum (also known as fetal calf serum [FCS])
FKBP	FK506 binding protein
FKBP37V	FKBP with a 37 V mutation
g	gram
g	gravitational force
GAP	GTPase-activating proteins
GDP	guanosine-5'-diphosphate
GEF	guanine nucleotide exchange factor
GPCR	G-protein coupled receptor
GST	glutathione-S-transferase
GTP	guanosine-5'-triphosphate

GTPγS	guanosine 5'-O-(3-thiotriphosphate)
h	hour(s)
HRas	Harvey Rat sarcoma viral oncogene homolog
HVR	hypervariable region
ICMT	protein-S-isoprenylcysteine carboxyl methyltransferase
IPTG	isopropyl β-D-1-thiogalactopyranoside
kDa	kilo Dalton
Ki	inhibitor constant
KRas	Kirsten rat sarcoma viral oncogene homolog
KSR	kinase suppressor of Ras
L	Liter
LB	lysogeny broth
M	Molar concentration, moles per liter (mol/L)
mAb	monoclonal Antibody
MAP	mitogen-activated protein
MAPK	mitogen-activated protein kinase, also known as ERK
MCF7	Michigan Cancer Foundation 7
MCF 10A	Michigan Cancer Foundation 10A
MDCK	Madin-Darby canine kidney
MEF	mice embryonic fibroblasts
Mek	mitogen-activated protein kinase kinase, MAP2K or MAPKK
Milli-Q	Quality, high purity water
min	minute
MKP	mitogen-activated protein kinase phosphatase
mL	milliliter
mM	milli molar
mTFP	monomeric Teal Fluorescent Protein 1
mTOR	mammalian target of rapamycin
mTORC1	mammalian target of rapamycin complex 1
NA	numerical aperture
NEAA	non-essential amino acids
NF	Neurofibromatosis
ng	nanogram
NGF	nerve growth factor
nm	nanometer
nM	nanomolar
NRas	Neuroblastoma Rat sarcoma viral oncogene homolog
OIS	oncogene-induced senescence
PA	photoactivatable/ photoactivation
pAKT	a family of serine/threonine protein kinases
PAS	photoactivation system
PAT	palmitoyl acyl transferase
PBS	phosphate buffered saline
PD	Pulldown
PDAC	pancreatic ductal adenocarcinoma
PDEδ	phosphodiesterase 6 delta subunit
pERK	phosphorylated ERK, also known as MAPK
PFA	paraformaldehyde

PH	pleckstrin homology
pH	potential of Hydrogen
PHLPP	pleckstrin homology domain leucine-rich repeat protein phosphatase
PI3K	phosphatidylinositol 3 kinase
PIP2	phosphatidylinositol (4,5) bisphosphate
PIP3	phosphatidylinositol (3,4,5) trisphosphate
PKB	protein kinase B, also known as AKT
PKC	protein kinase C
PM	plasma membrane
PP2A	protein phosphatase 2A
PTB	phosphotyrosine binding domain
PVDF	polyvinylidene fluoride
RALGDS	Ral guanine nucleotide dissociation stimulator
Raf	rapidly accelerated fibrosarcoma, mitogen-activated protein kinase kinase kinase, MAP3K or MAPKKK
Ras	rat sarcoma viral oncogene homolog
RasGRF	Ras guanine nucleotide releasing factor
RasGRP	Ras guanine nucleotide-releasing protein
RBD	Ras Binding Domain
RCE1	Ras converting enzyme 1
REM	Ras exchange motif
rG12D KRas	recruitable KRas with a G12D mutation
rG12V KRas	recruitable KRas with a G12D mutation
Rheb	Ras homolog enriched in the brain
rKRas	recruitable KRas
ROI	region of interest
rpm	revolutions per minute
RSK	ribosomal s6 kinase
RTK	receptor tyrosine kinase
rWT KRas	recruitable KRas wild-type form
s	seconds
sd	standard deviation
SDS	sodium dodecyl sulfate
SDS PAGE	sodium dodecyl sulfate polyacrylamide gel electrophoresis
sem	standard error of the mean
SLF’	synthetic ligand of FKBP
Spred	sprout related EVH1 domain containing protein
Src	proto-oncogene tyrosine-protein kinase Src
SOC	super optimal broth
SOS	son of sevenless
$t_{1/2}$	half-life
TB	terrific broth
TBS	Tris-buffered saline
TBS-T	Tris-buffered saline containing Tween
TEMED	tetramethylethylenediamine
tKRas	tail end of KRas (C-terminal end)
TMP	trimethoprim
Tris	tris(hydroxymethyl)aminomethane

v	volts
WB	western blot
WCL	whole cell lysate
WT	wild-type
%	percent
°C	Degrees Centigrade or Degrees Celsius

1 Abstract

Ras proteins play an important role in various signaling cascades, transducing external signals into phenotypic and behavioral responses. In many cancers, however, Ras-mediated signaling is dysregulated, with mutated, constitutively active KRas proteins being the most pervasive in pancreatic ductal carcinoma and colorectal cancer.

The mechanisms driving this dysregulation are complex. Wild-type Ras isoforms, including the cognate wild-type Ras counterpart to the oncogenic Ras, are thought to play distinct roles in how they mediate Ras signaling and alter cell behavior in cancerous cells. Moreover, overexpressed oncogenic Ras proteins can cause senescence when heterogeneously expressed with wild-type Ras isoforms. The molecular mechanism of this oncogene-induced senescence is not fully understood, although the involvement of tumor suppressor proteins such as p53 has been shown. Whether an interaction between oncogenic and wild-type Ras also plays a role here remains unclear.

To investigate how oncogenic KRas activity affects wild-type Ras activity and subsequent signaling, a two-component chemical genetic approach was developed. This technique allows bioorthogonal chemical control of the amount of KRas oncoproteins at the plasma membrane. It leverages the important feature of plasma membrane localization of Ras proteins in signal transduction.

The results herein show that a reversible, chemically-induced dimerization system can effectively control plasma membrane localization of ectopically expressed KRas in cells. Using this approach, we found that cytosolic oncogenic KRas (possessing G12V or G12D mutations) has higher GTP-loading compared to wild-type KRas, providing further evidence for its constitutive activity. We also show that acutely enriching overexpressed wild-type KRas and oncogenic KRas at the plasma membrane resulted in transient activation of endogenous wild-type Ras and the downstream signaling effectors ERK and AKT. As Epidermal Growth Factor (EGF) – mediated-Ras signaling is often dysregulated in cancer, an investigation into the effects of plasma membrane localization of oncogenic KRas on this network was performed by way of EGF dose-response experiments. Results suggest that accumulation of oncogenic KRas proteins at the plasma membrane causes an ultrasensitive response in endogenous wild-type Ras activity and downstream effectors at lower EGF doses, compared to wild-type cells. Additionally, clonogenic assays revealed that over-expressed KRas G12V and G12D oncoproteins were associated with reduced proliferation, regardless of whether they were localized in the cytosol or at the plasma membrane.

Collectively, these findings indicate that KRas oncoproteins have an activating interaction with the wild-type Ras proteins at the plasma membrane and initiate downstream signaling. Furthermore, oncogenic Ras may increase the sensitivity of transformed cells to growth factor stimulation by this interaction with wild-type Ras. However, these effects alone are likely insufficient to drive tumorigenesis when oncogenic KRas is overexpressed, as proliferation was suppressed. Thus, further mechanisms may be required for cancer formation. Altogether, these results help to explain some of the changes in signaling responses to growth factors in KRas-driven carcinogenesis.

2 Zusammenfassung

Ras-Proteine spielen eine wichtige Rolle in verschiedenen Signalkaskaden, indem sie externe Signale in phänotypische und verhaltensbezogene Reaktionen umwandeln. Bei vielen Krebsarten ist die Ras-vermittelte Signalübertragung jedoch dysreguliert, wobei mutierte, konstitutiv aktive KRas-Proteine beim duktalen Pankreaskarzinom und beim kolorektalen Karzinom am weitesten verbreitet sind.

Die Mechanismen, die dieser Dysregulation zugrunde liegen, sind komplex. Es wird angenommen, dass Wildtyp-Ras-Isoformen, einschließlich des komplementären Wildtyp-Ras-Gegenstücks zum onkogenen Ras, unterschiedliche Rollen bei der Vermittlung von Ras-Signalen spielen und das Zellverhalten in Krebszellen verändern. Darüber hinaus können überexprimierte onkogene Ras-Proteine Seneszenz verursachen, wenn sie heterogen mit Wildtyp-Ras-Isoformen exprimiert werden. Der molekulare Mechanismus dieser Onkogen-induzierten Seneszenz ist noch nicht vollständig geklärt, obwohl die Beteiligung von Tumorsuppressorproteinen wie p53 bereits nachgewiesen wurde. Ob dabei auch eine Interaktion zwischen onkogenem und Wildtyp-Ras eine Rolle spielt, bleibt unklar.

Um zu untersuchen, wie die onkogene KRas-Aktivität die Wildtyp-Ras-Aktivität und die anschließende Signalübertragung beeinflusst, wurde ein chemisch-genetischer Zwei-Komponenten-Ansatz entwickelt. Diese Technik ermöglicht eine bioorthogonale chemische Kontrolle der Menge der KRas-Onkoproteine an der Plasmamembran. Sie macht sich die wichtige Eigenschaft der Plasmamembranlokalisierung von Ras-Proteinen bei der Signaltransduktion zunutze.

Die vorliegenden Ergebnisse zeigen, dass ein reversibles, chemisch induziertes Dimerisierungssystem die Plasmamembranlokalisierung von ektopisch exprimiertem KRas in Zellen wirksam steuern kann. Mit diesem Ansatz konnten wir feststellen, dass zytosolisches onkogenes KRas (mit G12V- oder G12D-Mutationen) im Vergleich zu Wildtyp-KRas eine höhere GTP-Beladung aufweist, was ein weiterer Beweis für seine konstitutive Aktivität ist. Wir zeigen auch, dass die akute Anreicherung von überexprimiertem Wildtyp-KRas und onkogenem KRas an der Plasmamembran zu einer vorübergehenden Aktivierung von endogenem Wildtyp-Ras und den nachgeschalteten Signalgebern ERK und AKT führt. Da die durch den epidermalen Wachstumsfaktor (EGF) vermittelte Ras-Signalübertragung bei Krebs häufig gestört ist, wurden die Auswirkungen der Plasmamembran-Lokalisierung von onkogenem KRas auf dieses Netzwerk mit Hilfe von EGF-Dosis-Wirkungs-Experimenten untersucht. Die Ergebnisse deuten darauf hin, dass die Akkumulierung von onkogenen KRas-Proteinen an der Plasmamembran bei niedrigeren EGF-Dosen im Vergleich zu Wildtyp-Zellen eine überempfindliche Reaktion der endogenen Wildtyp-Ras-Aktivität und der nachgeschalteten Effektoren verursacht. Darüber hinaus zeigten klonogene Untersuchungen, dass überexprimierte KRas G12V- und G12D-Onkoproteine mit einer verringerten Proliferation verbunden sind, unabhängig davon, ob sie im Zytosol oder an der Plasmamembran lokalisiert sind.

Insgesamt deuten diese Ergebnisse darauf hin, dass KRas-Onkoproteine eine aktivierende Wechselwirkung mit den Wildtyp-Ras-Proteinen an der Plasmamembran haben und nachgeschaltete Signalwege aktivieren. Darüber hinaus kann onkogenes Ras durch diese Wechselwirkung mit Wildtyp-Ras die Empfindlichkeit der transformierten Zellen für die Stimulation durch Wachstumsfaktoren erhöhen. Diese Effekte allein reichen jedoch wahrscheinlich nicht aus, um die Tumorentstehung zu fördern, wenn onkogenes KRas überexprimiert wird, da die Proliferation unterdrückt wurde. Daher sind möglicherweise weitere Mechanismen für die Krebsentstehung erforderlich. Insgesamt tragen diese Ergebnisse dazu bei, einige der Veränderungen in den Signalreaktionen auf Wachstumsfaktoren bei der KRas-gesteuerten Karzinogenese zu erklären.

3 Introduction

Signaling networks are important features of life as they enable communication within and between living systems, from the subcellular to the ecosystem level (1), (2), (3). Thus, detecting, processing, and responding to environmental changes is imperative not only for temporal adaption to changes in the environment but also for life itself (1), (2). Hence, dysregulation in signaling and communication threatens the existence and maintenance of life systems.

Understanding the systems biology of life, as well as the biochemical and molecular biology of living systems offers a comprehensive approach to research in the life sciences (4), (5), (6). In this Ph.D. thesis, elements of these approaches were employed to study KRas, a ubiquitous protein involved in multiple cellular signaling networks. The roles of wild-type and mutated KRas and other Ras isoforms in health and disease have been studied for over half a century, with more to be explored and understood. Its involvement in multiple cancers is continuously being researched and contextualizes the work herein.

3.1 A brief history of Ras proteins

In the 1960s, carcinogenic viruses were discovered in rats that developed sarcomas (7), (8). Jennifer Harvey identified the Harvey sarcoma virus in 1964, whereas Werner H. Kirsten discovered the Kirsten sarcoma virus in 1967 sarcomas (7), (8). With the advancement of molecular biology techniques, Edward M. Scolnick was able to discover the viral genes associated with the Harvey sarcoma viruses and the Kirsten sarcoma viruses (9), (10). These genes were dubbed Ras, from Rat sarcoma. The short-hand forms today, HRas and KRas, were adopted to denote the Harvey rat sarcoma virus gene and the Kirsten rat sarcoma virus gene respectively.

Scolnick later discovered in the 1970s and 1980s that the viral HRas and KRas genes are translated into GDP and GTP-binding proteins with a molecular weight of 21kDa (11), (12), (13), (14), (15). They also discovered the plasma membrane-localized vertebrate equivalents of HRas and KRas viral genes, as well as their association with transformation into cancer (16), (17), (18), (19).

In 1982 it was discovered that human HRas was involved in bladder cancer, and subsequently that KRas genes were involved in human lung and colon cancers (20), (21). A missense mutation in codon 12 of both oncogenic human HRas and KRas was confirmed in the viral counterparts (22), (23) (24). These were the first oncoproteins discovered in humans (25), (26).

Neuroblastoma Ras (NRas) was discovered later from DNA obtained from neuroblastomas (27), (28). These discoveries marked the dawn of research into the molecular basis of cancer, which has evolved to what it is today. Thus, Ras proteins are significant in understanding the pathophysiology of carcinogenesis.

The discovery of Ras proteins has grown over the last 6 decades such that multiple proteins have now been classed under the Ras superfamily of proteins, all of which possess a catalytic G-domain. Of the over 150 small GTPases discovered to date, Ras forms the largest subdivision, with other members being Rab, Ran, Rho, and Arf GTPases, to name a few (29), (30).

3.2 Post-Translational Modifications

Translation of the three main Ras genes, HRas, KRas, and NRas, results in 4 proteins as KRas genes give rise to two splicing variants of exon 4, KRas-4A and KRas-4B (31). Of the two KRas splice variants, KRas-4B is the most highly expressed (31). All expressed Ras proteins have 189 amino acids in their sequences, except KRas-4B, which has 188. These Ras isoforms share high sequence homology of about 80% (32) as the first 165-167 amino acids from the N-terminus, which form the catalytic G-domain, are conserved. Variations occur in the remaining 21-22 amino acids of the C-terminal region which are termed the hypervariable region (HVR), and it is this HVR tail that specifies the targeting of Ras proteins to membranes (33) after post-translational modifications (Figure 1).

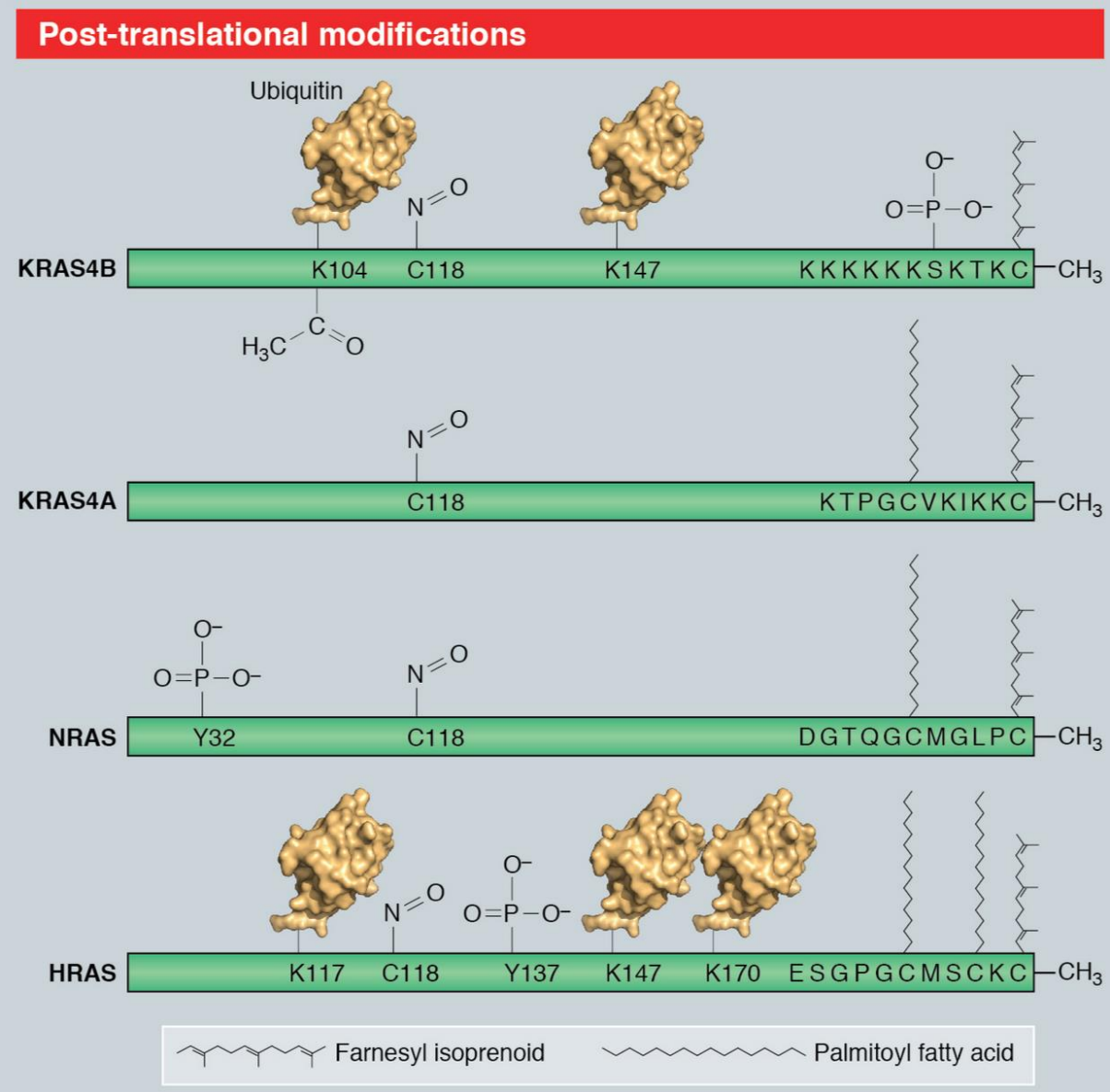

Figure 1. Post-translational modifications of Ras isoforms.
The amino acid residues that are post-translationally targeted in the 4 common Ras isoforms, KRas4B and its splice counterpart KRas4A, as well as NRas and HRas. Towards the C-terminal end on the right are the polybasic amino acids of KRas4B and KRas4A, as well as the cysteine sites of lipidation by farnesyl isoprenoid and palmitoyl fatty acid. Additionally, sites for phosphorylation, ubiquitination, and acetylation are shown. Image from Hobbs et al., 2016 (34).

Ras proteins are targeted to the endoplasmic reticulum and Golgi apparatus membranes through post-translational modifications of the CAAX box (35). The CAAX tetrapeptide sequence consists of a Cysteine (C), two aliphatic amino acids (A), and one more amino acid (X) and is located at the C-terminal end of the Ras isoforms (35). It goes through S-prenylation and is S-farnesylated (C15) irreversibly by cytosolic farnesyl transferase in the cytosol (36), (37), (38). Alternatively, geranylgeranyl polyisoprene (C20) is added by geranylgeranyltransferase I especially in KRas-4B, but also in the case of HRas and NRas (39), (40), (38). This takes place in situations where farnesylation cannot occur such as under farnesyltransferase-inhibiting drugs, or geranylgeranylation is preferred by certain C-terminal motifs (39), (40). The increased hydrophobicity increases binding to membranes, and interaction with the endoplasmic reticulum ensues.

At the endoplasmic reticulum, the action of Ras converting enzyme 1 (RCE1) on Ras lyses the AAX amino acids, following which protein-S-isoprenylcysteine O-methyltransferase (ICMT) changes the ending to a methyl ester, counteracting the negative charge of the carboxyl group on Cysteine (41) (42), (38). These irreversible modifications increase the attraction of the electrostatic charges of Ras to negatively charged phospholipids, increasing hydrophobicity with lipid membranes (38).

HRas contains two additional Cysteine residues (Cysteine 181 and 184) in the HVR compared to NRas (Cysteine 181) and KRas4A (Cysteine 180) which contain only one (43). It is here that Palmitoyl-S-transferases (DHHC9 and GCP16) reversibly palmitoylate Ras isoforms at the Golgi apparatus (44), (45), increasing its affinity to bi-layered phospholipids such as the plasma membrane (38), (46). Palmitoylation of Ras isoforms allows for the localization to the Golgi apparatus (44), (47), (48). KRas-4B is not palmitoylated as it does not have a cysteine after the Cysteine 186 residue (43), (49).

These PTMs increase lipophilicity which is important for plasma membrane localization. KRas-4B also contains a polybasic sequence of 6 Lysine amino acids (Figure 1), which are positively charged under physiological pH. These can interact with negatively charged phospholipids at the plasma membrane PM (50). KRas4A on the other hand contains lysine and arginine amino acid sequences forming two small polybasic regions (50).

Other post-translational modifications of Ras isoforms have also been observed. For example, HRas ubiquitination and localization to the PM and mitochondrial endomembranes suggests that it carries out signal transductions in the mitochondrial domains (51). Mono-ubiquitination of Ras at Lysine 147 has also been shown to increase the amount of active, GTP-bound wild-type Ras, as well as signaling in oncogenic KRas (52). Additionally, phosphorylation of KRas at Serine-181 (53), (54) and acetylation of Ras at Lysine-104 (55) may enhance or inhibit its signaling capabilities.

3.3 Plasma Membrane Localization and Ras Spatial Cycle

Post-translational modifications of Ras endow affinity to endomembranes. However, this is insufficient for maintaining the concentration of Ras proteins at the PM. Ras proteins are therefore actively cycled to enrich them on the plasma membrane (Figure 2) (56), (57).KRas-4B, despite its affinity towards negatively charged lipids of the plasma membrane, can still spontaneously dissociate from them (49), (58), (56). Additionally, a reduction of the plasma membrane concentration of Ras occurs via endocytosis (56).

As the membranes of endocytic vesicles become less negative in the cytosol, Ras is more readily released from the endosomes into the cytosol where it is continually de-palmitoylated by Acyl Protein Thioesterases (APTs) (59), (56). Energy is needed to maintain Ras at the PM as this endosomal-

cytosolic localization would entropically distribute the Ras across all endomembranes at equilibrium (60), (56), (57).

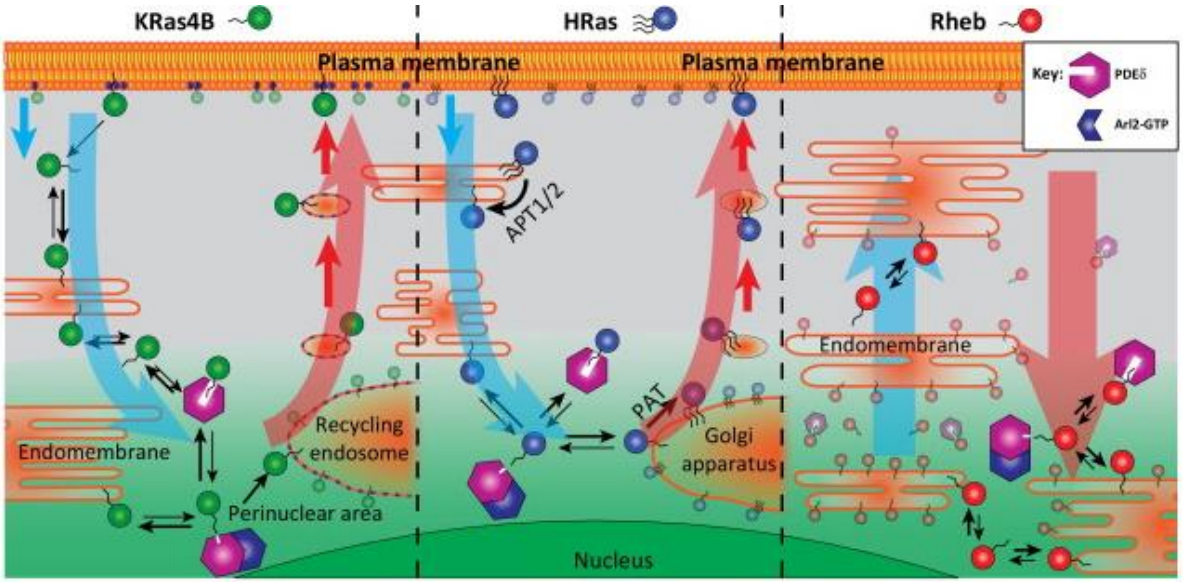

Figure 2. Spatial cycling maintains Ras proteins at the plasma membrane.
The scheme shows the spatial cycles of KRas4B (left panel) and HRas (middle panel). KRas4B and HRas move from the plasma membrane into the cytosol by spontaneous entropic displacement and endocytic vesicle formation where they associate with endomembranes or are solubilized by PDEδ (phosphodiesterase 6δ). Arl2-GTP (GTP-bound Arf-like2) frees KRas and HRas proteins from PDEδ in the perinuclear area. Here, KRas can associate with negatively charged recycling endosomes and HRas with the Golgi apparatus due to palmitoyl transferase (PAT)-mediated palmitoylation of HRas. This then allows them to be carried back to the plasma membrane. Rheb proteins (Ras homolog enriched in the brain) on the other hand are kept on perinuclear membranes by the same PDEδ-Arl2 mechanism but are carried to the plasma membrane only by entropic processes, thus it is not concentrated on the plasma membrane. Image from Schmick et al., 2015 (61).

In the cytosol, the farnesyl terminus of membrane-dissociated Ras proteins can bind to the farnesyl-binding pocket of PDEδ (phosphodiesterase 6), which is a Guanine nucleotide dissociation inhibitor (GDI-) like factor which solubilizes farnesylated Ras (60), (62). Allosteric binding of active Arf-like GTPases Arl2-GTP and Arl3-GTP leads to a conformational change of PDEδ, causing the release of Ras from PDEδ into the perinuclear area (63), (64), (56). Thus, Ras can re-associate with recycling endosomes or the Golgi complex if palmitoylated (38), (46), (56), (61).

Vesicular transport allows for Ras (H, N, and KRas4A) to be trafficked to the plasma membrane from the recycling endosomes and the Golgi apparatus (59), (48). KRas4B on the other hand is carried back to the plasma membrane via recycling endosomes and not via the Golgi Apparatus since it is not palmitoylated, but possesses the positively charged polybasic region instead (Schmick 2014). Therefore, KRas cycles spatially via equilibration to endomembranes, PDEδ-mediated solubilization, release to the perinuclear area by GTP-bound Arl2, electrostatic binding to recycling endosomes, and ultimately return to the plasma membrane by vesicular transport where it is maintained (56).

3.4 Structure of Ras proteins

Ras proteins contain Switch I and II regions which make up the catalytic G-domain. These undergo conformational changes depending on nucleotide binding (65). When GTP-bound, the gamma-phosphate-mediated conformational change (via Threonine 35 and Glycine 60 binding) results in a

"loaded spring" state, which is the active state of Ras (66). GTP hydrolysis to GDP reverses this "loaded spring" conformation to an inactive conformation. The "on" or active, GTP-bound conformation of Ras proteins allows them to interact with the Ras binding domain (RBD) or Ras associating domains of other molecules (Nassar, Horn, et al 1995, Ponting and Benjamin 1996). Thus, in the GDP-bound state, Ras proteins are said to be "off" as interaction with effector molecules is only possible when Ras is bound to GTP. For this reason, Ras proteins are often referred to as molecular switches in signaling cascades (67).

3.5 Regulation of Ras activity state

The defining characteristic of the Ras family of small GTPases is their ability to hydrolyze guanosine-5'-triphosphate (GTP) to guanosine-5'-diphosphate (GDP), a function catalyzed by the G-domain. Ras has a picomolar affinity for both GDP and GTP (68). Spontaneous switching from GDP-bound Ras to GTP-bound Ras is slow with an off-rate of 2×10^{-3} s^{-1}, and requires the release of GDP and re-binding of the more highly concentrated GTP (69), (70), (71). Therefore, despite the concentration of GTP being 10 times higher than that of GDP in the cytosol (72), the baseline state of Ras proteins is to be GDP-bound.

The conversion of Ras-GTP to Ras-GDP, via intrinsic hydrolysis, is also slow at a rate between 6×10^{-4} s^{-1} and 68×10^{-5} s^{-1} (71), (73), (74). Thus, regulators are required to facilitate efficient GDP- and GTP-exchange and to catalyze the hydrolysis of GTP to GDP. The regulation of Ras activity (nucleotide) state occurs via Ras Guanine Nucleotide Exchange Factors (Ras GEFs) and Ras GTPase Activating proteins (GAPs). GEFs allow for the substitution of GDP with GTP, thus activating the Ras protein (75), whereas GAPs enhance the intrinsic GTPase activity of Ras, resulting in the hydrolysis of GTP to GDP (76), (77), and the inactivation of Ras proteins.

3.6 Ras GEFs and GAPs

3.6.1 GEFS

The human Ras GEF family of proteins consists of Ras Guanine Nucleotide-Releasing proteins (RasGRPs), Ras Guanine Nucleotide-Releasing Factors (RasGRFs), and the two members of the son of sevenless (SOS) family (70), (78). Structurally, all possess a REM (Ras exchange motif) and a CDC25 homology domain which aid in guanine nucleotide exchange (78). An allosteric binding site for Ras-GTP (GTP-bound Ras) between the REM and CDC25 domains of SOS1 (75), (79), (80), is known to enhance the catalytic activity of SOS on Ras-GDP (GDP-bound Ras) 75-fold (81). This is because Ras-GTP stabilizes the catalytic domain of SOS via an allosteric site at the REM domain, to enhance nucleotide substitution in Ras (75), (79). This results in positive feedback (Figure 3) (79), (82).

There are two known human SOS isoforms, SOS1 and SOS2, of which SOS1 is the most studied. SOS is autoinhibited by its Dbl Homology – Pleckstrin Homology (DH-PH) domains in the cytosol (83). The DH domain of SOS covers the allosteric binding site for Ras when SOS is in its autoinhibited state (83). SOS is recruited to the PM (Figure 3) when the Src Homology 2 (SH2) domains of Grb2 bind to phosphorylated tyrosine on the growth factor receptor during growth factor-mediated signaling (84), (85), (86). Plasma membrane-binding of SOS to Ras, Ras-GTP, and phosphoinositide phosphates (PIPs) frees it from its autoinhibited state, contributing to a positive feedback loop in which multiple Ras molecules are activated (87), (88), (89).

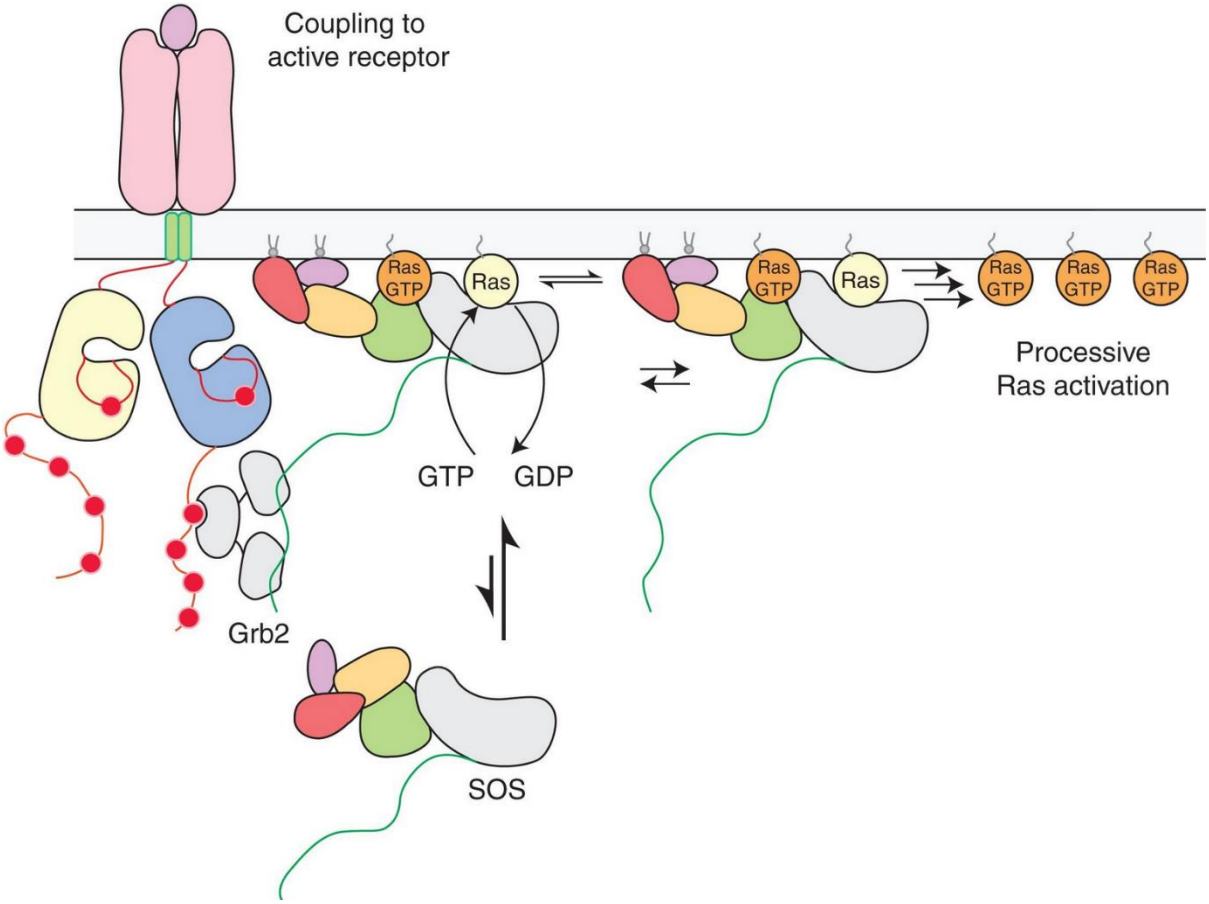

Figure 3. Activation of SOS and Ras at the plasma membrane.
In the cytosol, SOS is autoinhibited. Plasma membrane recruitment of SOS upon Tyrosine-phosphorylation of a ligand-bound receptor allows it to interact with Grb2, PIPs, and Ras-GTP to rapidly catalytically activate Ras proteins. The large, grey subunit of SOS is the catalytic cdc25 domain, while the adjacent green subunit is the REM domain. The yellow, red, and purple subunits indicate the DH, PH, and Histone domains respectively. Image from Bandaru et al., 2019 (80).

Of importance is also the role of magnesium ions. In the nucleotide-binding pocket, Mg^{2+} ions stabilize the beta-phosphates of both GDP and GTP, but also the gamma-phosphate of GTP (70). Additionally, they aid in orienting and coordinating the guanine nucleotides as well as mediating GTP hydrolysis. GEF binding to Ras causes Mg^{2+} release, which is a co-factor for nucleotide-binding (65). This reduces nucleotide binding affinity, subsequently freeing the bound nucleotide (75). Picomolar affinity allows immediate binding of another nucleotide, usually GTP due to its higher concentration in the cytosol (68), (72). GTP binding allows for GEF release, freeing the Ras-GTP (70). It has also been suggested that Ras-GDP can also bind allosterically to SOS conferring low GEF activating activity (83), such that fast SOS1 catalysis occurs when KRas-GTP is bound allosterically, and slow catalysis occurs when KRas-GDP is bound allosterically (82).

3.6.2 GAPs

There are six groups of Ras GAPs in mammals, namely p120GAP, GAP1, Neurofibromin, IQGAPs, SynGAPs, and Plexins (90). They each have different structures and cellular localizations. IQGAPS are non-canonical in that they do not activate intrinsic GTP hydrolysis in Ras proteins. A commonly studied GAP is Neufibromin-1 (NF-1) (91). NF-1 GAP is localized to the cytosol and is recruited to the plasma membrane by Spred1 (Sprouty-related EVH1 domain containing 1) during signaling (92). Degradation of NF-1 occurs via growth factor stimulation-induced ubiquitination which results in proteasomal degradation (93), (94), (95).

GAPs increase the intrinsic hydrolysis of Ras proteins by 10^5-fold (69), (77) as they alter the structure of the GTPase domain (73). Nucleophilic attack on the gamma-phosphate which hydrolyzes GTP occurs when a water molecule is correctly positioned by Glutamine 61 in the Switch II of Ras and is stabilized by an arginine finger motif of GAPs (70). GAPs are likely recruited to the PM or localized to cellular compartments where scaffold proteins hold signaling complexes together (96).

Collectively, Ras GEFs and GAPs work together to modulate Ras activity levels by catalyzing GTP-binding and the hydrolysis of GTP to GDP. Therefore, these Ras activity regulators are important in Ras-mediated signaling in both healthy and diseased states.

3.7 Ras-mediated signaling

Extracellular ligands bind cell-surface receptors such as G-protein Coupled Receptors (GPCRs) and receptor tyrosine kinases (RTKs), initiating a cascade of reactions that results in various cellular responses (1), (97). Ras proteins play a fundamental role as a signaling node for several signaling networks involving RTKs, GPCRs, and other proteins, mediating processes such as proliferation, survival, migration, and differentiation (Figure 4).

Epidermal Growth Factor (EGF) is a common ligand for the RTK Epidermal Growth Factor Receptor (EGFR), also known as ErbB1. At physiological (98) or sub-saturating EGF concentrations (below 100 ng/ml), the majority of EGFR proteins are monomeric and not bound to ligand (99). Thus signal transduction occurs through catalytic and autocatalytic activation of the monomers (57), (100). Conversely, at high, saturating EGF doses (over 100 ng/ml), EGFR forms asymmetric dimers upon ligand binding, leading to a conformational change that autophosphorylates itself at Tyrosine residues via activation of the intracellular kinase domain (101), (102), (103). Additionally, at lower EGF concentrations, EGFR is maintained at the PM via vesicular recycling to sustain signaling, while at high EGF concentrations, it is internalized and degraded to limit signaling (104), (105), (106), (100).

The SH2 domain of the adapter protein Grb2 binds to these phosphorylated Tyrosines (107), (108) and aid the plasma membrane recruitment and activation of GEFs such as SOS (84), (85) as mentioned above. This forms an EGF-Grb2-GEF-Ras complex as the initial stages of signal transduction (109), (110). A higher plasma membrane concentration of SOS leads to more GDP being substituted for GTP on Ras proteins (111).

The out-of-equilibrium enrichment of KRas-GTP on the plasma membrane actuates signal transduction as downstream effectors such as those along the MAPK cascade can bind to active Ras (56), (61). The different Ras isoforms bind to effector proteins with varying proclivities and strengths. For example, KRas4B activates Raf and induces cell migration more than NRas and HRas (112). KRas also more potently activates Rac than HRas (113). Conversely, HRas activates Raf and subsequently ERK at the Golgi apparatus and the endoplasmic reticulum membranes (114).

Ras can also be activated by non-RTK mechanisms. GPCRs activate Ras via RasGRF (115), and hormones such as Insulin can also activate Ras via GEF activity (116). Calcium-dependent, Phospholipase C (PLC) activation of HRas at the Golgi apparatus via RasFRP1 is another mechanism by which Ras isoforms can be activated (117).

The differential activation and effector proclivities of Ras isoforms can therefore give rise to a host of different cellular outcomes. Mitogen-Activated Protein Kinase (MAPK) signaling is one such important network, which plays a key role in proliferation, cell cycle progression, and differentiation (118), (119).

Another important signaling cascade is the Phosphoinositide 3-Kinase signaling network, which mediates cell survival (120).

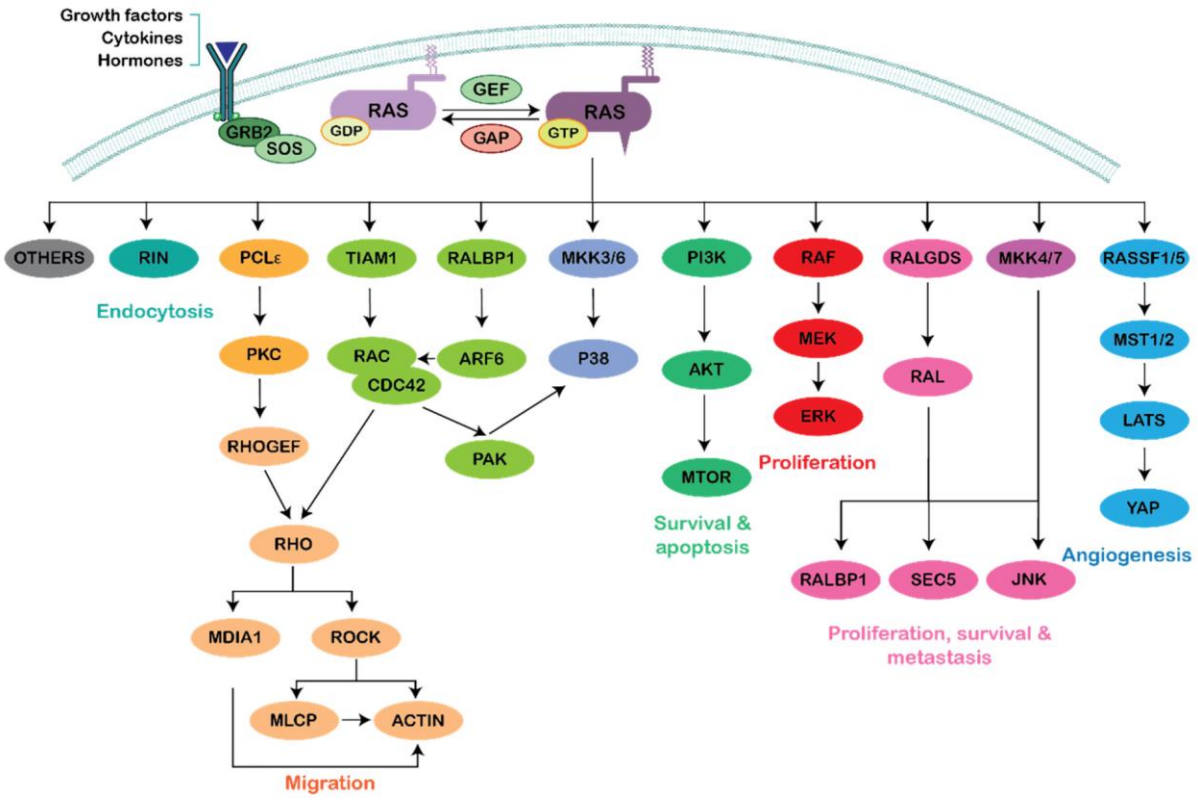

Figure 4. Ras-mediated signaling network.
Activation of Ras proteins by different ligands leads to a myriad of responses via several signaling cascades that mediate processes such as proliferation, migration, survival, and angiogenesis. Dysregulation of Ras-mediated signaling cascades can therefore drive cancer. Image from Soriano et al., 2021 (121).

3.7.1 Mitogen-Activate Protein Kinase signaling

Effectors downstream of Ras that are involved in MAPK signaling are Raf (MAPK Kinase Kinase), MEK (MAPK Kinase), and ERK (Extracellular Receptor Kinase, or MAPK) (122), (123). Thus, the sequential phosphorylation and activation of Raf-MEK-ERK proteins is what constitutes the MAPK signaling cascade (124), (125). MAPKs are serine/threonine kinases that phosphorylate serine/threonine amino acids which are followed by proline (124), (126).

Three Raf isoforms are described in the literature: A-Raf, B-Raf, and C-Raf. Raf proteins are inactive and autoinhibited in the cytosol (127), (128). Upon Ras activation, they are recruited to the plasma membrane and bind to Ras via their RBD (129). Dimensionality reduction (130), (131), (132) and a decrease in the diffusion speed of Ras-bound Raf kinases enables Raf dimerization which is often asymmetric, involving B-Raf and C-Raf (133). Dimerization results in the transactivation of Raf monomers (134). MEK family kinases are then phosphorylated and activated by the active Raf proteins. Subsequently, MEK-mediated phosphorylation of Threonine 202/Tyrosine 204 and Threonine 185/Tyrosine 187 leads to the activation of ERK1 and ERK2 respectively (135), (136). Cytosolic and nuclear substrates of phosphorylated ERK can then be activated leading to a variety of responses affecting transcription and replication (137) (138), (139) (140) (141).

Non-catalytic proteins and scaffold proteins such as 14-3-3 and KSR (kinase suppressor of Ras) are involved in Ras-mediated MAPK signaling at the level of the PM, by aiding the localization of signaling complexes (142). This gives credence to the importance of plasma membrane localization of Ras proteins for signal transduction. A review by Fehrenbacher et al., 2009 (143), suggested that Ras-mediated MAPK signaling can occur not only on the plasma membrane, but also at the level of the Golgi apparatus, endoplasmic reticulum, and endosomes.

Dynamic ERK responses mediated by spatiotemporal and dynamic regulation of growth factors are important and can yield different cell fate decisions or phenotypes (122), (144), (145), (146), (147). For instance, proliferation occurs as a result of transient activation of ERK via EGF signaling, while differentiation occurs when ERK activity is sustained upon stimulation with NGF (Nerve Growth Factor) in PC12 cells (147). Another example is that GPCR-mediated MAPK signaling is transient when it occurs via cross-talk with RTKs, or more sustained when it is cytosolic and modulated by β-arresting (148).

3.7.2 Phosphoinositide 3-Kinase signaling

Another important Ras-mediated signaling cascade is that of Phosphoinositide 3-Kinase (PI3K) acting via Ak strain transforming thymoma (AKT) protein, which is a serine/threonine kinase. AKT is a Ras effector (149), (150) but more strongly activated by HRas than KRas (151). It can also be activated by other ligands such as Insulin-like Growth Factor 1 and Insulin. During signaling, phosphatidylinositol-4,5-bisphosphate (PIP2) is activated by PI3K forming phosphatidylinositol-3,4,5-bisphosphate (PIP3). PIP3 associates with the plasma membrane (152) and activates effectors including AKT. Activation of AKT leads to its phosphorylation at threonine 308 and serine 473 residues (153), (154). Downstream of this, the mammalian Target of Rapamycin (mTOR) can be activated and influence cell survival and metabolism (155), (156).

Cross-talk between signaling networks can occur and add a layer of complexity to cellular information processing and communication. There is cross-talk between ERK and AKT signaling as they can compensate for each other's inhibition in pancreatic cancer cell lines (157), (158), (159). ERK inhibition can result in increased pAKT via the release of upstream negative feedback of pERK (160). AKT can also partially be phosphorylated by a MAPK-mediated mechanism (153), (161). It has also been shown that mTOR Complex 1 (mTORC1) can activate MAPK signaling via an S6K-PI3K-Ras mechanism (162).

3.8 Up- and down-regulation of Ras signaling cascades

Many factors influence the outcomes mediated by MAPK signaling such as the length and strength of the input signal, cross-talk with other signaling cascades, as well as scaffold proteins and intracellular localization (163). Non-linear dynamics of biological systems have been modeled mathematically to understand how signaling in living systems can result in multiple dynamic behavioral and morphological states (164). These dynamics of biological systems often contain properties such as positive and negative feedback loops, and adaptive and oscillatory behavior (164). This is also true for Ras-mediated signaling networks which can be viewed as more than just a molecular switch, due to the complex array of outcomes it modulates by the dynamic regulatory mechanisms that govern its function (165). This too involves feedback mechanisms and adaptive and oscillatory dynamics.

3.8.1 Positive feedback mechanisms in Ras-mediated signaling

Positive feedback loops form part of the EGF-EGFR-Ras-MAPK signaling. Autocatalytic activation of EGFR under physiological EGF concentrations has been shown to rapidly increase EGF-mediated signaling responses in downstream effectors (57). SOS positive feedback on Ras activation as a result of freeing it from its autoinhibited state upon plasma membrane recruitment (89) or by allosteric binding of Ras-GTP also increases Ras activation and thus the activation of downstream effectors. These positive feedback loops give rise to a switch-like or ultrasensitive response of Ras on MAPK signaling observed upon growth factor stimulation (166), (167). Positive feedback can sustain MAPK signaling and cell division responses with transient growth factor stimulation and mediate irreversible cell fate decisions in Xenopus oocytes, for example (168), (169).

3.8.2 Negative Feedback mechanisms in Ras-mediated signaling

Negative feedback mechanisms are also at play in Ras-mediated signaling along both the MAPK and PI3K-AKT cascades. Negative feedback loops influence the length and strength of ERK activity (Figure 5). ERK-mediated negative feedback acts via the inhibition of several proteins including SOS, Raf, and Mek (170). ERK can phosphorylate Threonine 669 of EGFR and downregulate its activity (171). Multiple serine sites on SOS1 can be phosphorylated by ERK, disrupting the EGFR-Grb2-SOS complex (172), (173), (174). Raf-1 (C-Raf) can also be phosphorylated by ERK, rendering it unable to bind to Ras-GTP at the plasma membrane (175).

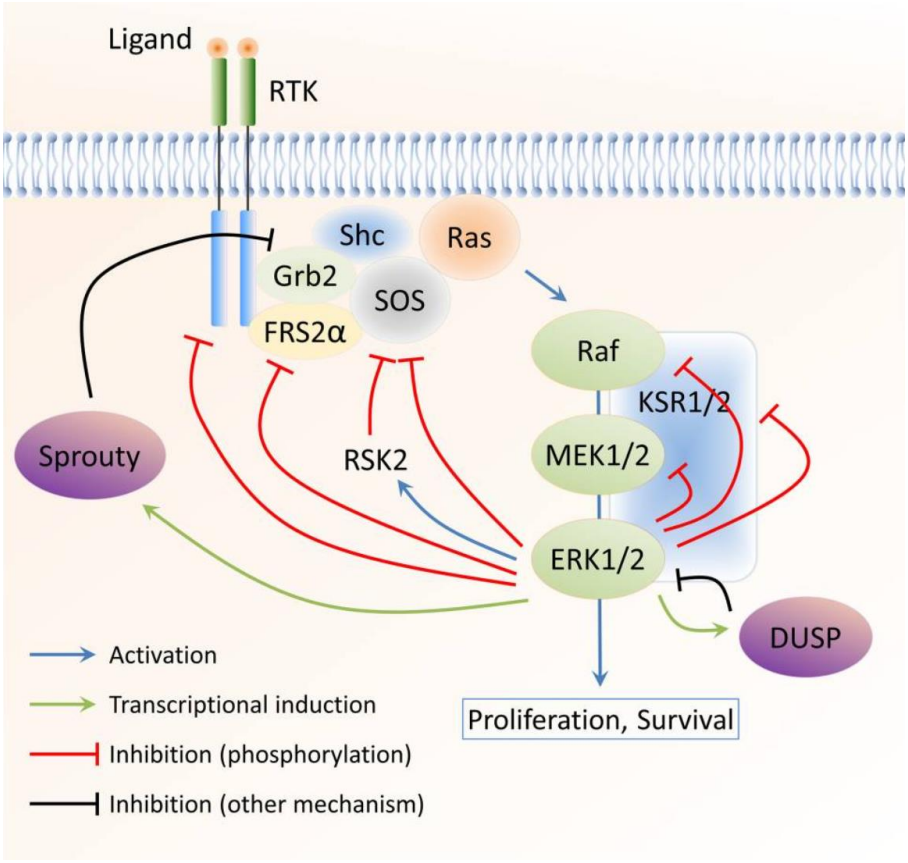

Figure 5. MAPK-associated negative feedback mechanisms.
The scheme shows the various levels of negative feedback regulation in the MAPK signaling cascade which is mediated by proteins such as ERK, DUSP, and Sprouty. Image from Lake et al., 2016 (170).

Phosphorylated ERK can itself be inactivated by proteins such as MAPK phosphatases and Dual-Specificity Phosphatases (DUSPs) which de-phosphorylate phosphorylated ERK (176), (170). Additionally, Sprouty (SPRY) proteins also downregulate MAPK signaling by inhibiting SOS-binding to Grb2 (177), (178), (170). SPRED 1 and 2 proteins inhibit FGF- and EGF-mediated MAPK signaling by preventing Raf activation (179), while EGFR is downregulated by protein tyrosine phosphatases (180).

The oscillatory behavior of phosphorylated ERK has been reported, the dynamics of which are a result of negative feedback mechanisms along the Ras-Raf-MEK-ERK signaling cascade (181), (182), (183). They have also been modelled computationally (184). These ERK waves have been described as asynchronous at steady-state (185).

Negative regulatory mechanisms are also present in PI3K-AKT signaling. Protein phosphatase 2A (PP2A) and the PH domain leucine-rich repeat protein phosphatases (PHLPP) 1 and 2 are known negative regulators of active phosphorylated AKT (153), (186), (161). P70s6K also acts as a negative regulator of AKT after growth factor stimulation (187)

There are multiple layers of complexity and regulation governing biological signaling systems. There is also tight regulation in the form of negative feedback or down-regulatory mechanisms to modulate the strength and length of the signal. However, even with such varied levels of control, errors still occur that can result in diseases.

3.9 Rasopathies

Given the central role of Ras in signaling, it follows that aberrations in the signaling network involving Ras can give rise to diseases. Ras-associated pathologies, or Rasopathies, are defined as germline mutations affecting aspects of the Ras-MAPK signaling cascade (188), (189). This includes a range of conditions such as neurofibromatosis type 1 where neurofibromin function is lost, Noonan syndrome where multiple gene mutations occur in Ras-MAPK proteins, and Costello syndrome where HRas is mutated (190), (191), (192) (188). Many of these conditions display similar symptoms and signs such as altered morphological features in the face, heart, skin, muscles, and eyes, as well as challenges in neurocognition (188). Patients with these conditions also have a greater propensity to developing cancers, many of which are Ras-associated (188), (193) Indeed, it is thought that up to a fifth of all human cancers are related to Ras isoform mutations, with KRas being the most frequently mutated (194).

3.10 Cancer

Carcinogenesis, or cancer formation, is viewed as a progressive phenomenon (195) involving multiple genetic defects (196) and chromosomal instability (197) and epigenetic factors such as DNA methylation (198), (199). These changes lead to dysregulated proliferation, survival, differentiation, and migration, which enable disordered growth and replication of cells and thus tumor formation, and the ability to metastasize through disordered migration. The 6 key aspects of cancer have been described, and they include the ability to replicate unhindered, evasion of apoptosis, mitogenic growth signaling autonomy (200). The environment surrounding a tumor, dubbed the tumor microenvironment, eventually also contributes to the maintenance and progression of cancer (201).

Gain-of-function mutations in oncogenes and loss or inactivation of tumor suppressor genes are commonly the primary contributing factors to tumor formation (202), (203), (204). The notion of oncogene addiction describes how cancerous cells depend on one or more oncogenic mutations for

growth, maintenance, and survival, despite having several genetic and epigenetic aberrations (205), (206). It has been suggested that addiction to oncogenic Ras in Ras-associated tumors is important for tumorigenesis via MAPK and PI3K signaling (207), (159), (154), with PI3K signaling playing a greater role in tumor maintenance than MAPK (207), (208), (152). Supporting the theory that Ras-mediated MAPK signaling is involved in cancer formation, one study suggested that ERK may be constitutively active in some colon, pancreatic, lung, and kidney tumors or cancer cell lines and that this may be linked to Raf activation (209). Suffice it to say, it is clear that aberrant Ras signaling plays a crucial role in cancer.

3.11 The role of Ras in cancer

About 19% of cancer patients possess a Ras mutation, with KRas mutations being implicated in about 75% of cases (194). An increase in wild-type KRas gene copy number and expression is also associated with the pathophysiology of some cancers (210), (211), (212). For example, overexpression of wild-type KRas is associated with worse outcomes in terms of remission and survival in acute myeloid leukemia patients (213). Thus both overexpression of and mutations in Ras proteins are significant. Following an oncogenic mutation in one of these isoforms, the loss of tumor-suppressors such as p53, and other genetic and epigenetic changes (214) that drive cells toward cancer formation.

Many Ras mutations are activating, missense mutations on positions Glycine 12 (G12), Glycine 13 (G13), and Glutamine 61 (Q61) and are involved in many cancers including pancreatic, colon, and lunch cancers (19), (66), (34), (215), (24), (157). G12 and G13 mutations are more common in KRas, whereas Q61 mutations are more common in HRas and NRas (216). Mutations in the G12 region result in a structural shift of the Switch II region (217). Differences in G12 and G13 Ras mutations are observed in responses to anti-EGFR chemotherapy, with slightly better survival in G13 patients (218). Mutations in these loci disrupt GTP hydrolysis and limit GAP activity on the mutated Ras (73), (216). Mutated Ras is therefore constitutively activated in the GTP-bound state, engaging MAPK and PI3K signaling in pathogenesis (219), (187), (220). Altered effector binding and changes in feedback mechanisms may also play a role in cancer formation in Ras-associated carcinogenesis (221), (219), (222), (160).

Different Ras isoform mutations are observed in different cancers with varying tissue specificities (216). For instance, HRas mutations are often involved in bladder cancers, while NRas mutations are associated with melanoma (25), (26), (193). KRas mutations on the other hand are often seen in pancreatic, colorectal, and lung adenocarcinomas.

About 93% of early-stage pancreatic ductal adenocarcinoma are observed to have an oncogenic Kras mutation (223), (224). Additionally, the growth of pancreatic cell lines was suppressed by inhibiting oncogenic KRas (225), (226) suggesting that these tumors depend, to a high degree, on the oncogenic KRas for growth.

Colorectal cancer (CRC) is the second deadliest cancer globally (227), characterized by upregulation of oncogenes and downregulation of tumor suppressor genes (228). Although mutations of the tumor suppressor gene product adenomatous polyposis coli and dysregulated Wnt signaling are important aspects of CRC, up to half of colorectal cancers involve an oncogenic KRas mutation, often conferring a treatment resistance (229), (223). KRas mutations, especially of the G12 codon, confer worse survival in CRC (230), (231). These patients often do not benefit from anti-EGFR therapies (232), (233), (234).

Mutations in Ras-signaling regulators can also be involved in Ras-associated cancers. As mentioned, a reduction in the function of mutated Neurofibromin is involved in several cancers such as melanoma,

lung adenocarcinoma, and glioblastoma (235), (236). Additionally, some T-cell leukemias involve overexpressed RasGRP1, a Ras GEF, which elevates active Ras-GTP (237).

3.12 Oncogene Induced Senescence and Apoptosis

It is evident that mutated Ras proteins play a role in many cancers. However, in certain situations, the presence of oncogenic Ras does not lead to hyperproliferation and increased cell survival, but rather growth inhibition. This phenomenon is termed oncogene-induced senescence (OIS). OIS can occur when co-expression of an oncogenic and a wild-type RAS allele drives cells towards senescence or apoptosis, rather than proliferation (238), (239), (240). The mechanism by which this occurs involves overexpression of mutant KRas (238), (241).

OIS appears not to occur at endogenous levels of expression of KRas G12V and G12D as shown in mice embryonic fibroblasts (MEFs) (242) (241). Conversely, endogenous-level expression of KRas G12D in MEFs increased proliferation and partial transformation (241). Thus, isogenic levels of mutant KRas in one allele drive proliferation toward cancer formation (243).

Oncogenic Ras alone is insufficient to cause senescence, but constant MAPK signaling, loss of GAPs like NF-1, and activation of tumor suppressors such as p53 and p16 INK4a are also required (238), (244), (245). To this end, a model was proposed by Tuveson et al, where overexpression of mutant KRas does occur and engages tumor inhibitory mechanisms, which must be overcome to eventually lead to cancer formation (241), (246), (247), (248). This also suggests that overexpression of mutant Ras is important for carcinogenesis as was suggested by a study on MCF-10A cells (249). However, tumor suppression should be overcome (246).

3.13 The roles of Ras proteins in tumorigenesis

OIS shows that oncogenic Ras alone may not be sufficient to cause cancer. From studies on OIS, it is clear that Ras expression level can affect the proliferation and survival of cells containing mutant Ras. However, another layer of complexity to Ras-associated carcinogenesis is the action and interplay of the other Ras proteins. Studies suggest that the wild-type counterpart of the mutant Ras, as well as other wild-type Ras isoforms, play distinct roles.

3.13.1 The role of the mutated Ras protein

The mutated Ras protein is constitutively active, in the GTP-bound state. Oncogenic KRas for example, is thought to modulate baseline effector levels, raising pERK, and mediating proliferation (250). Additionally, mutant Ras is thought to diminish responses to EGF via an inhibitory mechanism on wild-type Ras signaling (250)

Oncogenic KRas can increase wild-type HRas and NRas activity via allosteric activation of SOS1 (251), (252), (253). It can also cross-activate the cognate wild-type KRas via allosteric binding to SOS (254). In contrast to this, mutant KRas in pancreatic cancer can negatively regulate WT Ras signaling via Ribosomal S6 Kinase (RSK) and NF-1 mechanisms (255)

In KRas-mutant cells, activation of wild-type Ras, that is the cognate Ras and the other two Ras isoforms, likely occurs via two primary mechanisms. One mechanism involves allosteric activation of SOS by KRas oncoprotein, which then activates the wild-type HRas and NRas proteins in the cell, promoting tumor formation (253). Another mechanism is through growth factor-mediated activation.

As the wild-type Ras proteins are not constitutively active, they can still be activated by growth factor signaling cascades such as via RTKs. Additionally, activation of wild-type Ras proteins can occur via PI3K-AKT-NOS (endothelial Nitric Oxide Synthase) mediated C118 S-nitrosylation of wild-type Ras variants and is thought to encourage tumorigenesis (256)

3.13.2 The role of the cognate, wild-type Ras protein

Several studies suggest that the cognate, wild-type Ras counterpart of an oncogenic Ras plays a tumor-inhibitory role (Figure 6) in the early stages of tumorigenesis (257), (258). This is because, in human and mouse cancer models, it is often observed that this wild-type counterpart of the oncogenic Ras during cancer formation is lost, a process known as loss of heterozygosity, (258), (248).

Loss of heterozygosity (LOH) was seen in mice with mutated HRas that developed integumentary tumors (259). LOH has also been observed in lymphomas with mutant NRas and KRas-mutant lung tumors in mice (260), (258). This was also the case in a p16 knockout mouse line modeling pancreatic cancer (248). In human samples of lung cancer with mutated KRas, LOH was also observed (261). Additionally, samples from Costello Syndrome patients with mutated HRas who also developed cancer were observed to have LOH (262).

Further evidence for the tumor-suppressive ability of the cognate wild-type Ras comes from transfection experiments. Transfection of HRas-mutated rat fibroblasts with wild-type human HRas inhibited tumorigenesis (263). Similar results were observed when wild-type NRas was transfected into NRas-mutated thymic lymphoma model (264). Additionally, in KRas-mutated tumors, it has been shown that loss of wild-type HRas and NRas promotes DNA damage by an increased MAPK and AKT signaling mechanism, which encourages tumorigenesis (265).

The studies mentioned above provide evidence supporting an inhibitory role of the cognate wild-type Ras. Contrary to this, other research suggests that wild-type Ras may promote tumorigenesis under certain conditions. For instance, mutant KRas can activate signaling, resulting in apoptosis (266). However, expression of wild-type KRas in KRas-mutated colorectal cancer was associated with autocrine-mediated EGFR signaling that opposes this apoptosis, suggesting a tumor-promoting function of wild-type KRas (266). Adding a further layer of complexity is that some studies suggest that the cognate wild-type Ras neither encourages nor inhibits tumorigenesis in mutant KRas cell lines. In NRas (G12D)-mutated myeloproliferative neoplasia, wild-type NRas did not inhibit tumorigenesis (267).

3.13.3 The role of the non-mutated Ras isoforms

The non-cognate wild-type Ras proteins of the non-mutated Ras isoforms (for example, HRas and NRas in a KRas-mutated system) are thought to play a tumor-promoting role (Figure 6). In human cancer cell lines, the wild-type isoforms of Ras have been reported to drive cancer formation by mediating growth factor responses, which the constitutively active oncogenic Ras does not (250). It was shown in a KRas-mutant endometrial cancer cell line that growth factor-mediated ERK signaling occurs via wild-type HRas and NRas, while AKT signaling occurs via HRas (268). Signaling, however, may still occur independent of growth factor stimulations, as it was shown that in serum-deprived cells, wild-type NRas mediated MAPK signaling in G12V HRas mutated cells (222).

Although not commonly investigated, in KRas-mutated lung tumors, the wild-type KRas4A splice variant may promote tumorigenesis in the initial stages, but not maintain tumor growth (269).

The roles of different Ras proteins in cancer are therefore multilayered, with some opposing results in the literature. One study suggested that the contexts within which these observations are made are important as they affect whether the cognate and other wild-type Ras isoforms encourage or inhibit tumorigenesis (257).

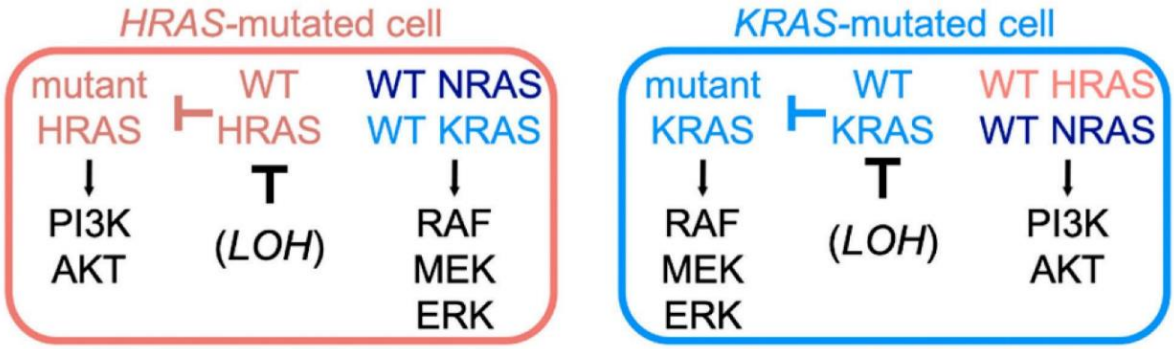

Figure 6. Theory on the roles and interactions of Ras isoforms in HRas- and KRas-mutated cells.
The scheme on the left shows the likely functions and interactions of Ras isoforms in HRas-mutated cells, where mutated, oncogenic HRas drives tumorigenesis via PI3K-mediated signaling and the WT KRas and NRas mediate MAPK signaling. The scheme on the right shows the proposed roles and relationship between mutated, oncogenic KRas and other Ras isoforms during tumorigenesis, whereby mutant KRas drives tumorigenesis via MAPK signaling, while WT HRas and NRas mediate PI3K signaling. In both HRas- and KRas-mutated cells, the cognate WT isoform is thought to be inhibitory to its mutated, oncogenic counterpart. Image from Sheffels et al., 2021 (270).

3.14 Other considerations of Ras-mediated signaling in cancer

Non-mutated Ras is also observed in several cancers. Oftentimes, gene duplication and Ras protein overexpression play a role in the development of cancer. Human HRas overexpressed in transgenic mice was associated with tumor formation, regardless of mutation state (271). Liver tumors can develop in mice models expressing only wild-type HRas through carbon tetrachloride induction (272).

Other genes of proteins involved in Ras signaling cascades, such as NF-1, are often mutated in ovarian and lung cancers (273), (274). DUSP6, a negative regulator of MAPK signaling, is thought to have an inhibitory function on proliferation in lung cancer cells (275). Even though SOS1 mutations are seldom reported in cancer (276), RasGRPs are involved in many cancers, as reviewed by Ksionda et al., 2013 (237).

Collectively, these studies show a complex relationship that exists between mutated and non-mutated Ras proteins in the development and maintenance of different cancers. It is possible that mutated Ras can activate the other wild-type Ras proteins. However, the functions of each of these is likely dependent on the context. Other proteins in the Ras signaling network, such as the GEF RasGRP, and negative regulators of MAPK signaling likely also play important roles.

3.15 Control of Protein Localization in vivo

There is experimental value in being able to manipulate the spatiotemporal dynamics of a protein or its expression. Chemically induced dimerization (CID) is one such molecular biology technique that allows for spatiotemporal control of proteins in vivo. Thus, it can be used to investigate signaling, protein localization, and gene expression (277), (278), (279), (280).

The CID system consists of dimerization domains, which are usually natural or modified ligand binding domains of selected proteins, which can be brought together by a chemical inducer or dimerizer that binds to both dimerization domains (281), (282). The dimerization domains are linked to split proteins or proteins of interest, at least one of which can be targeted to a specific cellular compartment, offering spatial control (281), (282).

One commonly used CID system is the FK506-binding protein (FKBP) – FKBP – rapamycin binding (FRB) system, or FKBP-FRB for short (278), (283), (284). The FKBP-FRB system allows for the use of Rapamycin or a related molecule as a dimerizer for FKBP12 and FRB dimerization domains (283), (284). While Rapamycin is a ligand for FKPB12, FRB is an mTOR domain that can bind to FKPB12 via Rapamycin.

Other systems have also been established with the capacity to be reversible and with less interference with endogenous systems. One such example is a system employing the use of an *E. coli* dihydrofolate reductase (eDHFR) and modified FKBP dimerization domains with a synthetic bivalent ligand as the dimerization molecule (285). Such systems are widely used for global control of protein localization in groups of cells.

Fine-tuned spatial control can be achieved by using chemical-optogenetic techniques. Chemical-optogenetic approaches contain photocaged and/or photocleavable molecules where light is used to control the dimerization and reversal of dimerization of proteins in a spatiotemporal manner (286), (287), (288). Different approaches employ light-based systems such as the Light-Oxygen-Voltage (LOV2) protein domain of phototropin 1 of Avena sativa, where blue light leads to a conformational change that can allow controlled binding of LOV2 to a designed domain. (289), (290). Combining the CID with optogenetics for multidirectional modulation of the localization of a protein of interest has also been proposed (291).

CID and optogenetic techniques therefore offer a way to investigate Ras signaling by controlling its plasma membrane localization.

4 Objectives

Ras proteins play an important role in several signaling cascades, transducing external signals into phenotypic and behavioral outputs. The significance of KRas oncoproteins in the pathophysiology of cancer is undeniable, as they regulate processes such as proliferation, differentiation, and survival – processes that are dysregulated in cancer. Constitutive activation of mutated KRas proteins is thought to drive tumor formation. However, this notion has proven to be more convoluted than previously thought. Oncogene-induced senescence occurs when oncogenic KRas is over-expressed relative to the other wild-type isoforms, adding nuance to the paradigm. Additionally, the loss of the cognate wild-type Ras during transformation points to this wild-type Ras playing an inhibitory role against its mutated counterpart. Although distinct roles in Ras signaling of wild-type and oncogenic Ras have been described, how they interact remains unclear and requires further study. We hypothesized that there is an interaction between wild-type and oncogenic Ras activity and that this interaction influences cell behavior toward either a senescent or oncogenic state.

Ras protein signaling via MAPK and PI3K cascades is intrinsically linked to its localization at the plasma membrane. Thus, controlling Ras localization provides a way to temporally regulate its signaling activity. Using this concept, we aimed to apply a bioorthogonal chemically-induced dimerization technique to modulate the plasma membrane translocation of oncogenic KRas and assess its effect on wild-type Ras activity and downstream signaling.

In summary, we set out to do the following:

1. Develop a chemical genetic approach to control the concentration of oncogenic KRas at the plasma membrane.

2. Develop a biochemical assay for wild-type Ras activity and signaling to investigate the effects of chemically-induced translocation of KRas to the plasma membrane on Ras-mediated signaling.

With these objectives, the aim was to investigate whether the plasma membrane localization of KRas oncoproteins influences wild-type Ras activity and subsequent signaling.

5 Materials and Methods

5.1 Materials

5.1.1 Chemicals and Reagents

Table 1. Chemicals and Reagents

Name	**Supplier**
2-mercapto-ethanol (β-mercaptoethanol)	SERVA Electrophoresis GmbH
Acetic Acid	Sigma-Aldrich
Albumin bovine fraction V, pH 7.0 (BSA)	SERVA Electrophoresis GmbH
Ammonium persulfate (APS)	SERVA Electrophoresis GmbH
Bromophenol blue	Sigma-Aldrich
cOmplete ™, EDTA-free Protease Inhibitor Cocktail	Merck
Crystal Violet	Sigma-Aldrich Biochemie GmbH
Dimethyl sulfoxide (DMSO)	SERVA Electrophoresis GmbH
Dithiothreitol (DTT)	Fluka ® Analytical
(Human) Epidermal Growth Factor (hEGF) E9644	Sigma-Aldrich
Ethanol	J.T. Baker
Ethylenediaminetetracetic acid (EDTA)	Fluka ® Analytical
Glycerol	GERBU Biotechnik GmbH
Glycine	Carl Roth GmbH
Guanosine 5'- [γ-thio] triphosphate tetralithium	Sigma-Aldrich
Guanosine 5 - diphosphate salt	Sigma-Aldrich
Imagine Medium	PAN ™ Biotech
Isopropanol	J.T.Baker
Isopropyl-β-D-1-thiogalactopyranoside (IPTG)	Sigma-Aldrich
Kanamycin sulfate	GERBU
Magnesium chloride ($MgCl_2$)	Merck KG
Methanol	Sigma-Aldrich
N,N,N',N'-Tetramethylene-diamine (TEMED)	Carol Roth GmbH
Phosphatase inhibitor cocktail 2 + 3	Sigma-Aldrich
Phosphate Buffered Saline 10X Molecular Biology Grade	Corning ®
Poly-Lysine	Sigma-Aldrich
Precision Plus Protein TM Dual Color Standards	Bio-Rad
Puromycin	Sigma-Aldrich
Sodium Chloride (NaCl)	Fluka ® Analytical
Sodium Dodecyl sulfate (SDS)	Carl Roth GmbH
Trimethoprim	Sigma-Aldrich
Tris-base	Carl Roth GmbH
Tris-HCl	J.T.Baker
Triton X-100	SERVA
Tween 20	SERVA
Roti®-Histofix 4%	Carl Roth GmbH

Rotiphorese®Acrylamide/Bis-acrylamide 40% (29:1)	Carl Roth GmbH
Modified Synthetic ligand of FKBP – Trimethoprim (SLF'-TMP)	ChiroBlock GmbH
Trimethoprim (TMP)	Sigma-Aldrich

5.1.2 Molecular Biology

5.1.2.1 Plasmids

Table 2. Plasmid List

Name	**Vector**
mTFP-2xFKBP-KRasΔHVRwt-P2A-tagBFP-2xeDHFR-tK_pPB CAG IRES Puro	PiggyBac CAG IRES PuroR
mTFP-2xFKBP36V-KRasG12VΔHVR-P2A-TagBFP-2xeDHFR-tKRas	PiggyBac CAG IRES PuroR
mTFP-2xFKBP-KRasΔHVRG12D-p2a-tagBFP-2xeDHFR-tK_pPB CAG IRES Puro	PiggyBac CAG IRES PuroR

*Plasmids were created in the Lab of Prof. Dr. Philippe Bastiaens, Department of Systemic Cell Biology, Max Planck Institute of Molecular Physiology, Dortmund (292).

5.1.2.2 Escherichia Coli (E. coli) strains

Table 3. Escherichia coli strains

Name	**Supplier**
E. coli BL21-CodonPlus(DE3) competent cells	Agilent Technologies

5.1.2.3 Buffers and Media

Table 4. Molecular biology - buffers and media

Name	**Preparation**
LB (Lysogeny broth) medium	10 g/L Bacto-Trypton 5 g/L yeast extract 10 g/L NaCl pH 7.4
LB agar plates with antibiotics for selection	15 g/L agar in LB medium, autoclaved, supplemented with respective antibiotics: Kanamycin 50 µg/mL, Ampicillin 100 µg/mL
SOC (Super Optimal broth) medium	20 g/L Bacto-Trypton 5 g/L Bacto-yeast extract 0.5 g/L NaCl 2.5 mM KCl 10 mM $MGCl_2$

	20 mM glucose autoclave, then add 20 mM glucose
TAE (Tris-acetate-EDTA) buffer	40 mM Tris/Acetate (pH 7.5) 20 mM NaOAc 1 mM EDTA
TB (Terrific broth) medium	12 g/L Trypton 24g/L yeast extract 4 mL/L glycerol 17 mM KH_2PO_4 72 mM K_2HPO_4

5.1.3 Protein Biochemistry

5.1.3.1 Buffers and Media

Table 5. Protein biochemistry - buffers and media

Name	**Preparation**
Bacterial Lysis Buffer	50 mM Tris-HCl (pH 7.5) 400 mM NaCl 1 mM DTT 1% Triton X-100 1 mM EDTA 1 cOmplete ™ EDTA-free Protease Inhibitor tablet per 50 mL
GST-3xRafRBD pulldown wash buffer	50 mM Tris-HCl (pH 7.5) 50 mM NaCl 20% Glycerol 1 mM EDTA 1 mM DTT 1 cOmplete ™ EDTA-free Protease Inhibitor tablet per 50 mL
GST-3xRafRBD pulldown lysis buffer	50 mM Tris-HCl (pH 7.5) 200 mM NaCl 10% Glycerol 5 mM $MgCl_2$ 1% Triton X-100 1 cOmplete ™ EDTA-free Protease Inhibitor tablet per 50 mL
2x SDS sample buffer	150 mM Tris-HCl (pH 6.8) 1.2% SDS 30% Glycerol 2.1 M β-mercaptoethanol 0.1% bromophenol blue
5x SDS sample buffer	60 mM Tris-HCl (pH 6.8) 2% SDS 25% Glycerol 0.7 M β-mercaptoethanol 0.1% bromophenol blue

SDS running buffer	25 mM Tris-base 192 mM glycine 0.1% SDS
Transfer buffer	25 mM Tris-base 192 mM glycine 20% methanol
Tris-buffered saline (TBS)	50 mM Tris-HCl (pH 7.5) 150 mM NaCl
TBS-Tween	50 mM Tris-HCl (pH 7.5) 150 mM NaCl 0.1% Tween 20

5.1.3.2 Commercially available materials and kits

Table 6. Protein biochemistry - commercially available materials and kits

Name	**Supplier**
Odyssey ® Blocking Buffers (PBS) (#927-40000)	Li-Cor
Pierce ™ Glutathione Magnetic Agarose Beads (#78602)	Thermo Fisher Scientific
Precision Plus Protein™ Dual Color Standards (#1610374)	Bio-Rad
Micro BCA Protein Assay Kit (#23235)	Thermo Fisher Scientific

5.1.3.3 Casting gels

Table 7. Casting gels for SDS PAGE

Name	**Preparation**
Running Gel 15%	9.2 mL Milli-Q H_2O 20 mL 30% Acrylamide 10 mL 1.5 M Tris (pH 8.8) 400 µL 10% SDS 400 µL 10% APS 16 µL TEMED
Stacking gel 5% (25 mL)	14 mL Milli-Q H_2O 4.25 mL 30% Acrylamide 6.25 mL 0.5 M Tris (pH 6.8) 250 µL 10% SDS 250 µL 10% APS 25 µL TEMED

5.1.3.4 Antibodies

5.1.3.4.1 Primary Antibodies

Table 8. Primary antibodies

Name	Dilution	Supplier
Pan Ras monoclonal antibody (RAS10), (Lot VH307686)	1:1000 (Western Blot)	Invitrogen
Anti-alpha Tubulin monoclonal mouse antibody, (#T6074, Lot 118M4779V)	1:4000 (Western Blot)	Sigma Life Sciences
Phospho-AKT rabbit monoclonal antibody, (S473), (#12/2019, Lot25)	1:2000 (Western Blot)	Cell Signaling Technology
Phospho-AKT rabbit polyclonal antibody (S473), (#9271L)	1:1000 (Western Blot)	Cell Signaling Technology
Phosphorylated p44/42 MAPK (T202/ Y204), rabbit monoclonal antibody, (#4370S and #4370L)	1:2000 (Western Blot)	Cell Signaling Technology

5.1.3.4.2 Secondary Antibodies

Table 9. Secondary antibodies

Name	Dilution	Supplier
IRDye® 680 RD Donkey anti-Rabbit IgG (H + L) (#926-68073)	1:10 000 (Western Blot)	Li-Cor
IRDye® 800 CW Donkey anti-Mouse IgG (H + L) (#926-32212)	1:10 000 (Western Blot)	Li-Cor
IRDye® 800 CW Donkey anti-Rabbit IgG (H+L) (#926-32213)	1:10 000 (Western Blot)	Li-Cor
IRDye® 680 RD Donkey anti-Mouse IgG (H + L) (#926-68072)	1:10 000 (Western Blot)	Li-Cor

5.1.4 Cell Biology

5.1.4.1 Mammalian Cells

Table 10. Mammalian cells

Name	Supplier
Madin-Darby canine kidney (MDCK) cells, MDCK (NBL-2), ATCC® Number: CCL-34TM	ATCC

5.1.4.2 Stable cell lines of mammalian cells

Table 11. Stable cell lines of mammalian cells

Name	Incorporated Plasmid
Recruitable WT KRas-expressing MDCK cells (rWT KRas cells)	MDCK cells piggyBac transfected with mTFP-2xFKBP-KrasΔHVRwt-p2a-tagBFP-2xeDHFR-tK_pPB CAG IRES Puro

Recruitable G12V KRas-expressing MDCK cells (rG12V KRas cells)	MDCK cells piggyBac transfected with mTFP-2xFKBP36V-KRasG12VΔHVR-P2A-TagBFP-2xeDHFR-tKRas
Recruitable G12D KRas-expressing MDCK cells (rG12D KRas cells)	MDCK cells piggyBac transfected with mTFP-2xFKBP-KrasΔHVRG12D-p2a-tagBFP-2xeDHFR-tK_pPB CAG IRES Puro

* The MDCK cell lines stably expressing recruitable KRas constructs were previously created in the laboratory of Prof. Dr. Philippe Bastiaens, Department of Systemic Cell Biology, Max Planck Institute of Molecular Physiology, Dortmund (292).

5.1.4.3 Media components

Table 12. Cell biology - media components

Name	**Supplier**
DPBS without Ca^{2+}/Mg^{2+} (P04-361000)	PAN ™ Biotech GmbH
Dulbecco's Modified Eagle Medium (DMEM, #P04-03600)	PAN ™ Biotech GmbH
Fetal Bovine Serum (FBS, #F7524)	Sigma-Aldrich
L-Glutamine (#P04-80100)	PAN ™ Biotech GmbH
Non-essential amino acids (NEAA)	PAN ™ Biotech GmbH
Trypsin 0.05% /EDTA 0.02% in DPBS, without Ca^{2+} and Mg^{2+} (#P10-023100)	PAN ™ Biotech GmbH

5.1.4.4 Media Preparations

Table 13. Cell biology - media preparations

Name	**Preparation**
Complete culture medium (Full growth medium (FGM))	DMEM, 1% NEAA, 1% L-Glutamine, 10% FBS
Cryopreservation medium	Complete culture medium, 10% DMSO
Serum-deprived Medium	DMEM, 1% NEAA, 1% L-Glutamine, 0.1% FBS
Serum-free Medium	DMEM, 1% NEAA, 1% L-Glutamine, 0% FBS

5.1.5 Instruments and Equipment

Table 14. Instruments and Equipment

Name	**Supplier**
Centrifuge 5417R (with Temp function)	Eppendorf
DynaMag ™-2	Life Technologies AS, Norway (Made in UK, REF 12321D, Invitrogen)
Immobilon-FL Polyvinylidene Fluoride (PVDF)	Millipore, Merck KGaA
Multiskan Ascent	Thermo Electron Corporation
Odyssey Infrared Imager	Licor® Biosciences
Pherastar FS	BMG Labtech
Typhoon Trio Variable Mode Imager	GE Healthcare

XCell IITM Blot Module	InvitrogenTM Life Technologies
XCell SureLockTM Mini-Cell Electrophoresis Sys.	InvitrogenTM Life Technologies

5.1.6 Software

Table 15. Software

Name	**Supplier**
Adobe Illustrator	Adobe Systems
DNASTAR Navigator v2.2.1.1	DNASTAR Inc.
FV10-ASW Fluoview Software	Olympus
Fiji	http://fiji.sc/Fiji (293)
GraphPad Prism 6 and 9	GraphPad Software Inc.
Inkscape Version 1.0.1 and 1.3.2	Download Inkscape 1.0 | Inkscape
Leica Application Suite X	Leica Microsystems
Microsoft Office 2016	Microsoft Corporation
Multiscan Ascent Software Version 2.6	ThermoElectron Coorperation
Odyssey Infrared Imaging System	Licor® Biosciences
Python v3.7.4	Python Software Foundation

5.2 METHODS

5.2.1 Cell Biology

5.2.1.1 Cell culture

5.2.1.1.1 Cultivation of cells

Dulbecco's Modified Eagle's Medium supplemented with 10% Fetal Bovine Serum (FBS), 1% nonessential amino acids, and 1% (10 mM) L-Glutamine was used to culture MDCK cells in a humidified incubator with 5% CO_2 at 37 °C. The standard culture procedure was to seed and culture 1 x 10^6 MDCK cells in a T-75 flask and passaged every 2 days.

5.2.1.1.2 Passaging cells

To passage the cells, the growth medium was aspirated and the cells were washed with 10 mL PBS without Ca^{2+}/Mg^{2+}. To detach the cells from the culture flask, 1.5 mL of 5% Trypsin-EDTA was added to the T-75 culture flask, and the cells incubated for 10-15 minutes in a humidified incubator (5% CO_2 at 37 °C). The trypsin-EDTA was neutralized by adding 8.5 mL of DMEM FGM. The cells were centrifuged at room temperature for 5 minutes at 200 g, and the FGM-Trypsin-EDTA was removed. The cell pellet was then resuspended in 6 mL growth medium and a 500 µL aliquot was used to determine the cell count and viability using an automated hemocytometer. Two million cells were then reseeded in a fresh T-75 with 10-12 mL medium for 2 days before the following passage.

5.2.1.1.3 Cryopreservation of cells

To cryopreserve cells, cells were detached from the culture flask with Trypsin-EDTA and pelleted as above. The cell count was determined, and the desired volume of cells was transferred to a new falcon tube and centrifuged again at 200 g for 5 minutes at room temperature. The pellet was resuspended in FGM containing 10% DMSO and stored in cryovials at 1 x 10^6 or 2 x 10^6 cells per milliliter per cryovial. The cells were stored at 70 °C for 24 hours before long-term storage at -150 °C.

5.2.1.1.4 Thawing cells from long-term storage

When thawing cryovials, the cells were quickly heated in a water bath for 1 – 2 minutes, then immediately diluted in FGM to a total volume of 10 mL in a falcon tube. The cells were then centrifuged at 200 g for 5 minutes at room temperature and the supernatant aspirated to remove the DMSO. The cells were then resuspended in fresh, warm medium (37 °C), and seeded in a T-75 flask with 12 – 15 mL total FGM before culturing until confluence (or for 2 – 3 days) in a humidified incubator with 5% CO_2 at 37 °C.

5.2.1.2 Characterization of the EGF temporal response of wild-type MDCK cells

To understand the effects of EGF on Ras signaling in cells, an EGF time series was carried out in WT MDCK cells using low (10 ng/mL) and saturating (160 ng/mL) doses of EGF. WT MDCK cells were seeded in 6 cm dishes at 6 x 10^5 cells per dish and cultured in FGM under standard culture conditions for 2 days (N= 14 x 6cm dishes). The cells were washed with room temperature PBS and then cultured in 3600 µL of serum-deprived DMEM for 2 hours under standard culture conditions (in a humidified incubator at 37 °C, 5% CO_2) to reset signaling to baseline levels.

A fresh working solution of 100 ng/mL or 1600 ng/mL EGF dissolved in cold, serum-free medium was prepared and warmed up in a water bath to 37 °C shortly before use. Cells were then stimulated with 10 ng/mL or 160 ng/mL EGF by adding 400 µL of 100 ng/mL or 1600 ng/mL EGF respectively to each 6cm dish of cells containing 3600 µL serum-deprived medium. The cells were cultured under standard conditions for various time points up to 60 minutes, and the experiment was stopped by placing the culture dish on ice, then washing the sample(s) with cold PBS containing protease and phosphatase inhibitors. Time points used (in minutes) were 0 (unstimulated), 3, 5, 7, 10, 13, 15, 20, 30, 40, 50 and 60. The samples were immediately lysed and snap-frozen in liquid nitrogen until further processing, or immediately prepared for western blotting of whole cell lysates (WCL), or for 3xRafRBD pulldown for active Ras (two samples in which no EGF stimulation was carried out). See Cell lysis. Determination of Protein Concentration, SDS-PAGE and Western Blot, and 3x-RafRBD GST Pull Down.

5.2.1.3 Effect of plasma membrane recruitment of rKRas on Ras activity and signaling

To as assess the effects of translocating rKRas to the PM on Ras-GTP levels and signaling via MAPK and PI3K, MDCK cells (1x WT MDCK, 7x rWT KRas, and 6x rG12V or rG12D KRas cells) were seeded in 6cm Petri dishes at 6.0 x 10^5 cells per dish and cultured in FGM for 2 days under standard conditions. Cells were washed once with 2 mL PBS then serum-deprived for 2 h in 3.6 mL serum-deprived DMEM containing 0.1% FBS, under standard culture conditions.

Fresh working solutions of SLF'-TMP (20 µM), DMSO (0.2% v/v), and EGF (1 µg/mL) dissolved in serum-deprived medium were prepared and kept on ice until needed. Shortly before use, they were warmed up in a water bath. To recruit rKRas to the plasma membrane, 400 µL of the working solution of SLF'-TMP (final concentration 2 µM) were added to the cells in 3600 µL serum-starved medium. For controls, 400 µL DMSO (final concentration 0.02% v/v) and EGF (final concentration 100 ng/mL) were also added. Two samples for each stable cell line used were also cultured and deprived of FBS, but not exposed to the dimerizer. These were used as positive and negative controls for the 3xRafRBD Pulldown assay as their lysates were in vitro loaded with GTPγS or GDP nucleotides.

Table 16. Effect of plasma membrane recruitment of rKRas on Ras activity and signaling

Cell Line	**Ligand/chemical added**	**Final concentration in 4 mL serum-deprived medium**	**Incubation time of experiment (minutes)**
rWT KRas cells	DMSO	0.02% v/v	10
rWT KRas cells	-	-	0
rWT KRas cells	SLF'-TMP	2 µM	10
rWT KRas cells	SLF'-TMP	2 µM	20
rWT KRas cells	SLF'-TMP	2 µM	60
rWT KRas cells	*sample for in vitro loading of GDP	-	0
rWT KRas cells	*sample for in vitro loading of GTPγS	-	0
rG12V (or rG12D) KRas cells	-	-	0
rG12V (or rG12D) KRas cells	SLF'-TMP	2 µM	10

rG12V (or rG12D) KRas cells	SLF'-TMP	2 µM	20
rG12V (or rG12D) KRas cells	SLF'-TMP	2 µM	60
rG12V (or rG12D) KRas cells	*sample for in vitro loading of GDP	-	0
rG12V (or rG12D) KRas cells	*sample for in vitro loading of GTPγS	-	0
WT MDCK cells	EGF	100 ng/mL	5

The cells were cultured under standard conditions, and the experiment stopped at the mentioned incubation times by placing the culture dish on ice, then washing the sample(s) with cold PBS containing protease and phosphatase inhibitors. The samples were then immediately lysed and snap-frozen in liquid nitrogen until further processing, or immediately prepared for western blotting of whole cell lysates (WCL), or for 3xRafRBD pulldown for active Ras. See Cell lysis, Determination of Protein Concentration, SDS-PAGE and Western Blot, and 3x-RafRBD GST Pull Down.

5.2.1.4 Effect of plasma membrane translocation and reversal on rKRas-GTP levels

We also sought to investigate the effect of plasma membrane recruitment and de-recruitment on rKRas GTPase levels. For this, MDCK cells (1x WT MDCK, 4x each of rWT, rG12V, and rG12D KRas cells) were seeded in 6 cm Petri dishes at 6 x 10^5 cells per dish and cultured for 2 days in FGM under standard culture conditions. As above, cells were washed once with 2 mL of room temperature-PBS then serum-deprived for 2 h in 3.6 mL of serum deprived medium (0.1% FBS).

Fresh working solutions of DMSO (0.2% v/v), SLF'-TMP (20 µM), TMP (20 µM), and EGF (1 µg/mL) dissolved in serum-deprived medium were prepared and kept on ice until needed. Shortly before use, they were warmed up in a water bath. 400 µL of the working solutions of DMSO (final concentration 0.02% v/v), SLF'-TMP (final concentration 2 µM), TMP (final concentration 2 µM), were added to the cells in 3600 µL serum-starved medium for 60 minutes. For reversal, 400 µL SLF'-TMP (2 µM final concentration) was added and cells incubated for 30 minutes, followed immediately by the addition of 444 µL of TMP (final concentration 2 µL) for a further incubation period of 30 minutes. 400 µL of EGF (final concentration 100 ng/mL) were also added and cells were incubated for 5 minutes as a positive control.

Table 17. Effect of plasma membrane translocation and reversal on rKRas-GTP levels

Cell Line	**Ligand/chemical added**	**Final concentration in 4 mL serum-deprived medium**	**Incubation time of the experiment (minutes)**
rWT KRas cells	DMSO	0.02% v/v	60
rWT KRas cells	SLF'-TMP	2 µM	60
rWT KRas cells	TMP	2 µM	60
rWT KRas cells	Reversal (SLF'-TMP then TMP)	2 µM	30 (SLF'-TMP), then 30 (TMP)
rG12V KRas cells	DMSO	0.02% v/v	60
rG12V KRas cells	SLF'-TMP	2 µM	60
rG12V KRas cells	TMP	2 µM	60

rG12V KRas cells	Reversal (SLF'-TMP then TMP)	2 µM	30 (SLF'-TMP), then 30 (TMP)
rG12D KRas cells	DMSO	0.02% v/v	60
rG12D KRas cells	SLF'-TMP	2 µM	60
rG12D KRas cells	TMP	2 µM	60
rG12D KRas cells	Reversal (SLF'-TMP then TMP)	2 µM	30 (SLF'-TMP), then 30 (TMP)
WT MDCK	EGF	100 ng/mL	5

The cells were cultured under standard conditions. At the stopping time, the samples were immediately placed on ice, washed with cold PBS, lysed, and snap-frozen in liquid nitrogen until further processing, or immediately prepared for western blotting of whole cell lysates (WCL), or for 3x-RafRBD pulldown for active Ras. See Cell lysisDetermination of Protein Concentration, SDS-PAGE and Western Blot, and 3x-RafRBD GST Pull Down.

5.2.1.5 EGF Dose-response

To determine the effects of recruitable KRas on EGF sensitivity and signaling responses, 6 cm Petri dishes were seeded with 6.0 x 10^5 of wild-type MDCK or rKRas-MDCK cells and cultured for 2 days in FGM under standard culture conditions. All samples were then serum-deprived for 2 hours in 3.6 mL serum-deprived medium as above before. 400 µL of SLF'-TMP (final concentration 2 µM) or DMSO (final concentration 0.02% v/v) as before was added and the cells were incubated for 60 minutes. A serial dilution of EGF (final concentrations of 0, 0.5, 1.0, 2.0 5.0, 10, 20, 40, 80 and 160 ng/mL) in serum-free medium was prepared and used to stimulate the cells for 5 minutes under standard culture conditions. Two samples for each cell line used were also cultured and deprived of FBS, but neither was exposed to the dimerizer nor EGF. These were used as positive and negative controls for the 3x-RafRBD Pulldown assay as their lysates were in vitro loaded with GTPγS or GDP nucleotides. The experiment was stopped by placing the culture dishes on ice, then washing the samples with cold PBS containing protease and phosphatase inhibitors. The samples were immediately lysed and snap-frozen in liquid nitrogen until further processing or immediately prepared for western blotting of whole cell lysates (WCL), or for 3x-RafRBD pulldown for active Ras. See Cell lysisDetermination of Protein Concentration, SDS-PAGE and Western Blot, and 3x-RafRBD GST Pull Down.

5.2.1.6 Clonogenic Assays

Clonogenic assays were done to determine the effect of long-term (7 days) exposure to the dimerizer SLF'-TMP on proliferation.

5.2.1.6.1 Determination of the optimal seeding density for clonogenic assays

First, the optimal seeding density was determined by seeding wild-type MDCK cells at different seeding densities (100, 250, 500, 1000, and 2000 cells) per well in a 6-well plate. These were grown for 7 days in FGM under standard culture conditions, with a media change on day 4. Cells were then washed twice with PBS, fixed with 4% PFA(v/v) (Roti-Histofix) in PBS (Corning) for 20-30 minutes at room temperature, and washed once more with PBS. The cells were then stained with 0.05% crystal violet diluted in PBS (stock solution of 5% crystal violet in Ethanol). Three further washes with PBS were carried out to remove excess crystal violet before drying the 6-well plates upside-down overnight. The plates were then scanned using the Typhoon Imager, and the images were quantified and analyzed using Fiji (293). See Analysis of Clonogenic Assays.

Stock solution: 5% Crystal Violet dissolved in ethanol
Working solution: 0.05% crystal violet dissolved in 1X PBS (Corning).

5.2.1.6.2 Effects of long-term localization of recruitable KRas to the plasma membrane on proliferation

Once the optimal seeding density was determined, the procedure was repeated using WT MDCK cells and MDCK cell lines stably expressing rWT, rG12V, and rG12D KRas seeded at that density. Different culture media conditions were used; FGM, 0.02% v/v DMSO in FGM, and 2 µM SFL'-TMP. For reversal, cells were cultured in FGM containing 2 µM SLF'-TMP for the first 4 days, and when the media was changed, they were cultured in FGM containing 2 µM TMP for the remaining 3 days. The cells were cultured under standard conditions (humidified incubator at 37 °C, 5% CO_2) throughout. After 7 days, the dishes were then washed with PBS, cells fixed with 4% PFA, stained with 0.05% crystal violet, washed again, and dried as before.

5.2.1.6.3 Scanning Clonogenic Assays

A Typhoon Scanner (Amersham Biosciences Trio +) was used to scan stained 6-well dishes used for the clonogenic assays. The acquisition mode was set to fluorescence and the set-up used was as follows:

- 670 nm Band Pass 30 Cy5 filter
- PMT 500 Volts
- Excitation in the Red channel [633 nm]
- 1000 µm pixel size for the pre-scan used to check the saturation of the plates
- Final scan at 50 µm pixel size]
- Focal plane +3 mm.

5.2.2 Biochemistry

5.2.2.1 Cell lysis

To terminate an experiment, culture plates were immediately placed on ice and the medium aspirated. A wash was carried out with cold (4 °C) PBS containing protease and phosphatase inhibitors (DPBS without Ca^{2+}/Mg^{2+}, cOmplete ™, EDTA-free Protease Inhibitor Cocktail (1 tablet per 50 mL PBS), and 1% Phosphatase inhibitor cocktail 2+3). Cells were lysed on ice using GST-3x-RafRBD pulldown lysis buffer (120 µL per 6cm dish) and scraped off into pre-cooled 1.5 mL Eppendorf tubes. The samples were either snap-frozen in liquid nitrogen and stored or immediately processed. Lysates were vortexed for 2 seconds before centrifugation at 4 °C for 12 minutes at 14000 rpm using the 5417R Eppendorf Centrifuge with temperature function (Eppendorf). The supernatant was transferred to new pre-cooled 1.5 mL Eppendorf tubes and used for protein determination using the Micro BCA Protein Assay Kit, western blot of whole cell lysates (32-40 µL), and for 3x-RafRBD Pulldown assay (remaining supernatant). See Determination of Protein Concentration, SDS-PAGE and Western Blot3x-RafRBD GST Pull Down

5.2.2.2 3x-RafRBD GST Pull Down

The protocol for the 3x-Raf-RBD-GST Pull Down of active, GTP-bound Ras was adapted from the Ph.D. Thesis of Holger Vogel (292) from the lab of Prof. Dr. Philippe Bastiaens at MPI Dortmund.

5.2.2.2.1 Transformation and Cultivation of Chemically Competent *E. Coli* for Pulldown

Transformation of *Escherichia Coli (E. coli)* BL21-CodonPlus(DE3)-RIL was performed by mixing bacterial cells with DTT (78 mM final concentration) and 10 ng plasmid DNA coding for GST-3xRafRBD. Cells were incubated for 20 minutes on ice, heat-shocked for 45 seconds at 42 °C, and immediately placed on ice for an additional 2 minutes. SOC media (200 µL) was added to the mixture which was incubated for one hour at 37 °C under constant shaking. Transformed E. col BL21DE3 RIL containing the GST-3xRafRBD plasmid were plated on LB-Ampicillin plates and transformed cells selected for using 50 mL of TB (100 µg/mL Ampicillin).

5.2.2.2.2 Expression of GST-3x-RafRBD

Colonies of transformed *E. coli* bacteria were inoculated into 50 mL of TB (100 µg/mL Ampicillin) and incubated at 37 °C overnight under constant shaking (200 rpm). A preculture of 20 mL *E. coli* was added to 480 mL of TB-ampicillin and the OD_{600} (UV-1900 Spectrophotometer) was monitored hourly until a value of 0.8 was reached. Addition of 0.1mM IPTG induced protein expression after which the bacteria were cultured for a further 5 hours at 30 °C under constant rotation (200 rpm). Bacterial cells were harvested by centrifugation at 4300 rpm at 4°C for 30 minutes (Rotor F9-6x 100 LEX centrifuge Lynx 6000 or Sorvall Lynx 6000 Centrifuge; Thermo Fisher Scientific). The pellets were stored at -20 °C or lysed immediately.

5.2.2.2.3 Bacterial Lysis

Approximately 6 g of the bacterial pellet was mixed with 15 mL cold bacterial lysis buffer and run through a Microfluidizer (LM10 by Unitronics) at 10,000 PSI, for 6 cycles at 4 °C. After homogenization, the lysate was centrifuged at 17 600 g in high-speed falcon tubes using the rotor F13S-14x50 RC6+ centrifuge. The supernatant was transferred to a new pre-cooled falcon, the volume determined and glycerol added to make a final stock concentration of 20% glycerol in bacterial lysate supernatant. The mixture was snap-frozen in aliquots of 1000 µL and stored at -70 °C long-term.

5.2.2.2.4 GST-3x-RafRBD Purification

For 10 samples, 175 µL of GSH Sepharose 4B (GE) magnetic beads were used (Pierce ™ Glutathione Magnetic Agarose Beads (#78602), Thermo Fisher Scientific). Beads were washed twice with 1 mL bacterial lysis buffer before being mixed with a 1000µL aliquot of thawed bacterial lysate containing GST-3x-RafRBD, then incubated for 60 – 90 minutes at 4 °C under constant rotation. After incubation, the 3x-RafRBD-bound magnetic beads were washed 4 times with 1.5 mL pulldown wash buffer, then subsequently twice with 1.5 mL pulldown cell lysis buffer. The beads were then resuspended in 300 µL cell lysis buffer (containing 1% protease inhibitor cocktail 2+3) and divided into 30 µL aliquots in pre-cooled 1.5 mL tubes.

5.2.2.2.5 In vitro loading of nucleotide

During the purification step of the 3x-RafRBD on the magnetic beads, the positive and negative control samples for the pulldown were prepared. The total protein amount used for each sample was equal to that used for the experimental samples in the Active Ras Pull Down below (100 – 200 µg protein). For 500 µL lysate, 10 µL of 0.5 M EDTA (pH 8.0) was added for a final concentration of 10 mM and vortexed for 2 seconds. For the negative control, 5 µL of 100 mM GDP was added, whereas 5 µL of 10 mM GTPγS was added for the positive control. The samples were vortexed for 2 seconds and then incubated at 30 °C for 15 minutes under constant agitation (300 rpm). The loading reaction was stopped by placing the samples on ice and adding 32 µL of $MgCl_2$ for a final working concentration of 60 mM).

5.2.2.2.6 Active Ras Pull Down

For the pulldown, thawed cell lysate volumes of 200 µg of total protein for each sample (or up to a minimum of 100 µg if insufficient lysate) were added to pre-cooled 1.5 mL tubes containing 30 µL of purified 3x-RafRBD-bound magnetic beads in cell lysis buffer and incubated for 30 minutes under constant rotation at 4 °C. The protein concentration was equal for all samples used for each experimental replicate. This was also done for the negative and positive control samples already loaded with GDP or GTPγS. Each reaction tube was then washed 3 times with 500 µL cell lysis buffer and all remaining cell lysis buffer was aspirated. In preparation for SDS-PAGE and western blotting, 50 µL of 2X SDS sample buffer was added to each tube and boiled at 95 °C for 10 minutes. After cooling on ice, the samples were centrifuged for 10 seconds, and the supernatant was removed with the aid of the magnetic stand and stored in fresh pre-cooled 1.5 mL tubes at -20 °C ready for SDS-PAGE.

During the washing steps, the DynaMag 2 magnetic stand (Dynal Invitrogen bead separations, Invitrogen) was used to separate the magnetic beads from solution, thus eliminating the need to centrifuge. Aspiration of the lysates was done using the Vacusafe comfort pump and a 200 µL pipette tip.

5.2.2.3 Determination of Protein Concentration

Protein concentration was determined by performing a BCA (bicinchoninic acid) assay using the reagents and protocol of the Micro BCA Protein Assay Kit (Thermo Fisher Scientific). A serial dilution of aqueous BSA (Bovine Serum Albumin) was used as the standard. Concentrations of 5, 2, 1, 0.5, 0.25, and 0 µg/mL BSA dissolved in GST-3x-RafRBD pulldown lysis buffer were used. Four microliters of the BSA standard concentrations, as well as each lysed sample, were pipetted into a 96-well plate in duplicate. Following this, 80 µL of BCA reagent mixture was added to each well as per the BCA Protein Kit protocol and incubated at 37 °C for 30 – 60 minutes. The 96-well plate was read at 562 nm using the Multiscan Ascent plate reader (Thermo Electron Corporation), and the protein concentrations of the lysed cell samples were calculated in an Excel spreadsheet.

5.2.2.4 SDS-PAGE and Western Blot

SDS-PAGE gels of 15 mm thickness were cast containing a 15% acrylamide separating gel and a 5% acrylamide stacking gel with 15 well combs inserted before the gels polymerized.

For whole cell lysate analysis via western blotting, up to 40 µL of whole cell lysate supernatant were mixed with 8 µL or 10 µL of 5x SDS buffer respectively, then heat-treated at 95 °C for 5 minutes before cooling on ice. Samples from the 3x-Raf-RBD pulldown were also prepared accordingly See **Error! Reference source not found.**.

SDS-PAGE was carried out in the X-cell II Mini Electrophoresis apparatus, following the instruction manual, in SDS running buffer. For the whole cell lysates (WCL), 20 µg of proteins were loaded per well, whereas 20 µL of GST-3x-RafRBD pulldown lysates were loaded per well. Up to 4 µL of molecular weight standard was loaded in one well. The gels were run at constant voltage (80 V for 30 minutes, then 120V for 1 h 40 min).

Samples were transferred onto a PVDF (Immobilon-FL Polyvinylidene Fluoride) membrane at a constant voltage of 20 V for 70 minutes in a transfer buffer. After blocking for 1 h at room temperature with blocking solution (Odyssey blocking buffer), an overnight incubation at 4 °C with selected primary antibodies (dissolved in Odyssey blocking buffer) was carried out. Three washes of 5 minutes each with 1% TBS-Tween were done to remove excess antibodies prior to 1h incubation with selected IRDye 800 and IRDye 680 secondary antibodies diluted in Odyssey blocking buffer at room temperature, under constant rocking. Excess secondary antibody was removed by washing the blot 3 times for 15 minutes using 1% TBS-T. Following this, the PVDF membrane was scanned using the LI-COR Odyssey R CLx Imaging system, and the scanned images were quantified and analyzed using the Gel Analyzer plugin tool on Fiji (293). See Analysis of Western Blots - pulldowns and whole cell lysates.

5.2.3 Microscopy

5.2.3.1 Confocal Microscopy

Live cell images were obtained using a Leica TCS SP8 confocal microscope housed with an environmentally control chamber (Life Imaging Services, Switzerland) that was humidified, at 37 °C with a supply of 5% CO_2. A HC PL APO CS2 1.3 NA 63x oil objective set at 2x digital zoom (Leica Microsystems) was used. TagBFP (Tag Blue Fluorescent Protein) fluorophore was excited at 405 nm, and its emission was detected at 420 nm – 450 nm. Monomeric Teal Fluorescent Protein (mTFP) was excited at 470 nm and its emission was detected at 480 nm – 530 nm wavelength λ. A diode laser and a White Light Laser Kit (WLL2) were used to excite fluorophores at 405 nm and 470 nm wavelengths respectively, while emissions were restricted to the abovementioned wavelengths for detection using an acousto-optical beam splitter. Images of 16-bit depth at 512 x 512 pixels were obtained sequentially for the Tag-BFP and mTFP fluorescence, for the Validation of plasma membrane translocation and reversal of recruitable KRas by fluorescence microscopy. For Stability of plasma membrane localization of recruitable KRas over one week by fluorescence microscopy, images of Tag-BFP and mTFP fluorescence were obtained at 12-bit depth, 1024 x 1024 pixels. Captured images were analyzed to quantify changes in mTFP fluorescence at the plasma membrane using Fiji (293); See Analysis of Fluorescence Microscopy Images.

5.2.3.1.1 Validation of plasma membrane translocation and reversal of recruitable KRas by fluorescence microscopy

To validate the KRas CID system, stably transfected MDCK cells expressing WT, rG12V, and rG12D KRas proteins were used. Cells were seeded in black 24-well glass bottom plates at 1.0 x 10^5 or 5.0 x 10^4 cells per well and cultured in FGM under standard conditions for 1 or 2 days respectively. FGM was aspirated and the cells were gently washed with room temperature PBS at room temperature before adding 360 µL of fresh FGM.

Working dilutions of 20 µM SFL'-TMP and 20 µM TMP in FGM were made from stock solutions. A solution with DMSO of equal volume to that used for the 20 µM SLF'-TMP dissolved in FGM was also prepared. These were kept on ice and warmed up shortly before being used. Cells were selected via TagBFP and mTFP fluorescence and imaged (Confocal Microscopy) every minute for 5 minutes to obtain a baseline.

To validate plasma membrane translocation of recruitable KRas (rKRas), 40 µL of the working solutions of SLF'-TMP (final concentration 2 µM) or DMSO (negative control) were added to the 360 µL fresh FGM added to the cells. The cells were then imaged every minute for 60 minutes, at which point the experiment was ended.

For the reversal of translocation, 40 µL of the working solutions of SLF'-TMP (final concentration 2 µM) or DMSO (negative control) were added to the 360 µL fresh FGM added to the cells as before. The cells were then imaged every minute for 20 minutes, at which point 44.4 µL of the stock solution of TMP was added to the cells (final concentration 2 µM). the cells were then imaged for a further 30 minutes, at which point the experiment was ended.

5.2.3.1.2 Stability of plasma membrane localization of recruitable KRas over one week by fluorescence microscopy

To validate the long-term stability of plasma membrane localization of rKRas, stably-transfected MDCK cells expressing WT, rG12V and rG12D KRas proteins were used. Three culture medium conditions of cells were used; FGM as a control, 2 µM SLF'-TMP in FGM for plasma membrane translocation, and DMSO (with a volume equivalent to that used for the 2 µM SLF'-TMP condition) dissolved in FGM as an additional control were used.

The stably-transfected MDCK cells were seeded in 8-well Labtek chambers (chambers No. 1.0 Nunc by Thermo Fischer) at 100 cells per well and cultured with one of the 3 culture media for 7 days, under standard conditions (in a humidified incubator at 37 °C, 5% CO_2). A media change was carried out on day 4. Confocal microscopy images of the Tag-BFP and mTFP fluorescence for each condition were taken at days 2 and 7 after seeding.

5.2.4 Data Analysis

5.2.4.1 Analysis of Fluorescence Microscopy Images

Fiji software (ImageJ (294) distribution Fiji (293)) was used to concatenate the microscopy images to form time laps videos (tiff) for each set of cells per experiment containing both the mTFP (cytosolic G-domain) and the tagBFP (PM-localized tKRas) channels.

The concatenated images were imported into Python programming language (v3.7.4, Python Software Foundation) using the imageio.volread function from the Imageio package. A region of interest (ROI) where cells have similar fluorescence intensity was selected. Local thresholding (skimage packaged with the localtheshold function) in the tagBFP (tKRas) channel was used to create a binary mask of the PM. This mask was used to derive the corresponding pixels from the PM fluorescence in the mTFP channel. A final mask was made in the mTFP channel to include all cells in the ROI. To exclude spurious fluorescence outside the cell boundaries, the Binary_opening function from the scipy.ndimage package was used. At each time point (t), the mean integrated fluorescence intensity of the PM-localized mTFP and the total mTFP (cytosolic and PM-associated) was measured for the cells in the ROIs. The relative fluorescence at each time point was calculated using the following ratio:

Equation 1. Relative plasma membrane fluorescence

$$Relative\ PM\ Fluorescence\ at\ time\ (t) = \frac{PM\ mTFP}{PM\ mTFP + cytosolic\ mTFP}$$

Where PM mTFP = mean PM-associated mTFP fluorescence obtained using the tagBFP mask,
And cytosolic mTFP = mean mTFP fluorescence outside of the tagBFP mask, excluding extra-cellular spurious mTFP signals,
Thus total mTFP fluorescence for the cells in the ROI = PM mTFP + cytosolic mTFP.

To compare the trends in different experiments, the data for each experiment were normalized to the time t = 0 minutes. Data was visualized using the matplotlib Python package, and statistical analyses carried out on GraphPad Prism (versions 9 and 10.0.2 (232).

*These analyses were performed with the help of Dr. Luis Manuel Muñoz Nava, Department of Systemic Cell Biology, Max Planck Institute for Molecular Physiology, Dortmund.

Half-lives were calculated using the GraphPad Prism function for calculating half-lives for a one-phase association (translocation to the plasma membrane from the cytosol) or one-phase decay (translocation from the plasma membrane to the cytosol) by dividing the natural logarithm of 2 (ln(2)) by the rate constant, such that:

Equation 2. Half-life

$$Half - life\ \left(t\frac{1}{2}\right) = \frac{\ln(2)}{K}$$

Where K is the rate constant expressed as the reciprocal of time (minutes^{-1}).

5.2.4.2 Analysis of Western Blots - pulldowns and whole cell lysates

The Gel Analyzer functions from Fiji software ImageJ (294) distribution Fiji (293) was used to measure the fluorescence intensity of each western blot band which corresponded to antibody-tagged proteins of interest.

Briefly, a rectangle was drawn around the entire well lane to cover all tagged proteins. The same sized rectangle was used to mark all subsequent lanes which were then plotted to view signal profiles. Background subtraction was manually carried out by drawing a line using the line tool at the base of the area under the curve of the protein profiles to enclose the area, before using the magic wand tool to measure the integrated signal density, that is the area under the curve for each protein signal.

For the GST-3x-RafRBD pulldown of active GTP-bound Ras proteins, the value of GTP-bound Ras was normalized to the value of the GTP$\boldsymbol{\gamma}$S positive control for each experiment as follows:

Equation 3. Endogenous Ras-GTP (eRas-GTP)

$$Endogenous\ Ras-GTP = \frac{value\ of\ eRas-GTP}{value\ of\ eRas-GTP\gamma S\ for\ the\ experiment}$$

Equation 4. Recruitable KRas-GTP (rKRas-GTP)

$$Recruitable\ KRas-GTP = \frac{value\ of\ rKRas-GTP}{value\ of\ rKRas-GTP\gamma S\ for\ the\ experiment}$$

For total Ras Expression, values were normalized to the corresponding value for tubulin as follows:

Equation 5. Total endogenous pan-Ras (eRas)

$$Total\ Endogenous\ pan-Ras\ = \frac{value\ of\ total\ eRas}{value\ of\ Tubulin}$$

Equation 6. Total recruitable KRas (rKRas)

$$Total\ Recruitable\ KRas\ = \frac{value\ of\ total\ rKRas}{value\ of\ Tubulin}$$

The relative expression of rKRas to eRas was calculated as follows:

Equation 7. Total recruitable KRas relative to total endogenous pan-Ras (rKRas/eRas)

$$Total\ Recruitable\ KRas\ relative\ to\ total\ endogenous\ panRas = \frac{total\ rKRas}{total\ eRas}$$

Relative total phosphorylated ERK was normalized to Tubulin as shown:

Equation 8. Phosphorylated ERK relative to Tubulin (pERK/Tubulin)

$$phosphorylated\ Erk\ relative\ to\ Tubulin = \frac{(pErk1 + pErk2)}{Tublin}$$

Relative phosphorylated AKT was also normalized to Tubulin as shown:

Equation 9. Phosphorylated AKT relative to Tubulin (pAKT/Tubulin)

$$phosphorylated\ Akt\ relative\ to\ Tubulin = \frac{pAkt}{Tublin}$$

The calculated values for eRas-GTP/GTPγS, rKRas-GTP/GTPγS, pERK/Tubulin and pAKT/Tubulin were then normalized per experiment as follows:

a) Peak-normalization of values within the range 0 – 60 minutes for the EGF time-series experiments
b) Peak-normalization of values within the range 0 – 60 minutes for the rKRas plasma membrane recruitment experiments
c) Normalizing to the 3-point average at 80 ng/mL for calculated averages within the range 0.5 – 80 ng/mL EGF for the EGF dose-response experiments. These values were also converted to three-point moving averages before normalization, such that :

Equation 10. 3-point average values

$$3-point\ average\ value(x) = \frac{[value\ (x-1)] + [value(x)] + [value(x+1)]}{3}$$

It should be noted that for the Effect of plasma membrane translocation and reversal on rKRas-GTP levels, the Ras-GTP values were all normalized to the rKRas-GTP value of the DMSO condition for each rKRas cell line, instead of normalizing to GTPγS. Thus, the values were calculated as follows:

Equation 11. Recruitable KRas-GTP relative to recruitable KRas-GTP levels in the DMSO condition

$$Recruitable\ KRas-GTP = \frac{value\ of\ rKRas-GTP}{value\ of\ rKRas-GTP\ for\ the\ DMSO\ condition\ of\ the\ same\ cell\ line}$$

Additionally, a ratio of the amount of GTP-loading in rKRas G12V or rKRas G12D relative to the amount of GTP-loading in rKRas WT proteins was calculated as follows:

Equation 12. GTP-loading in rG12V KRas or rG12D KRas relative to rWT KRas

$$GTP-loading\ in\ rG12V\ KRas\ or\ rG12D\ KRas\ relative\ rWT\ KRas$$

$$= \frac{value\ of\ rKRas-GTP\ in\ rG12V\ or\ rG12D\ KRas\ cells}{corresponding\ value\ of\ rKRas-GTP\ in\ rWT\ KRas\ cells\ for\ each\ condition}$$

5.2.4.3 Analysis of Clonogenic Assays

Images scanned using the Typhoon scanner were analyzed using Fiji ImageJ (294) distribution Fiji (293).

Images were thresholded by intensity and background excluded to limit the counting areas to pixels corresponding to the area stained by cell colonies. From this a binary 8-bit mask was created and watershed areas were separated using the Watershed function in Fiji. The Analyze Particles command on Fiji was used to measure the area of the mask and obtain values for colony count and total occupied area relative to the area of the well. The area occupied per colony was calculated for each condition, and the results were graphically represented using GraphPad Prism.

5.2.4.3.1 Fiji Macro for Quantifying Clonogenic Assays once the ROI (circular border of 1 well from a 6-well plate) had been selected using the Oval/elliptical selection tool.

```
run("Duplicate...", " ");
setBackgroundColor(0, 0, 0);
run("Clear Outside");
run("Duplicate...", " ");
setAutoThreshold("Default");
//setThreshold(43, 255);
setOption("BlackBackground", false);
run("Convert to Mask");
run("8-bit");
run("Watershed");
run("Analyze Particles...", "  circularity=0.00-1.00 show=Outlines display exclude clear summarize");
```

Outcome measures from quantifying the clonogenic assay plates yielded values for total area, percentage occupied area, and the number of colonies counted. The area occupied per colony was then calculated as follows:

Equation 13. Area occupied per colony

$$Area\ occupied\ per\ colony = \frac{total\ area\ occupied}{number\ of\ colonies\ counted}$$

5.2.4.4 Statistical tests

Statistical tests were performed according to the type of data obtained and are specified in the figure legends for each figure, detailing the test, the number of independent samples (N) and the significance value (p). GraphPad Prism (versions 9 and 10.0.2 (232)) was used for these analyses.

Averages were expressed as either mean ± Standard deviation or mean ± Standard error of the mean.

Data were assessed for normality using a test for normality on GraphPad Prism. Unless strongly suggesting that data were normally distributed, a non-parametric statistical test was used to assess the data depending on the number of repeats and the number of types of variables for each experiment.

6 Results

Oncogene-induced senescence occurs when oncogenic Ras proteins are heterogeneously expressed with wild-type Ras isoforms (238), (241), (239), (240). The mechanism by which this happens involves constant MAPK signaling and is mediated by p53, p16 INK4a (238), (244), (246), (247). With studies suggesting different roles of oncogenic and wild-type Ras isoforms in tumor initiation and maintenance (257), (258),(250), more research is needed to further elucidate the complex interplay between Ras isoforms and their roles in cancer formation. Our research aimed to shed light on this relationship by spatially controlling the localization of KRas to the plasma membrane (PM), and assessing signaling responses.

6.1 A Chemically-Induced Dimerization system to control KRas localization

We employed an orthogonal, reversible, chemically induced dimerization (CID) adapted from Liu et al. (285) to control the plasma membrane localization of KRas-4B. Our efforts focused on the human KRas-4B splice variant, as KRas-4B is the most commonly mutated Ras isoform in cancer (66). Briefly, recombinant KRas-4B (henceforth referred to as KRas) was separated into the membrane-localizing polybasic tail end of KRas (tKRas) containing the hypervariable region (HVR), and the cytosolic catalytic G-domain of KRas without the HVR (KRas G-domain) (Figure 7).

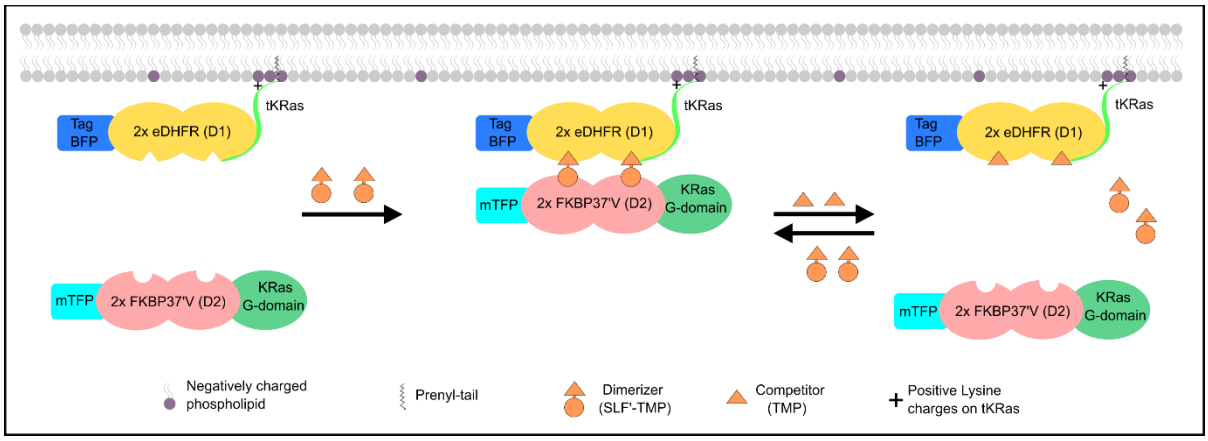

Figure 7. Schematic of the reversible recruitable KRas CID system.
Plasma membrane translocation of the recombinant recruitable KRas G-domain by the dimerization of the 2x-FKBP and 2x-eDHFR moieties using SLF'-TMP (synthetic ligand of FKBP-trimethoprim). Addition of TMP (trimethoprim) competitively binds to the 2x-eDHFR domains, displacing the SLF'-TMP dimerizer, thus displacing the KRas G-domain from the plasma membrane.

Blue fluorescent protein (tagBFP) and two moieties of eDHFR (*Escherichia Coli* Dihydrofolate Reductase) were linked to the tKRas moiety, while the G-domain was coupled with two moieties of FKBP37-V and monomeric teal fluorescent protein mTFP. This design allows for the controlled translocation of KRas G-domain to the plasma membrane-anchored tKRas by the addition of the bivalent dimerizer molecule, SLF'-TMP (Synthetic Ligand of FKBP – Trimethoprim), as SLF' and TMP are high-affinity ligands for FKBP and eDHFR respectively (Figure 7) (285). The KRas G-domain can subsequently be released from the plasma membrane by the addition of TMP as a competitor to the SLF'-TMP. This is schematically shown in (Figure 7). Thus, the cytosolic and plasma membrane localization of recruitable KRas can be chemically controlled. The recruitable KRas (rKRas) constructs

were then validated in these stably-transfected MDCK cell lines to verify their functionality by confocal fluorescent microscopy, and then by western blot analysis to confirm adequate expression.

6.2 Validation of recruitable KRas translocation by live-cell imaging

To assess the functionality of the construct in stably-transfected MDCK cells, cells were exposed to 2µM of SLF'-TMP for 60 minutes whilst observing mTFP (D2-G-domain) and TagBFP (D1-tKRas) fluorescence. Before exposure to SFL'-TMP, mTFP (mTFP-D2-KRas G-domain) was evenly distributed in the cytoplasm, while the tagBFP-D1-tKRas fluorescence was located at the plasma membrane. Upon the addition of 2µM SLF'-TMP, the accumulation of mTFP-tagged G-domain of KRas at the plasma membrane was evident, in contrast to no movement upon the addition of DMSO only (Figure 8 A-C). This was not observed when DMSO was added in all cells. A mask created from plasma membrane-associated Tag-BFP was used to detect and measure the changes in plasma membrane-associated mTFP fluorescence over time (See 5.2.4.1 Page 37). In this way, changes in PM-associated mTFP-D2-KRas G-domain for recruitable wild-type (rWT), recruitable G12V (rG12V) and recruitable G12D (rG12D) KRas expressing cells were quantified (Figure 8 D). On average, the PM-associated increase in mTFP fluorescence across the cells was 1.6 times higher than the baseline. Translocation was observed to be stable over 60 minutes, with PM-association half-lives (calculated as half-life t1/2 = ln(2)/K on GraphPad Prism) of 6.76 minutes, 2.42 minutes and 2.52 minutes calculated for rWT, rG12V, and rG12D KRas cells respectively (Figure 8 D).

Once plasma membrane translocation was successfully replicated, the reversibility of the CID system in MDCK cell lines was tested. After exposure to 2 µM SLF'-TMP and observation for 20 minutes, 2 µM TMP was added to the cells and the observation continued for another 30 minutes. (Figure 9). As before, the mTFP fluorescence was evenly distributed across the cells before the addition of the dimerizer. The addition of the SLF'-TMP dimerizer followed by TMP was associated with an increase followed by a decrease back to the baseline of plasma membrane-associated mTFP respectively in all cells expressing recruitable WT, G12V, and G12D KRas (Figure 9 A-C). The plasma membrane association half-lives, in this case, were 1.51 minutes, 4.56 minutes, and 4.82 minutes for the rWT, rG12V, and rG12D KRas cells respectively, whereas the respective plasma membrane dissociation half-lives were 5.86 min, 4.07 min, and 4.83 min (Figure 9D). Together, these data show that ectopic, stably-expressed recruitable KRas in MDCK cells translocates to the plasma membrane and back into the cytosol upon the addition of 2µM SLF-TMP and equimolar TMP respectively, with similar kinetics in all three variants tested.

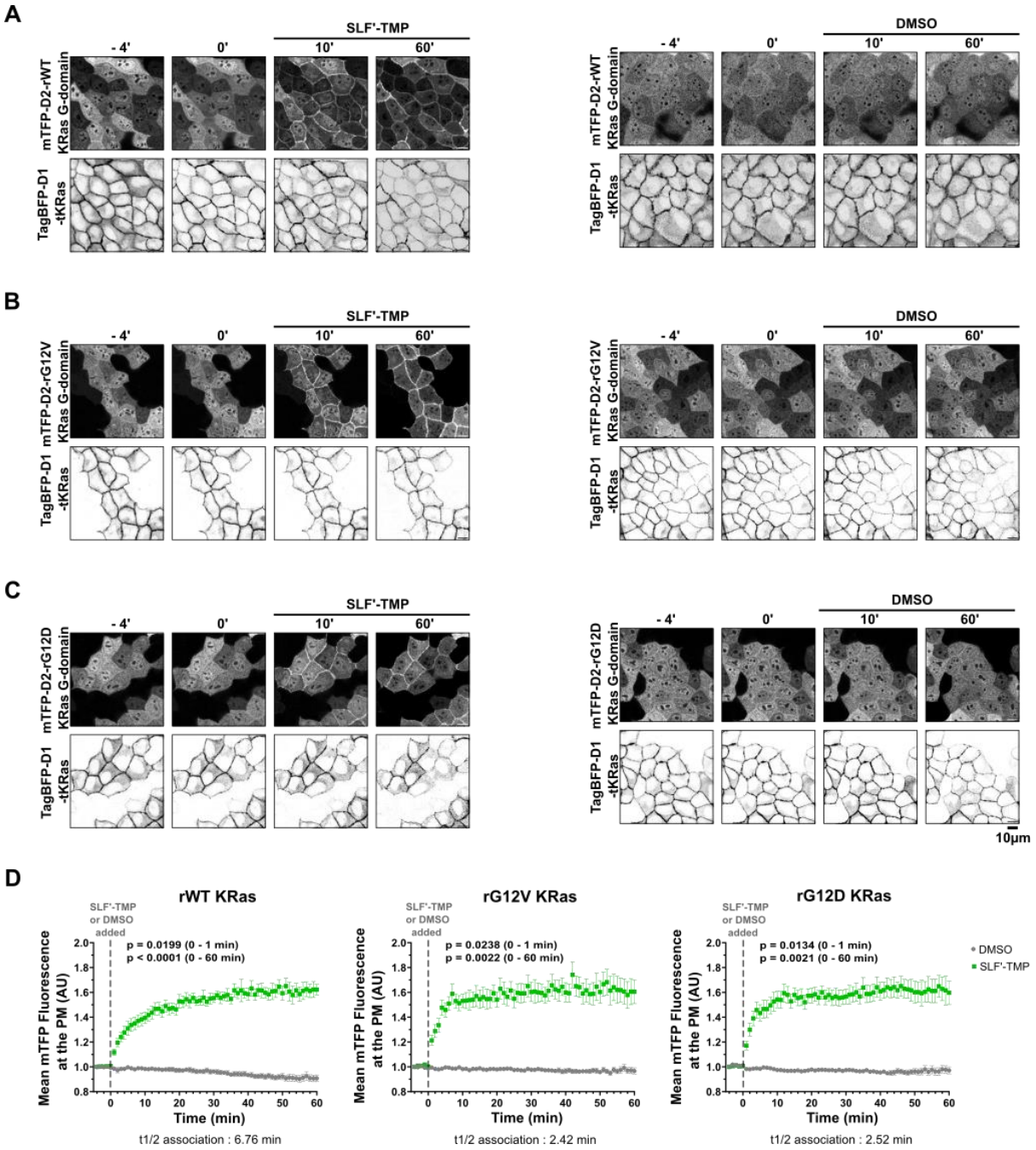

Figure 8. Plasma membrane translocation of recruitable KRas.
(A-C) Live-cell confocal fluorescence micrographs depicting a time series for non-serum deprived, stably-transfected MDCK cells expressing recruitable KRas before and after the addition of 2 µM SLF'-TMP. The upper panels show mTFP fluorescence of the KRas G-domain (mTFP-D2-X-KRas) whereas the lower panels show the Tag-BFP fluorescence (Tag-BFP-D1-tKRas) of tKRas in the cells. Scale bar: 10 µm. Images on the left show the effect of adding 2 µM SLF'-TMP dimerizer, while images on the right show the accompanying controls where only the DMSO driver was added to the cells.
(D) The quantification of the mean fluorescence of mTFP-tagged KRas G-domain at the plasma membrane (PM) at each time point, when 2 µM SLF'-TMP dimerizer (green) and the DMSO (grey) were added to the cells for 60 minutes. mTFP fluorescence at the PM was obtained from a mask of the PM associated Tag-BFP-D1-tKRas. The dashed line indicates the addition of the SLF'-TMP or DMSO at time 0 minutes. PM association half-lives are shown for each cell line below its respective graph. Values were expressed as mean ± SEM for N = 3 independent experimental repeats (n = 9 micrographs in total). Statistical significance was calculated using a Repeated Measures One-Way ANOVA with the Geisser-Greenhouse correction, and with Dunnett's test for multiple comparisons, with individual variances computed for each comparison.

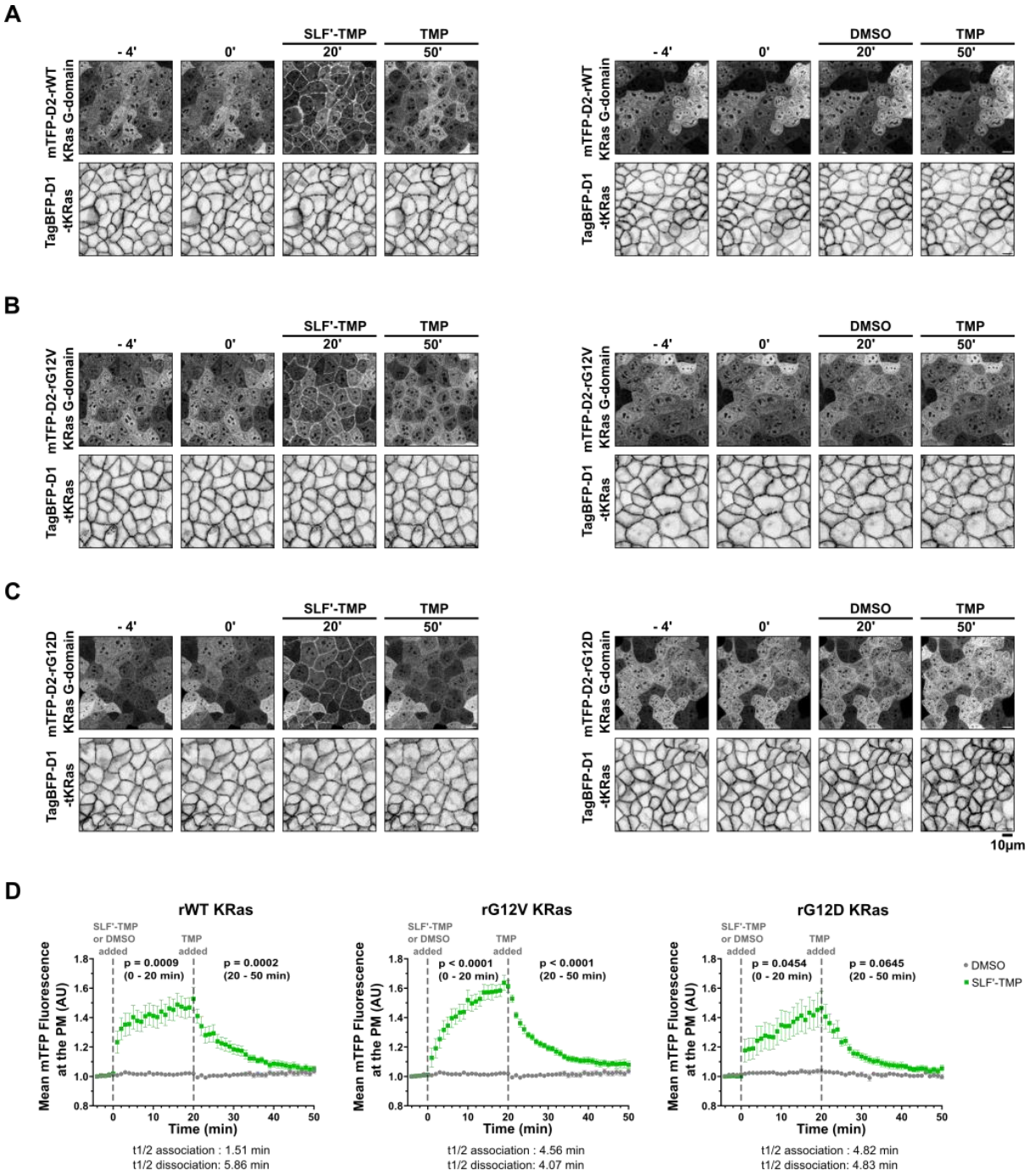

Figure 9. Plasma membrane translocation of recruitable KRas is reversible.
(A-C) Live-cell confocal fluorescence micrographs depicting a time series for non-serum deprived, stably-transfected MDCK cells expressing recruitable KRas before and upon exposure to 2 µM SLF'-TMP for 20 minutes, followed by exposure to 2µM TMP for 30 minutes. The upper panels show mTFP fluorescence of the KRas G-domain (mTFP-D2-X-KRas) whereas the lower panels show the Tag-BFP fluorescence (Tag-BFP-D1-tKRas) of tKRas in the cells. Scale bar: 10µm. Images on the left show the effect of adding 2 µM SLF'-TMP dimerizer followed by 2 µM TMP, and images on the right show the accompanying controls where only the DMSO driver was added to the cells followed by 2 µM TMP.
(D) The quantification of the mean fluorescence of mTFP-tagged KRas G-domain at the plasma membrane (PM) at each time point, when 2 µM SLF'-TMP dimerizer (green) and the DMSO (grey) were added to the cells for 20 minutes before reversal with 2 µM TMP. mTFP fluorescence at the PM was calculated as in (Figure 8). The first dashed line indicates the addition of the SLF'-TMP or DMSO at time 0 minutes and the second dashed line indicates the addition of 2 µM TMP at 20 minutes. PM association half-lives are shown for each cell line below its respective graph. Values were expressed as mean ± SEM for N = 3 independent experimental repeats (n = 9 micrographs in total). Statistical significance was calculated using a Repeated Measures One-Way ANOVA with the Geisser-Greenhouse correction, and with Dunnett's test for multiple comparisons, with individual variances computed for each comparison.

6.3 Stably-transfected recruitable KRas is overexpressed in MDCK cell lines

Once the functionality of the KRas CID system was shown via live-cell confocal fluorescence microscopy, a biochemical assay to assess the effects of rKRas PM translocation was tested. In an initial western blot, whole cell lysates of WT MDCK cells, and MDCK cells stably expressing rWT, rG12V, and rG12D KRas (Figure 10). Using a pan Ras antibody for all Ras proteins, both eRas and rKRas were detected and could be differentiated by their molecular weights of 21 and 72 kDa respectively. From this initial blot it was clear that rKRas was overexpressed in all MDCK cell lines stably expressing rKRas.

The double-band of Ras seen on western blots is due to post-translational modifications (43), (295), (296). The differences in molecular weights between the endogenous Ras isoforms (21 kDa) and the recruitable KRas (72 kDa) are due to the additional mass of mTFP (27 kDa) (297), and the two FKBP37V domains (12 kDa each) (298), (299)

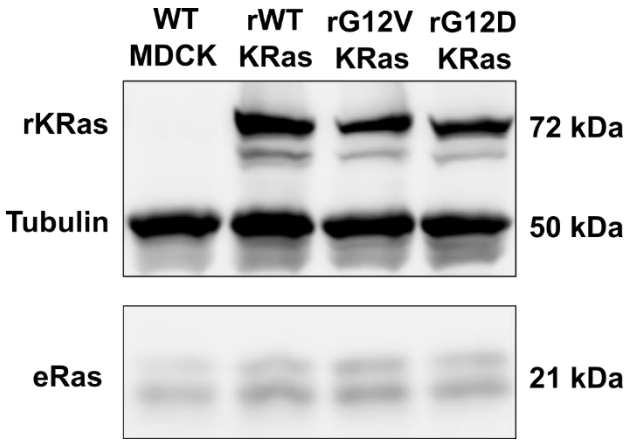

Figure 10. Recruitable Kras (rKRas) is expressed in stably-transfected MDCK cells.
The figure shows representative western blot bands from whole cell lysates of stable MDCK cells expressing rWT, rG12V and rG12D KRas proteins compared to WT MDCK cells. A pan-Ras antibody was used for staining all Ras isoforms, and Tubulin was the housekeeping protein stained (N = 1).

6.4 Characterization of the EGF temporal response of Wild-Type MDCK cells – Ras Signaling Responses

Given the importance of EGF-EGFR mediated activation of KRas signaling in cancer, the response of EGF stimulation in MDCK cells was tested. First, the aim was to characterize the signaling dynamics of wild-type (WT) MDCK cells to provide a knowledge basis and control for later comparison of the effects of PM translocation of rKRas on endogenous Ras and signaling. To characterize the EGF response in WT MDCK cells, the cells were stimulated with low (10 ng/ml) and saturating (160 ng/ml) doses of EGF (100) and incubated for increasing time durations of up to 60 minutes to resolve the Ras-GTP, pERK, and pAKT responses. A GST-3x-Raf-RBD pulldown for active Ras-GTP was performed on the cell lysates. These lysates, as well as whole cell lysates, were assessed by quantitative western blots analysis (Figure 11 and Figure 12).

At a high, saturating EGF concentration (160 ng/ml), a sharp rise in eRas-GTP was seen, peaking at 5 minutes post-stimulation, and sharply decreasing back to baseline within 30 minutes (Figure 11). This was similar to the eRas-GTP curve in the presence of low, 10 ng/ml EGF concentration. However, the

rise and fall in eRas-GTP in the 10 ng/ml EGF case was not as sharp as in the 160 ng/ml EGF, despite the average peak also being observed at 5 minutes post EFG stimulation (Figure 11 B).

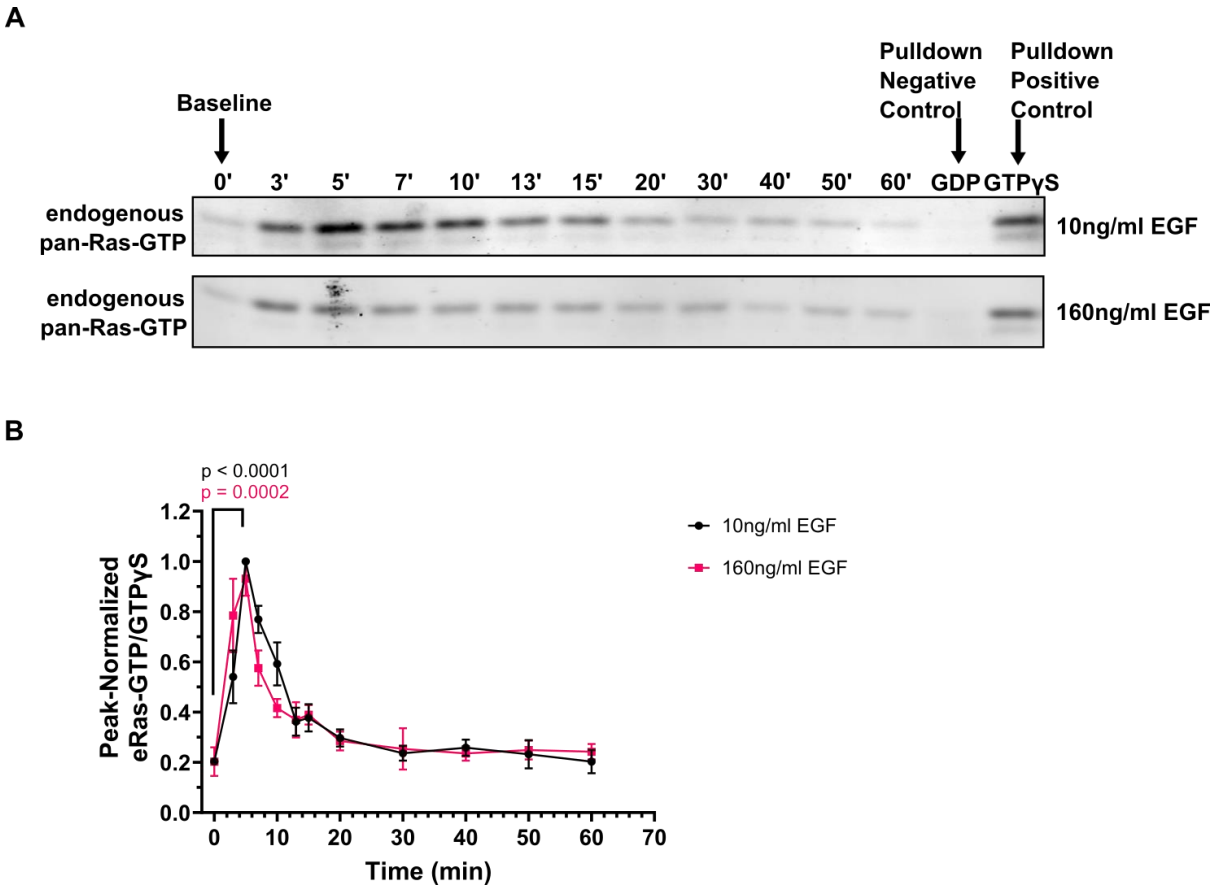

Figure 11. Active eRas-GTP signal in response to low and high EGF doses in time.
(A) Representative western blot following 3x-RafRBD-GST pulldown showing changes in active GTP-bound endogenous Ras (eRas-GTP) in time as a response to low (10 ng/ml) [top] and high (160 ng/ml) [bottom] EGF concentrations in WT MDCK cells. Samples stained with a pan Ras antibody.
(B) Graphical representation of the eRas-GTP signal in (A) for WT MDCK cells stimulated with 10 ng/ml EGF (black, N = 4) and 160 ng/ml EGF (red, N = 4) displayed as mean ± SEM. P-values calculated using an unpaired t-test with a Welch correction.

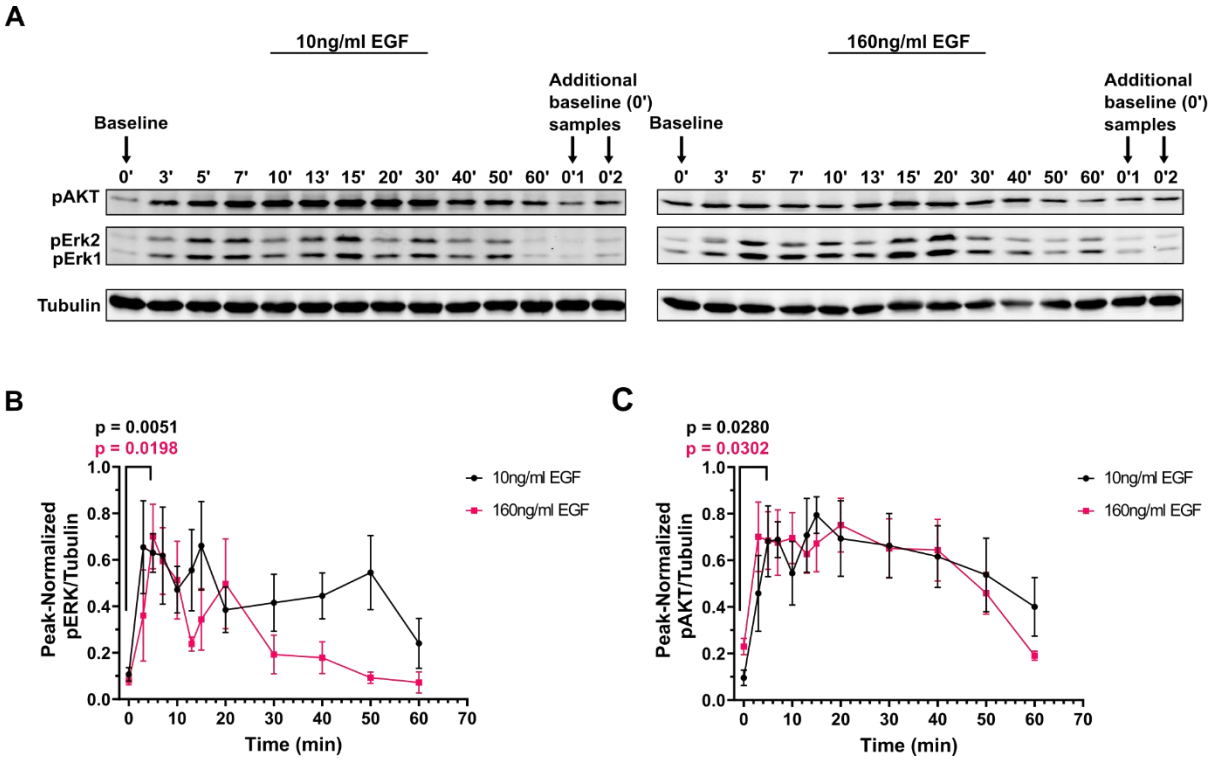

Figure 12. Responses in phosphorylation of ERK and AKT upon stimulation of WT MDCK with EGF.
(A) shows examples of western blots of the whole cell lysates of serum-deprived WT MDCK with 10 ng/ml (left) and 160 ng/ml (right) EGF. Samples were stained with pAKT, pERK and Tubulin antibodies.
(B) shows the changes in pERK with time upon stimulation of the cells with 10 ng/ml (black, N = 4)) and 160 ng/ml (red, N ≥ 3) EGF doses displayed as mean ± SEM. P-values calculated using an unpaired T-test with a Welch correction.

The average trends for phosphorylated ERK and AKT observed corresponded with the trend seen in eRas-GTP, in that they also peaked by 5 minutes after EGF addition (Figure 12 B and C). Interestingly, pERK responses showed a dampened oscillatory behavior upon EGF stimulation, most clearly in the saturating dose of 160 ng/ml (Figure 12 B). In the high EGF concentration case of 160 ng/ml, the first peak was observed at 5 minutes, with a second, smaller peak at 20 minutes and an overall decrease to baseline reached by 60 minutes after growth factor stimulation. The oscillations in the 10 ng/ml EGF case, however, appeared more sustained over 60 minutes with at least 3 peaks seen on average. The 10 ng/ml EGF pERK response also did not completely return to baseline levels within 1 hour.

The pAKT responses to EGF stimulation were similar in both low and high EGF concentrations (Figure 12 C). However, the amplitude of the peak was approximately 3.5 times higher than the baseline in the 160 ng/ml EGF case compared to an 8-fold increase in pAKT with 10 ng/ml EGF stimulation. Additionally, the pAKT levels returned to baseline at 60 minutes with 160 ng/ml EGF stimulation, whereas the more gradual decrease in pAKT in the 10 ng/ml EGF stimulation did not reach baseline levels by 60 minutes. Despite the differences, both pAKT peaks reached their maxima within 3-5 minutes on average and maintained this for up to 40 minutes before starting to decrease.

Collectively, these results show that the eRas-GTP, pERK, and pAKT response signals in WT MDCK cells reached an initial peak within 5 minutes of stimulation by both low and high EGF concentrations. While the eRas-GTP levels declined quickly to baseline after the peak, pERK showed oscillatory behavior that was dampened in the high EGF condition, and pAKT showed more sustained behavior before decreasing.

6.5 Changes in rKRas- and eRas-GTP levels upon plasma membrane translocation of rKRas

After characterizing EGF-mediated Ras and effector temporal signaling dynamics in WT MDCK cells, we investigated whether the translocation of rKRas to the plasma membrane affects endogenous Ras activity and subsequent downstream signaling. From western blot data of stably-transfected MDCK cells that were exposed to 2 µM SLF'-TMP for up to one hour, the changes in both active rKRas-GTP and eRas-GTP could be assessed after performing a GST-3x-RafRBD pulldown assay for active, GTP-bound Ras as before (Figure 13 A).

On average, the rWT KRas-GTP levels at baseline were comparable to the GDP-loaded samples (negative control for 3x-Raf-RBD pulldown) of the same cell line (Figure 13 B). Conversely, both rG12V and rG12D KRas-GTP each had a factor of 31.3 and 66.8 times higher GTP-binding respectively at time 0 minutes compared to the GDP-loaded samples (Figure 13 B). There were no statistically significant changes in the rKRas-GTP levels across the 3 cell lines from baseline over a period of 60 minutes after SLF'-TMP stimulation. However, there was a minimal decrease in the case of rG12D KRas-GTP (Figure 13 B).

Interestingly, in the case of eRas-GTP (Figure 13 C), the baseline samples at time 0 minutes had a GTP loading 2.18, 1.98, and 2.30 times higher than the average GDP-loaded samples for the rWT, rG12V, and rG12D KRas expressing cells respectively. In all three recruitable KRas cell lines, there was an increase in eRas-GTP that peaked at time 10 minutes and decreased back to baseline (or slightly lower than baseline in the rWT KRas case) by time 60 minutes after SLF'-TMP addition.

Comparing the trends between the rKRas variants, there were no significant differences in rKRas GTP-loading in time within all three cell lines (Figure 13 D). However, the average decrease in eRas-GTP after the peak at 10 minutes post PM translocation of rKRas was slower in the oncogenic rG12V and rG12D KRas expressing cells compared to the rWT KRas cells (Figure 13).

In summary, SLF'-TMP addition to translocate rKRas to the plasma membrane over a duration of 60 minutes was associated with no overall change in rKRas-GTP levels. However, a transient peak in eRas-GTP levels was observed, with a peak at 10 minutes that decreased to baseline at a slower rate in the rG12V and rG12D KRas cells than in the rWT KRas cells.

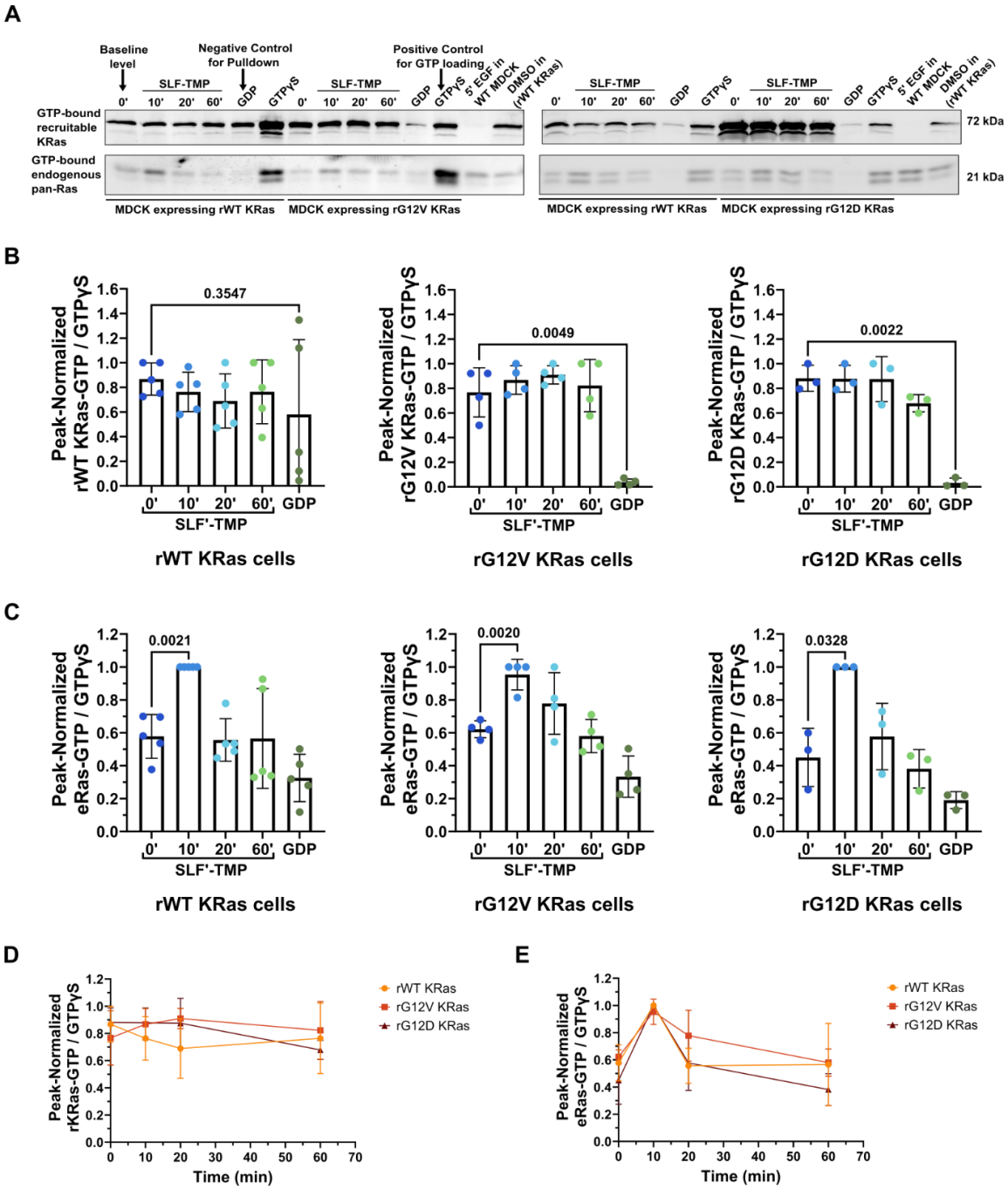

Figure 13. Changes in Ras-GTP levels upon plasma membrane translocation of recruitable KRas.
(A) representative western blots showing temporal changes in active GTP-Ras levels from 3x-RafRBD pulldown assays comparing levels in MDCK cells stably expressing rWT KRas and recruitable oncogenic (rG12V on the left, and rG12D on the right) KRas upon plasma membrane translocation of the recruitable KRas construct with 2 μmM SLF'-TMP up to 60 minutes. The upper panels show the recruitable KRas-GTP (rKRas-GTP), whereas the lower panels show the endogenous Ras-GTP (eRas-GTP), all stained with pan Ras antibody. Also shown are the GDP-loaded and GTPγS-loaded controls for each stable cell line for the pulldown, as well as a positive control of WT MDCK cells stimulated with 100 ng/ml EGF for 5 minutes, and a negative control of rWT KRas MDCK cells exposed to the same volume (as the dimerizer) of DMSO for 10 minutes.
(B) shows the quantified temporal changes in rKRas-GTP levels in comparison to the GDP-loaded controls for MDCK cells stably expressing rWT KRas (left), rG12V KRas (middle) and rG12D KRas (right).
(C) shows the quantified temporal changes in endogenous eRas-GTP up to 60 minutes, in comparison to GPD-loaded samples for MDCK cells stably expressing rWT (left), rG12V (middle) and rG12D (right) KRas.
(D) shows the comparison of the relative, peak-normalized levels of GTP-bound Ras with time amongst the MDCK cells expressing rWT (orange), rG12V (red) and rG12D (brown) KRas, showing the trends in rKRas-GTP (left) and eRas-GTP (right N = 5, N = 4, and N = 3 experiments for rWT, rG12V and rG12D KRas expressing cells. Values represented as Mean ± SD. Statistical significance calculated using the unpaired T test with a Welch correction. Statistical significance calculated using the unpaired T test with a Welch correction.

6.6 ERK and AKT responses upon plasma membrane translocation of recruitable KRas

Following the observed PM translocation of rKRas and the associated increase in eRas-GTP levels, the whole cell lysates from the same cells were used to evaluate downstream effector signaling. Whole cell lysates were used to quantify phosphorylated ERK and AKT (Figure 14), as well as total Ras expression via western blot (Figure 15).

In all cell lines, the pulse in eRas-GTP activity upon PM translocation of rKRas was associated with an adaptive response in both pERK and pAKT under serum-deprived conditions (Figure 14). A peak in pERK levels occurred 10 minutes after the addition of SLF'-TMP and returned to an average level just above baseline across all three cell lines (Figure 14 B and D). Relative to the mean baseline level, there was a 6.46, 20.8, and 7.38 fold increase in pERK levels in the rWT, rG12V, and rG12D KRas-expressing cells respectively. Despite the differences in magnitude, the average pERK trend was consistent across all 3 cell lines (Figure 14 D).

The peak in pAKT abundance (Figure 14 C) was on average observed to occur at 20 minutes post-addition of the dimerizer in rWT KRas cells, but occurred at 10 minutes post-addition of the dimerizer in the rG12V and rG12D KRas variant cells. However, the average pAKT levels at 10 minutes in the rWT KRas cells were close to the levels at 20 minutes. The mean decrease in pAKT after the peak was starker in the rWT KRas cells compared to the oncogenic KRas cells. There was a higher, more sustained pAKT level 60 minutes after SLF'-TMP addition in the oncogenic rKRas-expressing cells, especially in the rG12V KRas cells (Figure 14 D).

When looking at total Ras expression, the expression of rKRas relative to eRas was most homogeneous in the rG12V KRas-expressing cells and was also the lowest of the three cell lines (Figure 15). Furthermore, the rG12D KRas expression relative to eRas expression was the highest for this experimental cell line.

These results show that plasma membrane translocation of overexpressed rWT, rG12V, and rG12D KRas was associated with a peak in endogenous Ras-GTP and transient signals of pERK and pAKT that peaked at 10 minutes after initiation of PM translocation. All responses were adaptive, that is, they decreased towards baseline within a time duration of 60 minutes. This occurred regardless of differences in the expression of rKRas relative to eRas.

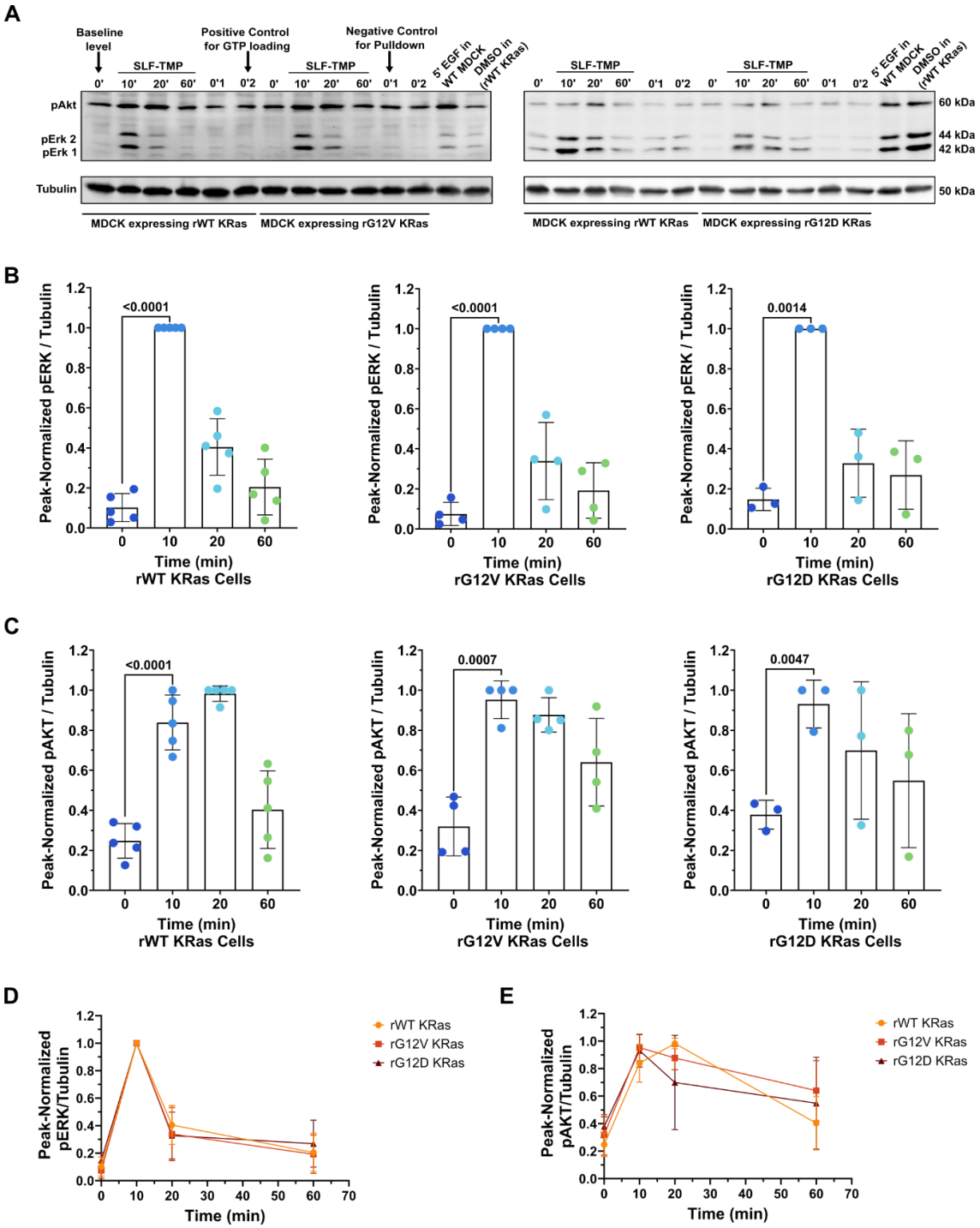

Figure 14. Changes in phosphorylated ERK and AKT in time upon plasma membrane translocation of recruitable KRas.
(A) Representative western blots showing changes in active pERK and pAKT levels comparing samples from MDCK cells stably expressing rWT KRas and recruitable oncogenic (rG12V on the left, and rG12D on the right) KRas with time upon plasma membrane translocation of the recruitable KRas construct with 2 μM SLF'-TMP up to 60 minutes. The upper panels show pAKT and pEkr levels, whereas the lower panels show the total alpha Tubulin levels. Also shown are the GDP-loaded and GTPγS-loaded control samples for the pulldown, which in this case are additional point for time 0 minutes, as well as a positive control of WT MDCK cells stimulated with 100 ng/ml EGF for 5 minutes, and a negative control of rWT KRas MDCK cells exposed to the same volume of DMSO for 10 minutes.
The quantified changes in pERK (B) and pAKT (C) with time in rWT (left), rG12V (middle) and rG12D (right) KRas expressing cells.
(D) shows the comparison of the trends in pERK (left) and pAKT (right) with time amongst the MDCK cells expressing rWT (orange), rG12V (red) and rG12D (brown) KRas. N = 5, N = 4, and N = 3 experiments for rWT, rG12V and rG12D KRas expressing cells. Values represented as Mean ± SD. Statistical significance calculated using the unpaired T test with a Welch correction.

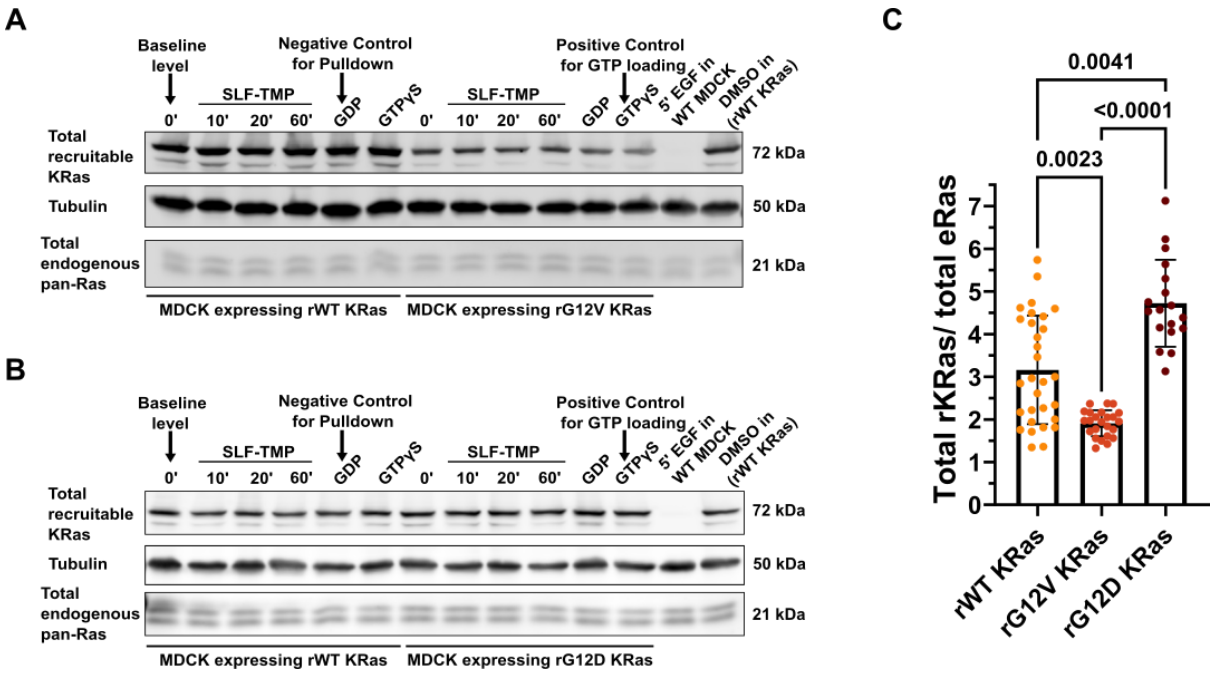

Figure 15. Total rKRas expression relative to total eRas expression.
Representative western blots of whole cell lysates showing total rKRas, Tubulin, and total eRas expression for PM recruitment experiments involving rG12V KRas (A) and rG12D KRas (B).
(C) shows the total rKRas/total eRas expression ratio for the whole cell lysates of stable MDCK cell lines expressing rWT, rG12V and rG12D KRas. N = 5 (n = 30), N = 4 (n = 24), and N = 3 (n = 18) experiments for rWT, rG12V and rG12D KRas-expressing cells. Values were expressed as Mean ± SD. Kruskal-Wallis test (nonparametric one-way ANOVA) with Dunn's test for multiple comparisons was used for statistics.

6.7 The effect of plasma membrane translocation on recruitable KRas GTP-loading

Upon confirming the overexpression of rKRas in stably-transfected MDCK cell lines, we quantified this further and assessed the GTP-loading of the rKRas proteins. This was achieved by performing a reversal experiment which also allowed us to investigate whether rKRas-GTP levels are influenced by plasma membrane localization. Stably-transfected MDCK cells were serum-deprived, following which plasma membrane translocation of rKRas was performed. Reversal of plasma membrane translocation of rKRas was also carried out. Exposure to 2 µM SLF'-TMP for PM translocation or 0.02% v/v DMSO as a control was carried out for one hour, while recruitment with 2 µM SLF'-TMP for 30 minutes followed by equimolar TMP for a further 30 minutes was carried out for the reversal. Western blots of whole cell lysates were used to assess total endogenous Ras (eRas) and total rKRas expression (Figure 16). Additionally, in the same samples, GTP-bound Ras levels were assessed by western blots after GST-3x-Raf-RBD pulldown assay for active, GTP-bound Ras (Figure 17).

Quantification of western blots for whole cell lysates (Figure 16 A) revealed that the expression levels of eRas isoforms were consistent across all cell lines for each of the independent (color-coded) experiments (Figure 16 B). Mean eRas/Tubulin expression was the lowest at 0.17 in rG12D KRas cells and highest at 0.27 in the rG12V KRas cells. This was similar to the average value of 0.19 for eRas/Tubulin expressed in Wild-type (WT) MDCK cells (Figure 16 B). Recruitable KRas expression however was varied when comparing the different rKRas variants (Figure 16 C). The mean rKRas/Tubulin values were 0.5121, 0.3962, and 0.7558 for the rWT, rG12V, and rG12D KRas cells respectively (Figure 16 C). Therefore, it follows that the mean expression levels of the rKRas relative to the eRas (rKRas/eRas) of 4.76, 2.68, and 4.35 for the rWT, rG12V, and rG12D KRas cells respectively

were quantified (Figure 16 D). Collectively, the average expression of rKRas was higher than the expression of eRas in all stable cell lines, with Total rKRas / Total eRas in rG12V KRas expression about 50% lower than rWT KRas- and rG12D KRas-expressing cells.

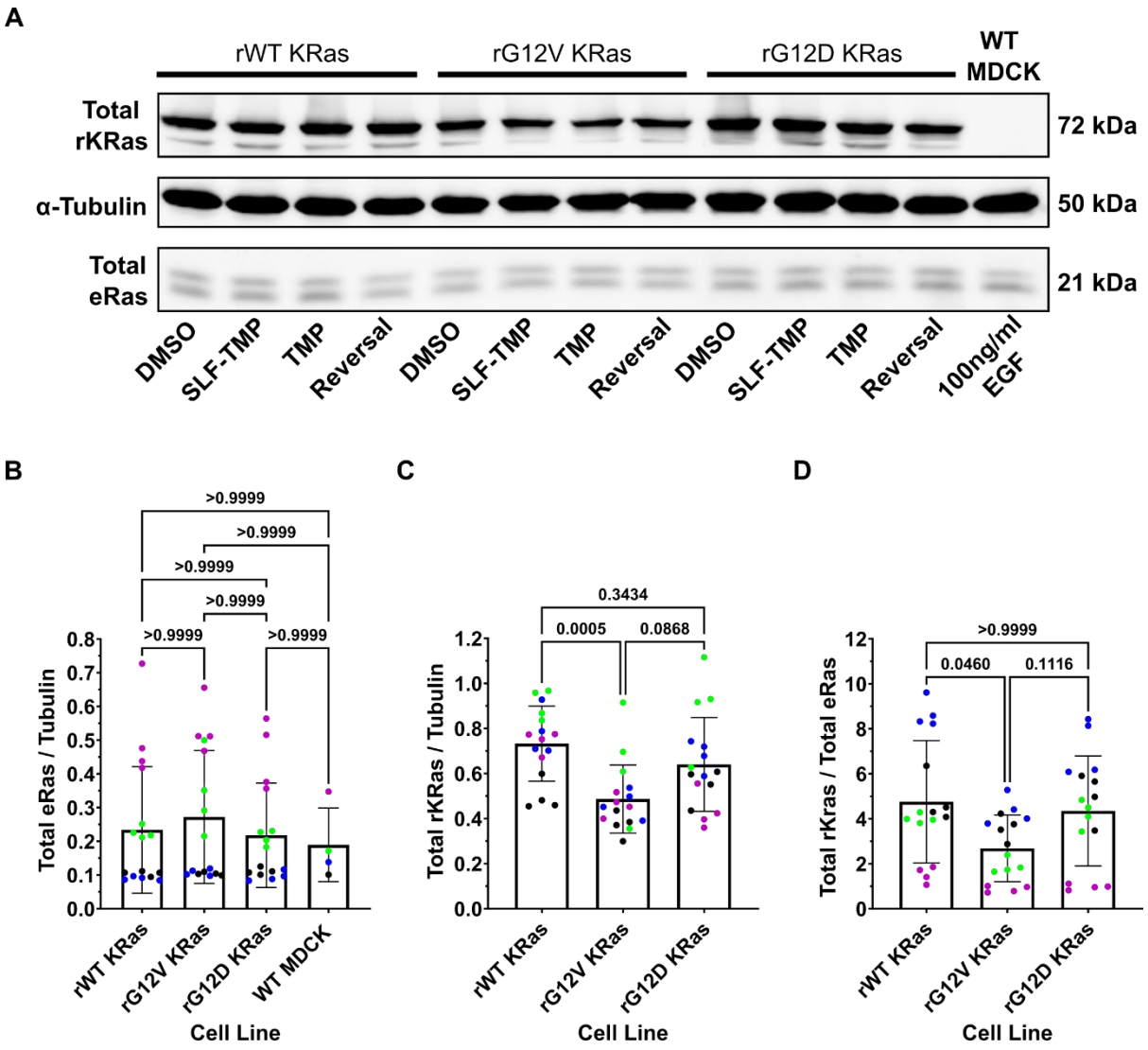

Figure 16. Endogenous Ras (eRas) and recruitable Kras (rKRas) expression levels in MDCK cells stably expressing recruitable WT, G12V, and G12D KRas.
(A) shows representative western blot bands from whole cell lysates of MDCK cells stably expressing rWT, rG12V, and rG12D KRas constructs compared to WT MDCK cells. Tubulin was used as a loading control.
The total eRas (B) and total rKRas (C) expression relative to Tubulin, as well the ratio of total rKRas to total eRas expression (D) are displayed. N = 4 (n ≥ 14). Data expressed as mean ± SD, with significance calculated using the Kruskal-Wallis test (non-matched, non-parametric analysis) with Dunn's multiple comparison test.

Following this, we assessed the activity state of the recruitable KRas proteins. A 3x-Raf-RBD pulldown for active GTP-bound Ras was performed on cell lysates from the same reversal experiments and assessed by quantitative western blotting (Figure 17 A). Translocation of rWT KRas to the PM and reversal, that is translocation back into the cytosol, had no significant changes in the amount of GTP bound to the rWT KRas (Figure 17 B). However, in the case of the oncogenic rKRas variants, rG12V and rG12D, PM recruitment of the rKRas by SLF'-TMP was associated with a significant (p = 0.0286) albeit

marginal decrease in rKRas-GTP to 0.7417 and 0.7608 of the DMSO levels respectively (Figure 17 C and D). This decrease in bound GTP was recovered in the Reversal condition wherein after TMP addition, rKRas-GTP was increased to DMSO control levels in the rG12V and rG12D KRas cells (Figure 17 C and D). This was only statistically significant in the rG12D KRas cells. TMP addition alone without prior PM translocation with SLF'-TMP showed no significant effect on GTP binding of rKRas in all cell lines, although there was a minimal increase in the rWT KRas-GTP in comparison to the DMSO control condition (Figure 17B-D).

Comparing the GTP-loading of rKRas, it was evident that the oncogenic rG12V and rG12D KRas were bound to higher amounts of GTP compared to the rWT KRas (Figure 17 E). Interestingly, even with about 50% lower expression of rG12V KRas compared to rWT and rG12D KRas, the GTP-loading of rG12V KRas was similar to that of rG12D KRas, and both were on average 4 times higher than in the rWT KRas (Figure 17 E).

Overall, these data show that all rKRas constructs are highly expressed within the stably-transfected MDCK cell lines and that the oncogenic variants bind more GTP than the wild-type rKras variant. Additionally, translocation of rG12V and rG12D KRas to the PM was associated with a slight decrease in GTP binding, which was restored upon reversal of translocation from the PM using TMP. GTP-binding in rWT KRas on the other hand remained largely unaffected by PM translocation and reversal.

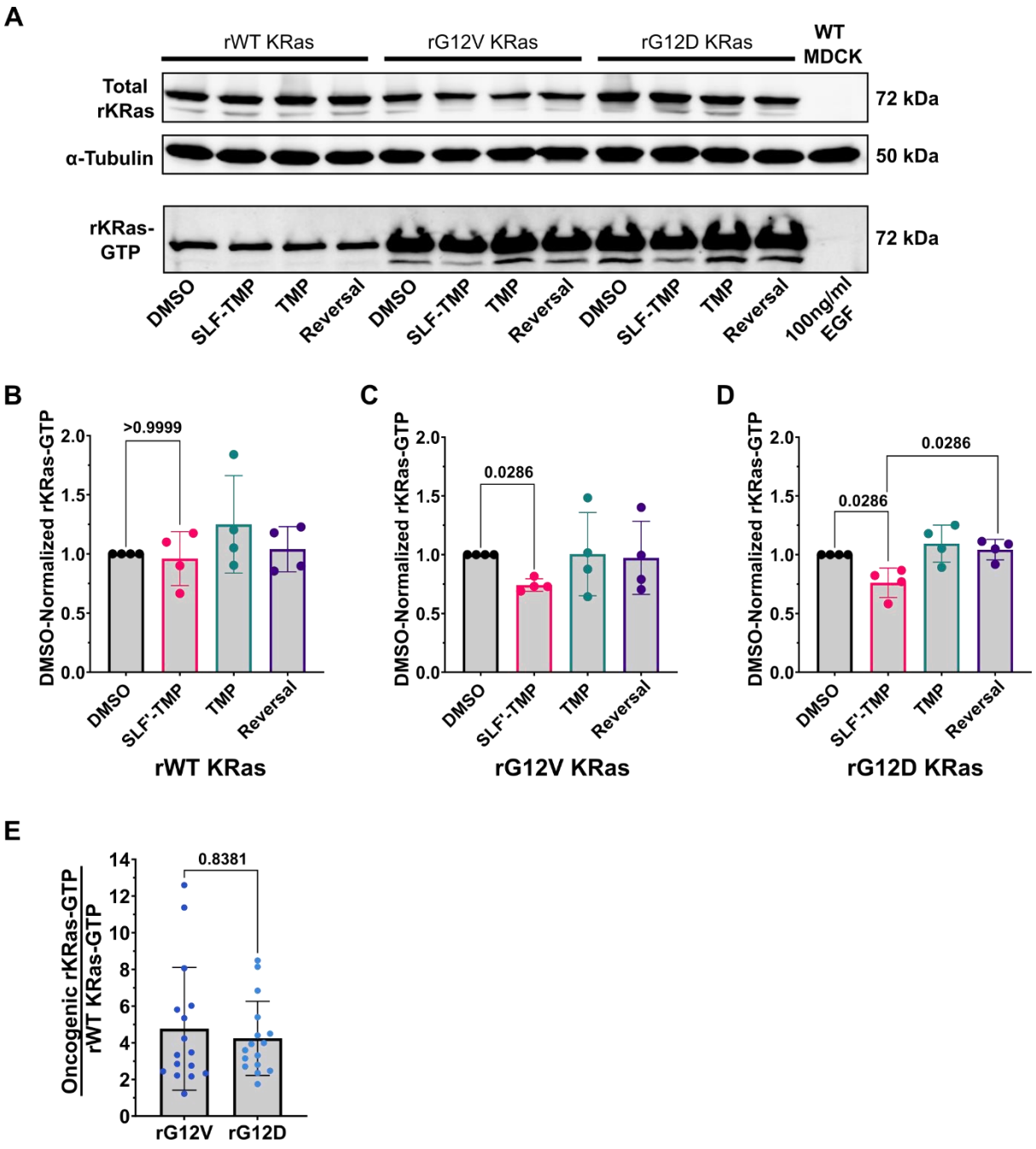

Figure 17. Changes in rKRas-GTP upon plasma membrane recruitment with SLF'-TMP and reversal with TMP.
(A) Representative western blot bands showing rKRas and Tubulin expression from whole cell lysates in the upper and middle bands. The lower band shows the rKRas-GTP levels after 3x-Raf-RBD pulldown of active GTP-bound Ras stained with panRas antibody.
(B-D) shows the changes in rKRas-GTP in rWT (B), rG12V (C) and rG12D (D) KRas cells upon recruitment with 2 μM SLF'-TMP, 2 μM TMP alone, or Reversal (initial recruitment with 2 μM SLF'-TMP then de-recruitment with 2 μM TMP) normalized to the DMSO control.
(E) shows the rG12V and rG12D KRas normalized to rWT KRas-GTP. N = 4, mean ± SD, and significance calculated using the unpaired, nonparametric Mann-Whitney U test.

6.8 Effects of long-term localization of rKRas to the plasma membrane on proliferation

Until this point, the effects of plasma membrane translocation of rKRas were assessed on short time scales of up to an hour. We next investigated the effect of plasma membrane localization of recruitable KRas on proliferation over one week using clonogenic assays. The stability of plasma membrane translocation of rKRas over 7 days was validated by confocal microscopy (Figure 18). Images were captured on days 2 and 7 after seeding the stably-transfected MDCK cells and growing them in full growth medium (FGM), FGM containing 2 µM SLF'-TMP dimerizer, or FGM containing an equivalent volume of DMSO (0.02% v/v). Plasma membrane translocation of rKRas was stable at 2 and 7 days of incubation with FGM containing dimerizer as the plasma membrane localization was visible with mTFP fluorescence at these time points when compared to the FGM and the DMSO conditions (Figure 18).

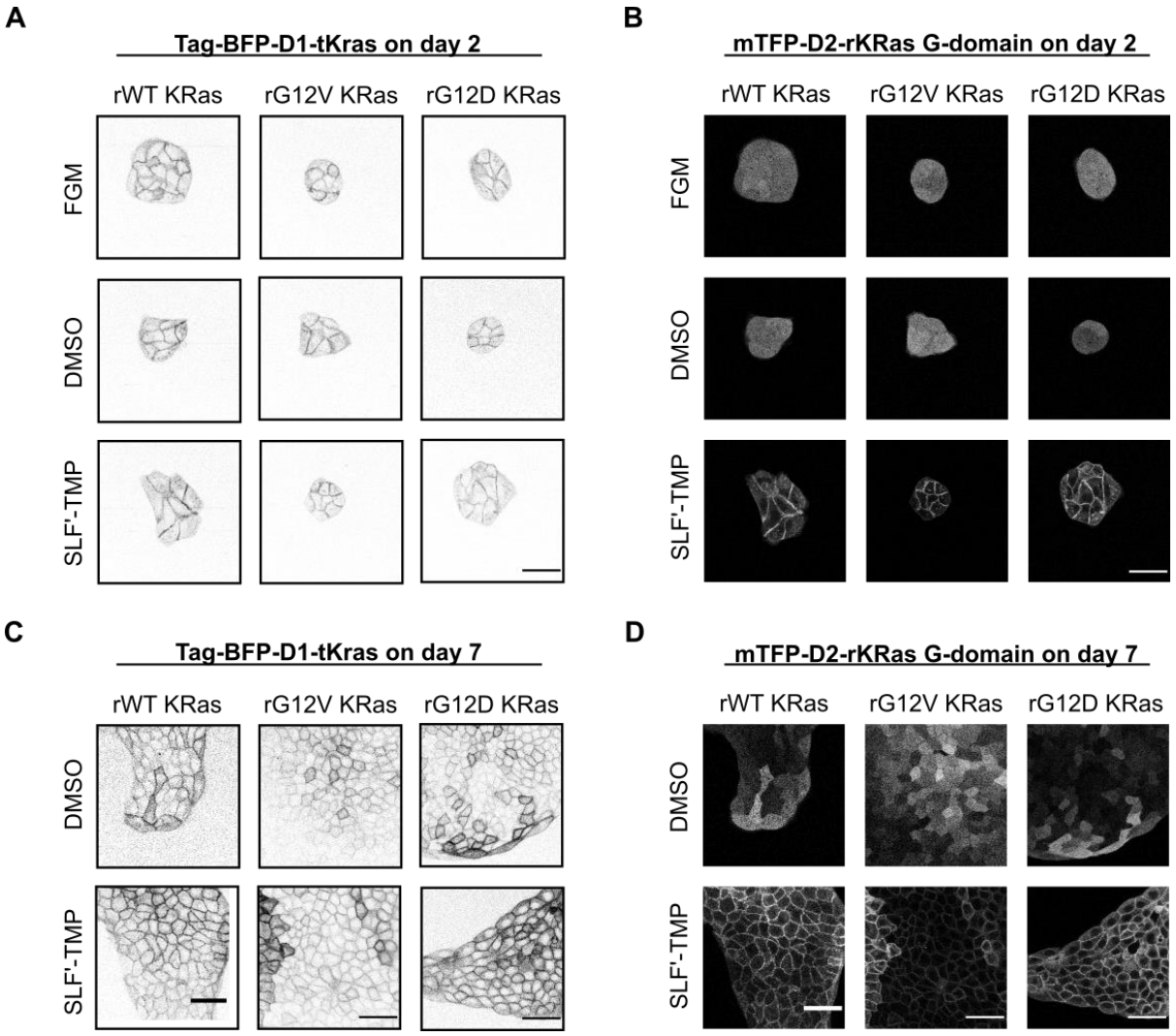

Figure 18. Stability of plasma membrane recruitment over 7 days.
Confocal microscopy images showing the tag-BFP-tKRas (A) and mTFP-G-domain (B) of stably-transfected MDCK cells grown in full growth medium (FGM), 0.02% v/v DMSO and 2 µM SLF'-TMP at day 2 after seeding 100 cells.
Confocal microscopy images of the tag-BFP-tKRas (C) and mTFP-G-domain (D) of stably-transfected MDCK cells grown in full growth medium DMSO and 2 µM SLF'-TMP at day 7 after seeding 100 cells. Scale bar: 50µm.

Upon successfully culturing the stably-transfected MDCK cell lines with constant exposure to DMSO and SLF'-TMP for a week, we determined to carry out clonogenic assays for the same time period.

Initially, WT MDCK cells were seeded at increasing densities of 100, 200, 500, and 1000 cells per well of a 6-well plate to determine the optimum seeding density for a clonogenic assay experiment (Figure 19 A). As the proliferation potential of the stably-transfected cell lines was unknown, it was decided that the lowest seeding density of 100 cells would be optimal after 7 days, since the 500 and 1000 cells/well density could yield high confluency that could increase the difficulty of distinguishing individual colonies. There was higher variation in the 200 cells/well density, and no statistical difference between the 100 cells/well seeding density (Figure 19 B) as colonies could easily be delineated at the end of the assay.

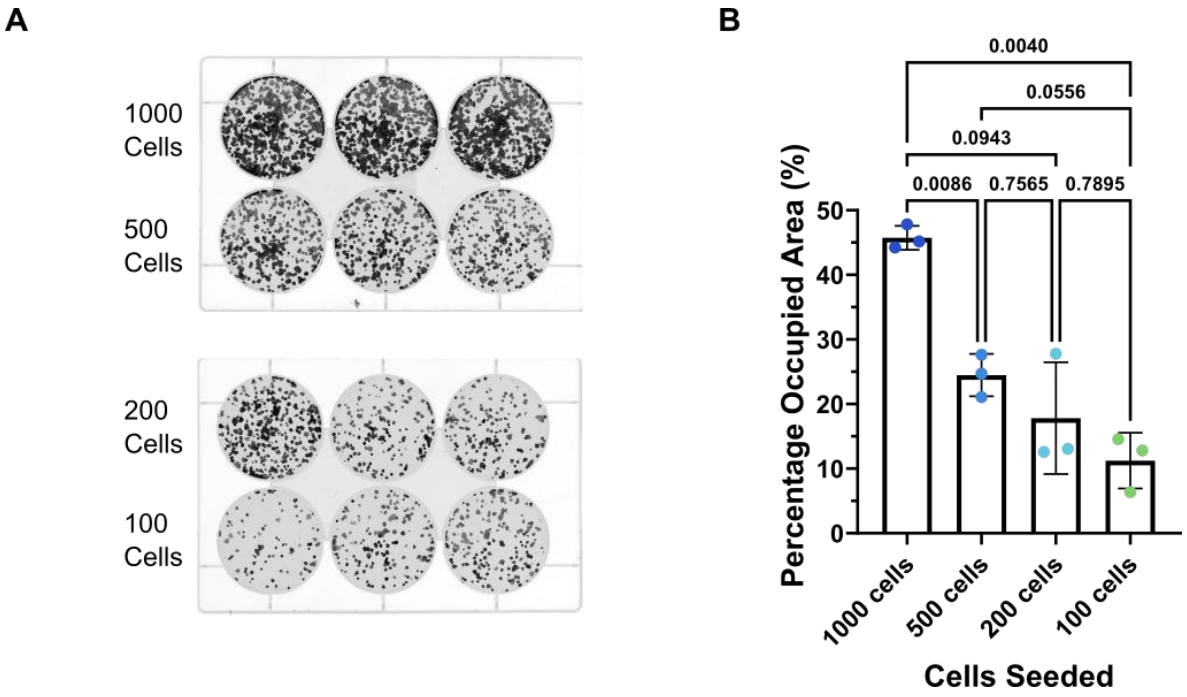

Figure 19. Determination of the seeding density for clonogenic assays.
(A) Representative image of the final growth after culture in full growth media for 7 days of WT MDCK cells seeded at 100, 200, 500 and 1000 cells per well of a 6-well plate.
(B) Quantified percentage of the occupied area of the well for each seeding density of WT MDCK cells (from A) after 7 days of growth. Statistics were calculated using the Brown-Forsythe and Welch ANOVA test with Dunnett's T3 multiple comparisons test.

Following this, clonogenic assays were performed on the MDCK cell lines stably expressing rKRas to assess the effects of prolonged plasma membrane localization on proliferation (Figure 20). Recruitable KRas was maintained at the plasma membrane for one week with 2 µM SLF'-TMP. Reversal of PM translocation of rKRas was carried out by maintaining rKRas at the plasma membrane for 4 days, followed by a washout with PBS and incubation for 2 days FGM containing 2 µM TMP). Visually, the colonies for the WT MDCK and the rWT KRas-expressing cells appeared to be of similar size and number, whereas the colony sizes in the oncogenic rG12V and rG12D KRas-expressing cells appeared to be smaller (Figure 20 A). Upon quantification, there was no difference in mean area per colony between FGM and the DMSO conditions in all 4 cell lines (Figure 20 B). In WT MDCK cells, SLF'-TMP was associated with an insignificant decrease in the mean area per colony of about 28% compared to the FGM and DMSO conditions. However, SFL'-TMP was associated with an insignificant increase in mean area per colony in rG12V KRas cells compared to the FGM and DMSO conditions (Figure 20 B).

Overall, there were no significant changes in mean area per colony between conditions within each cell line (Figure 20 B).

Under FGM and DMSO growth conditions, there were no differences in mean area per colony between the WT MDCK and rWT KRas expressing cells (Figure 20 C). The only difference observed was an insignificant increase in the mean area per colony in rWT KRas cells compared to the WT MDCK in the SLF'-TMP condition. This was obliterated in the Reversal condition.

Interestingly, in the FGM and DMSO conditions, the mean area per colony for the oncogenic variant cells (rG12V- and rG12V KRas-expressing cells) was almost identical. The oncogenic variant cells displayed about a 50% lower mean area per colony in both the FGM and DMSO conditions compared to the wild-type variant cells. However, the rG12D KRas cells displayed the lowest mean area per colony in the SLF'-TMP condition of all the cell lines.

Notably, the reversal condition after 4 days of plasma membrane localization was observed to have no effect in all cell lines. There was no difference when compared to the SLF'-TMP condition, especially in the G12D KRas cells where the mean area per colony was the lowest (Figure 20 C). Altogether, these data show that oncogenic KRas-expressing cells grew small colonies compared to WT MDCK and rWT KRas cells regardless of plasma membrane localization.

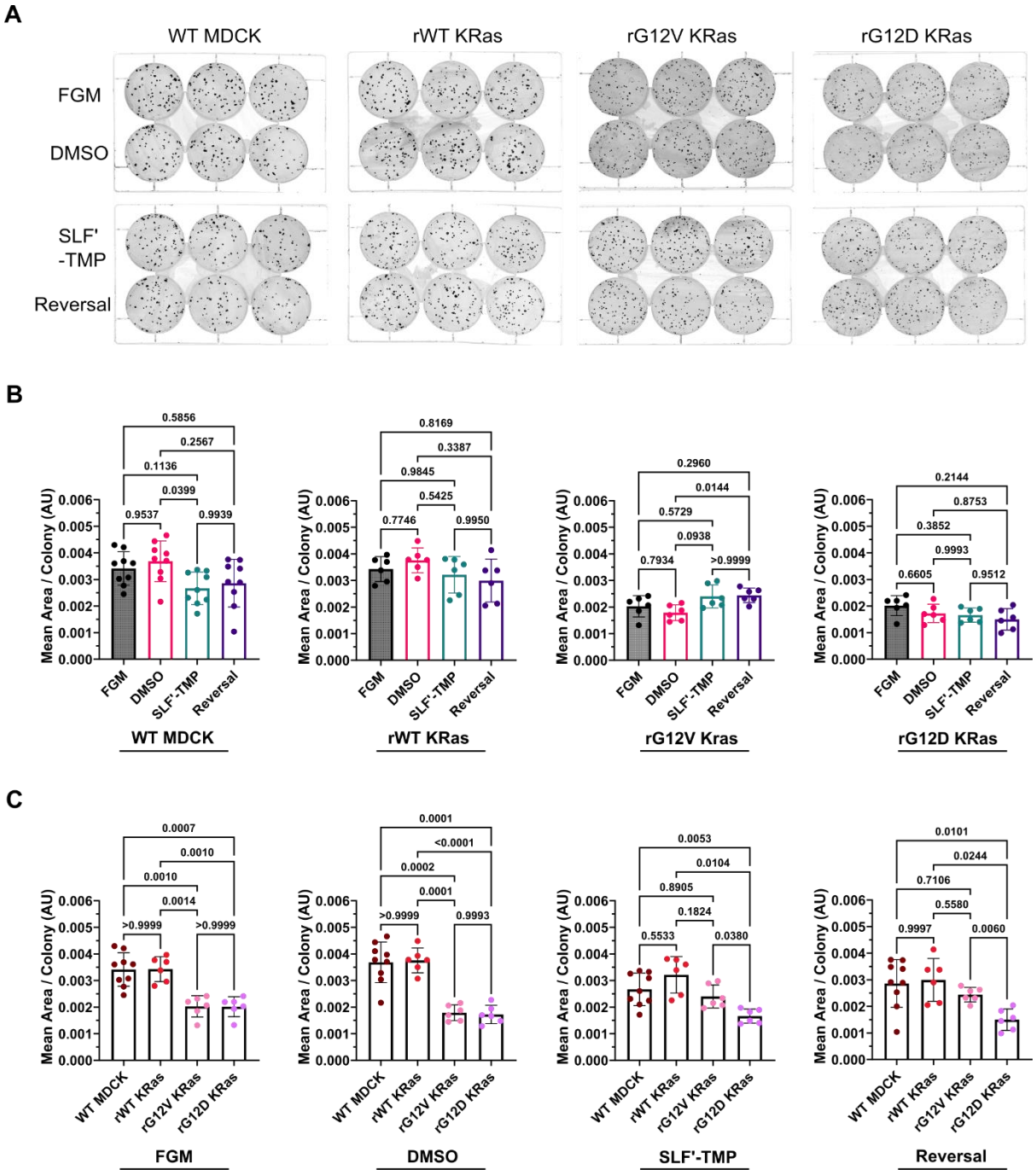

Figure 20. Differences in the average occupied area per colony.
(A) Representative images of the end growth state of WT MDCK cells, and MDCK cells stably expressing rWT, rG12V and rG12D KRas seeded at 100 cells per well, and grown for 7 days in Full Growth Medium (FGM), 0.02% v/v DMSO, 2 µM SLF'-TMP dimerizer, or a Reversal condition of 4 days with 2 µM SLF'-TMP followed by a washout with PBS then 3 days of 2 µM TMP in FGM.
(B) Shows the average occupied area per colony for WT MDCK, rWT KRas, rG12V KRas and rG12D KRas expressing cells cultured in FGM, FGM + 0.02% v/v DMSO, FGM + 2 µM SLF'-TMP and FGM + 2 µM TMP for 7 days (see Figure X).
(C) Shows graphs comparing the different cell lines to each other under each culture with FGM, DMSO, (2 µM) SLF'-TMP and (2 µM) TMP respectively. All statistics were calculated using the Brown-Forsythe and Welch ANOVA test with Dunnett's T3 multiple comparisons test.

7 Discussion

7.1 Control of KRas localization using a CID system

The applied CID system was used to control the concentration of KRas G-domain at the PM using micromolar concentrations of the bivalent dimerizer SLF'-TMP and its competitor TMP. Plasma membrane translocation of rKRas was confirmed in all 3 stable cell lines of MDCK cells expressing rWT, rG12V, and rG12D KRas constructs when exposed to SLF'-TMP (Figure 8). With half-lives under 10 minutes in all cases, maximum translocation was achieved in all cell lines by 40 minutes post SLF'-TMP addition (Figure 8). The translocation was stable over days, as observed in the clonogenic assay experiments where the dimerizer was included in the culture medium for 1 week (Figure 18). The reversibility of the system was also shown in confocal fluorescence microscopy where cells were exposed to the SLF'-TMP for 20 minutes before being exposed to TMP for 30 minutes (Figure 9). Dissociation half-lives were below 10 minutes in all cell lines, with return of the KRas-G-domain to the cytosol achieved within 30 minutes of exposure to TMP (Figure 9). However, movement of rKRas from the plasma membrane to the cytosol was slower than translocation to the plasma membrane. Thus, a higher concentration of TMP may enhance this.

This CID technique to control the localization of proteins within a cell is slower than light-induced dimerization techniques, where translocation to targeted cellular compartments occurs on a seconds time-scale. (288), (291), (280). However, the translocation kinetics were similar to those of a previous study where the CID system was tested in HeLa cells using 1µM SLF'-TMP and 10 µM TMP. (285).

7.2 Characterization of Wild-Type MDCK cells signaling responses to EGF stimulation

It was important to have an insight into growth factor-mediated signaling in MDCK cells, to offer a comparison for later experiments with the rKRas. Thus, we characterized the standard behavior of active, GTP-bound eRas activity and downstream signaling through pERK and pAKT in response to low (10 ng/ml) and high (160 ng/ml) EGF concentrations in WT MDCK cells (Figure 11 and Figure 12). The results showed that eRas-GTP peaked 5 minutes after exposure to EGF with both concentrations (Figure 11). An EGF concentration of 10 ng/ml is within the physiological range for humans (98), suggesting that ligand-bound EGFR is recycled to the PM as it is likely monomeric (99), (57). This might suggest that the eRas-GTP peak would have been sustained, however, this was not observed. Internalization of dimeric EGFR receptors likely mediated the faster decrease in eRas-GTP seen when MDCK cells were stimulated with 160 ng/ml EGF compared to 10 ng/ml (57), (180).

The increase in eRas-GTP observed correlated with the peak in pERK, which also occurred 5 minutes after EGF stimulation. This is consistent with data for MCF7 and MCF 10A cells (300). The pERK signal persisted beyond the decrease in eRas-GTP seen. This suggests that pERK regulation is uncoupled from Ras signaling after the initial peak in pERK, and after deactivation of active Ras-GTP. This is likely due to negative feedback mechanisms regulating ERK activity such as ERK negative feedback on Raf (301), (182), (175). There was likely a stronger negative feedback effect in the 160ng/ml EGF case which accounted for the sharper decrease in pERK. The dampened oscillations, more clearly visible in the 160 ng/ml EGF case had a period of about 15 minutes on average, similar to when human mammary epithelial cells were stimulated with EGF (182). In both cases, an increase in MAPK phosphatases likely mediated the dampening of pERK (302).

As with pERK, the peak in pAKT also occurred after 5 minutes of EGF stimulation. However, it was maintained for about 35 minutes before starting to decrease (Figure 12). This 5-minute peak was also

consistent with data for MCF7 and MCF 10A cells (300). Phosphorylated AKT levels were more sustained than pERK levels, with the gradual decrease observed likely mediated by AKT negative regulators such as PP2A and PHLPPs AKT (153), (186), (161). The extended pAKT signal duration suggests delayed feedback mechanisms at play after the initial pulse of increased eRas-GTP. That is, pAKT is also uncoupled from Ras activity, likely with self-sustaining, time-limited mechanisms. The negative feedback mechanisms acting on pAKT are likely stronger in the case of the higher EGF dose (160 ng/ml), explaining the steeper, more regulated return to baseline of pAKT as with pERK (Figure 12).

As the pERK response was measured by quantitative western blots, experimentally phase-matching the experiments proved challenging, however, this likely resulted in the variation of responses seen at each time point, especially in the case of pERK. Temporal confounding factors may be mitigated by using a fluorophore-tagged ERK reporter such as EKAREV to measure pERK responses.

7.3 Cytosolic oncogenic KRas is GTP-loaded

With the CID system, we could assess the average GTP state of rKRas in the cytosol and when localized to the plasma membrane. Differences in rKRas-GTP observed corroborate what is known, that mutated oncogenic Ras variants are constitutively active, as the rG12V and rG12D KRas variants had higher GTP-loading compared to rWT KRas (Figure 13 and Figure 17). This was the case regardless of cytosolic or plasma membrane localization. This is likely because intrinsic GTP hydrolysis of oncogenic Ras variants is much lower than in wild-type Ras protein.

When comparing KRas-GTP levels upon SLF'-TMP mediated PM translocation to DMSO control, there was a small decrease in rG12V and rG12D KRas, but not in rWT KRas (Figure 17). This was in contrast to the time-resolved PM translocation experiment where comparison was to a baseline of serum-deprived cells before rKRas translocation, that is, without the dimerizer and DMSO (Figure 13 and Figure 14). In this case, there was no change in rWT KRas-GTP and rG12V KRas-GTP levels, but there was still a small decrease in rG12D KRas-GTP seen (Figure 17). The use of DMSO solvent is beneficial for increased membrane permeability to other molecules (303). However, it was recently shown that DNA methylation, as well as the transcriptome and proteomes of cardiac and liver cells were altered by DMSO concentrations as low as 0.1% (304). Although a low DMSO concentration of 0.02% v/v was used in our experiments, it might still affect cells and membrane-associating proteins such as Ras.

Additionally, GAPs such as NF-1 are cytosolic (92), and are recruited to the PM to modulate Ras activity. Interestingly, neither intrinsic nor GAP-mediated hydrolysis is completely abolished in mutated Ras and may play a role in the hydrolysis of GTP in oncogenic Ras variants (71). This would also explain why no change in rWT KRas-GTP was observed upon translocation to the plasma membrane, but a small decrease in rG12V and rG12D KRas-GTP was seen. As no change in rWT KRas-GTP was observed upon plasma membrane translocation (Figure 13 and Figure 17), it suggests that an equilibrium between GTP-binding, intrinsic GTPase activity, and GAP activity was reached. Simply translocating to the PM does not change the equilibrium of GTP-loading in rWT KRas. Thus, GAPs likely regulate cytosolic Ras-GTP activity, and an increase in WT Ras-GTP in the absence of mutant Ras can only occur by growth factor stimulation or GEF-mediated mechanisms at the plasma membrane. The maintenance of high oncogenic Ras-GTP levels upon plasma membrane translocation can be explained by oncogenic KRas being constitutively on and having resistance to GAPs (73).

The presence of GTP-loaded cytosolic KRas begs the question of whether active, non-membrane-bound KRas has signaling capabilities. As Ras proteins can localize to cellular compartments such as

the endoplasmic reticulum and Golgi apparatus via the CAAX box motifs, it has been suggested that they can activate Raf in these compartments (114), (35). However, the KRas G-domains in the CID system are cytosolic and not bound to endomembranes as they do not possess the KRas tail.

7.4 Oncogenic KRas has an activating interaction with wild-type Ras at the plasma membrane

We translocated rKRas to the PM using SLF'-TMP to assess the initial effects of PM localization of oncogenic KRas on other wild-type Ras isoforms (Figure 13). Our results showed that all 3 rKRas variants in our study were GTP-bound regardless of PM localization. However, the oncogenic rG12V and rG12D KRas always had higher amounts of bound GTP compared to the rWT KRas. This presumably explains why PM translocation of oncogenic rG12V and rG12D KRas, as well as rWT KRas, activated endogenous wild-type pan Ras upon translocation to the plasma membrane in the absence of growth factor (Figure 13). This activating interaction of rKRas-GTP on eRas is assumed to occur via allosteric activation of SOS, potentiating its action on the endogenous wild-type Ras. This is consistent with the findings that oncogenic Ras can activate wild-type Ras without growth factor stimulation (253), (87).

The concentration of GTP-bound rWT KRas in our study was likely sufficient, due to its overexpression, to also activate eRas. Additionally, it has been shown that GDP-bound Ras can also activate SOS, however, at a much lower level (83). Interestingly, the change in eRas-GTP upon PM translocation of rKRas ranged from 1.6 – 2.4 fold compared to the 5-fold increase when WT MDCK cells were stimulated with low and saturating EGF doses. This suggests that full activation of eRas requires growth factor stimulation and that oncogenic KRas plays a role in maintaining baseline Ras activity while wild-type Ras isoforms mediate growth factor-induced signaling (250). Following the activation of eRas, the decrease in eRas-GTP at the PM was likely mediated by the action of GAPs.

A question that remains open is how the baseline levels of the endogenous wild-type Ras-GTP are also high or visible on pull-down of active GTP-bound Ras, before translocation of rKRas to the plasma membrane. This might be explained by mass action as the G-domain of the rKRas in all cell lines is highly concentrated, albeit in the cytoplasm. However, this high concentration may be sufficient for interaction with Ras signaling cascade molecules in the periphery of the PM by diffusion. Alternatively, eRas may be activated by paracrine and juxtacrine signaling cascades (305), (306), (307). Additionally, other GEFs may also play a small role in activating cytosolic oncogenic KRas (308). The robust nature of MDCK cells may also allow for signaling in the 0.1% FBS-containing medium used during serum deprivation.

7.5 Plasma membrane translocation of rKRas initiates Ras-MAPK and Ras-PI3K signaling independent of growth factor

The activation of endogenous wild-type Ras isoforms by PM translocation of rKRas was associated with signaling responses in ERK and AKT (Figure 14). These pERK and pAKT signals were observed in all rKRas-expressing cell lines. This gives further evidence that Ras-mediated MAPK and PI3K signaling occur at the plasma membrane. Deactivation of the pERK signal after the peak at 10 minutes in all three cell lines can be explained by the negative feedback regulation of pERK on MAPK signaling (175), (170), (170). This likely occurs at the levels of Raf and MEK, and less likely at the level of SOS-Ras in the case of oncogenic rKRas (175), (170), (160). This adaptive pERK signal was conserved in all three cell lines, regardless of the KRas mutation (Figure 14 B and D). This suggests that there is a standard, all-or-nothing pERK response upon Ras activation, and gives evidence to the notion of fold-change

detection, that cells respond to changes in signal (309), (310). The adaptive response of pERK is interesting because the negative feedback response to mutated Ras and Raf proteins has been proposed as a mechanism for oncogene-induced senescence rather than tumor progression (245). This differs from the results of a study that suggested that negative feedback regulation of MAPK signaling in cells expressing oncoproteins may be weaker than in WT cells (160).

The return to baseline of pERK in all cases poses the question of how much baseline ERK activity is influenced by PM localized oncogenic KRas. Baseline fluctuations in Ras-GTP signaling may occur as oncogenic KRas is cycled through the cytosol and shuttled back to the PM to maintain its localization (57). This maintenance may drive a baseline activation of MAPK signaling mediated by oncogenic KRas when oncogenic KRas is expressed at isogenic levels.

Considering AKT responses, phosphorylated AKT levels peaked quickly at 10 minutes post initiation of PM translocation of rKRas in rG12V and rG12D KRas cells, compared to 20 minutes in rWT KRas cells. The signal was also more sustained in the oncogenic KRas cells. Downregulation of the pAKT response that we observed likely occurred through protein phosphatase 2A (PP2A) and the PH domain leucine-rich repeat protein phosphatases (PHLPP) 1 and 2, which are known negative regulators of active phosphorylated AKT (153), (186), (161).

The more sustained pAKT signal observed in the oncogenic rKRas variants compared to the wild-type variant suggests that the downregulation pAKT signals is linked, in part, to oncogenic KRas activity. This prolonged pAKT signal also suggests a higher survival response which would favour tumorigenesis. This is in line with studies showing that Ras-mediated PI3K signaling is important in tumor formation and maintenance (208), (152). The similar responses in pERK and pAKT seen in our results between rG12V and rG12D KRas-expressing cells contrast what was suggested previously, that in non-small cell lung carcinoma cell lines, it was observed that G12D mutations activated pAKT and pERK more than G12V (187). Our results also contrast the notion that isogenic SW48 human colon cancer cell lines expressing G12 mutations of Ras did not activate AKT and ERK signaling in the absence of growth factors, in a study by Hood et al. (311).

There is likely cross-talk between ERK and AKT signaling as they can compensate for each other's inhibition in pancreatic cancer cell lines (157), (158), (159). In the case that pERK is down-regulated more strongly or for longer in the presence of oncogenic Ras, a faster more prolonged pAKT response may be compensatory. This would support the quick and sustained pAKT responses we observed upon plasma membrane translocation of rG12V and rG12D KRas in comparison to rWT KRas.

7.6 Reduced proliferation in cells harboring overexpressed rG12V and rG12D KRas

As the cell lines were created with the PiggyBac transposon system, copy numbers can vary, and this was evident in the differences in rKRas expression within the same cell lines across different experimental replicates (Figure 15 and Figure 16). However, this ensured effective, stable transfection of the construct with rKRas expression up to 5 times higher on average than the endogenous Ras expression within each pooled group of cells. This is important as oncogene-induced senescence occurs in heterogeneous cells containing over-expressed oncogenic KRas (238), (241), (239), (240).

The culturing of cells under constant exposure to the dimerizer SLF'-TMP was confirmed by live-cell confocal microscopy for 7 days (Figure 18). Additionally, we determined a seeding density suitable for performing clonogenic assays in MDCK cells stably expressing rKRas (Figure 19). Following this, clonogenic assays revealed that exposure to very low concentrations of DMSO (0.4 µl/2 ml or 0.02% v/v) did not affect proliferation potential (Figure 20).

The addition of SLF'-TMP to WT MDCK cells was associated with a decrease in proliferation compared to WT MDCK cells cultured in full medium or with DMSO added (Figure 20 B). This suggests that although the CID system is stable over 7 days, the dimerizer may have off-target effects in MDCK cells that limit proliferation. Thus, this CID system may not be completely bioorthogonal as previously described (285). Cytosolic oncogenic KRas on the other hand appeared to inhibit clonogenicity when cultured in full growth medium and DMSO, suggesting that cells can detect and respond to cytosolic oncogenic KRas. Plasma membrane translocation of the oncogenic KRas and reversal back into the cytosol had no significant effect on clonogenicity compared to no translocation (DMSO condition).

Together, these data suggest that oncogene-induced senescence can occur regardless of oncogenic KRas cellular localization. It also confirms the notion of oncogene-induced senescence occurring only in over-expressed oncogenic KRas, as this effect was not observed in the rWT KRas-expressing cells, which also had overexpressed rKRas in all western blots analyzed (Figure 20). Oncogene-induced senescence may therefore be a protective mechanism of cells against carcinogenic aberrations. Repeating the experiment in isogenic or low-expressing cells may help to elucidate whether low expression of oncogenic KRas (or expression at physiological levels) is also implicated in oncogene-induced senescence.

8 Limitations

Tuveson et al., 2004 (241) suggested that endogenous expression of oncogenic Ras at physiological levels, as opposed to high expression from ectopic oncogenic Ras, would lead to increased proliferation as opposed to cell senescence. Currently, our study cannot give evidence regarding this due to overexpression of rWT, rG12V, and rG12D KRas in the stably-transfected MDCK cell lines (Figure 15 and Figure 16). The use of a less aggressive promoter in the CID construct would be one avenue to explore. Finally, there was no discrimination biochemically between different Ras isoforms in our experiments, which is possible by using isoform-specific Ras antibodies. It is therefore challenging to ascertain how much downstream signaling was due to endogenous Ras, and how much of it was attributed to the recruitable KRas. Additionally, a few of the western blots showed some pre-activation of ERK and AKT at time 0 minutes, before the addition of SLF'-TMP. This suggests that the rKRas CID system may be leaky, in that a small proportion of the expressed rKRas is not split by the P2A ribosomal skipping site. This would result in plasma membrane localization of a small proportion of full-length ectopically-expressed rKRas that could increase baseline levels of phosphorylated ERK and AKT.

9 Conclusions and Future Considerations

The significance of KRas oncoproteins in the pathophysiology of cancer is unquestionable as they influence processes such as proliferation, differentiation, survival, and migration, which are dysregulated in cancer. However, the complexities of the roles of the wild-type and oncogenic variants of Ras proteins in cells, and their effect on tumor formation via altered Ras signaling require further study. The primary research question of this thesis was to assess whether oncogenic KRas activity affects wild-type Ras activity and signaling responses using a chemically inducible dimerization technique to temporally modulate plasma membrane translocation of KRas. Using pulldown assays

and western blots to assess changes in Ras-GTP and effector levels, some insights on the wild-type Ras–oncogenic KRas interaction could be gained.

The results shown in this thesis show that a reversible, chemically induced dimerization system can effectively be used to control the localization and dose of KRas proteins at the plasma membrane in MDCK cells. It was shown that cytosolic oncogenic rKRas already had a higher GTP loading in comparison to cytosolic wild-type rKRas, before translocation to the plasma membrane. Upon movement to the plasma membrane, both oncogenic KRas and over-expressed wild-type KRas resulted in transient, adaptive responses in eRas-GTP, pERK, and pAKT, suggesting an activating link between oncogenic KRas and wild-type Ras. The likely mechanism is through allosteric activation of wild-type Ras by the oncogenic and overexpressed wild-type rKRas. Additionally, the presence of overexpressed oncogenic G12V and G12D KRas, regardless of cytosolic or plasma membrane localization, was associated with decreased proliferation, pointing towards oncogene-induced senescence. Thus, this reduction in proliferation would need to be overcome for tumorigenesis to occur.

Future work can focus on delineating if indeed the activating link between recruitable oncogenic KRas and endogenous wild-type Ras isoforms is through allosteric activation of SOS by disrupting allosteric bind using a W729E mutation of SOS (81), (254). The effect of plasma membrane-localized oncogenic KRas on EGF signaling responses can be assessed by performing EGF dose-response experiments and comparing outcomes between cytosolic and plasma membrane-localized recruitable KRas. Initial results for this suggest that the plasma membrane localization of oncogenic rKRas causes an ultrasensitive response in endogenous Ras, ERK, and AKT, at lower EGF concentrations compared to WT MDCK cells and cells expressing rWT KRas proteins (Supplementary Figure 1Supplementary Figure 1. Changes in Ras-GTP levels in response to increasing EGF doses with (2µM SLF'-TMP) and without (DMSO) plasma membrane translocation of rKRas. and Supplementary Figure 2). This would suggest that oncogenic KRas enhances growth factor sensitivity by a wild-type Ras-activating interaction. This would not corroborate previous research suggesting that oncogenic Ras decreases the sensitivity of cells to growth factors, but when expressed at isogenic levels (250), (160). Furthermore, changes in the morphology or migration capacity of cells can also be assessed as described in other studies (300), (100), as morphological changes and migration capability are linked to cancer progression and metastasis. Finally, using the reversibility function of the CID may help to elucidate whether cells have memory of plasma membrane-localized KRas and whether targeting Ras localization may be a viable target for cancer therapies.

10 Supplementary Figures

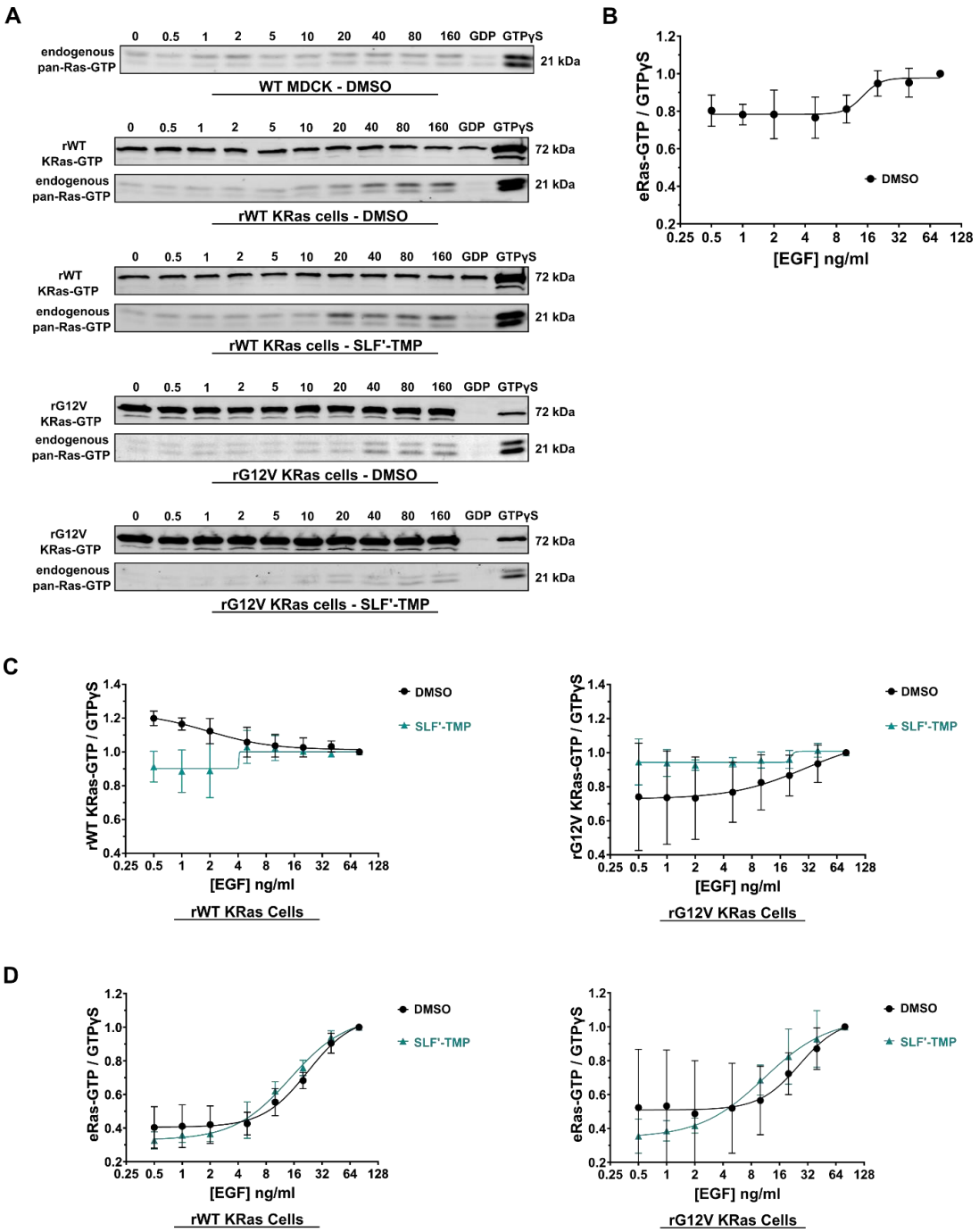

Supplementary Figure 1. Changes in Ras-GTP levels in response to increasing EGF doses with (2µM SLF'-TMP) and without (DMSO) plasma membrane translocation of rKRas.
(A) Representative western blot images of 3x-RafRBD Pulldown samples showing the levels of rKRas-GTP and eRas-GTP for Wild-type MDCK (top band only), rWT KRas cells with DMSO and SLF'-TMP, and rG12V KRas cells with DMSO and SLF'-TMP from top to bottom.
(B) shows the quantified average changes in eRas-GTP in WT MDCK cells.
(C) and (D) show the quantified changes in rKRas-GTP and eRas-GTP respectively, with rWT KRas expressing cells (Left) and rG12V KRas expressing cells (Right). Changes in Ras-GTP the presence of DMSO are in black, while Ras-GTP changes in the presence of SLF'-TMP are in teal. N = 4 for WT MDCK cells, N = 3 for rWT KRas cells, N = 3 for rG12V KRas cells in DMSO (black) and N = 4 for rG12V KRas cells in SLF'-TMP (teal). Data displayed as mean ± SD for 3-point moving averaged data points normalized to the point at 80 ng/ml EGF Least square line fitted with output as 95% confidence interval of the parameters.

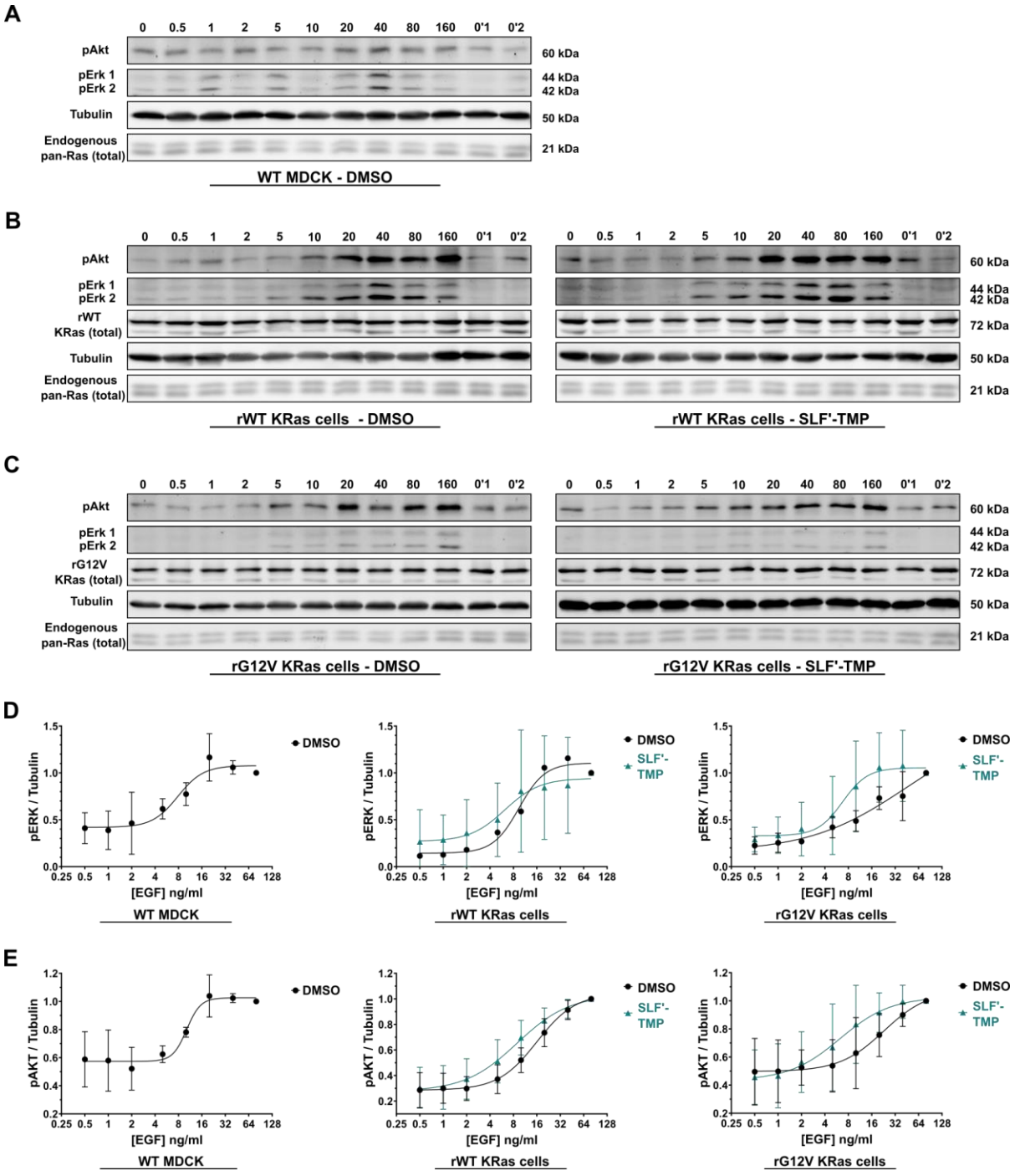

Supplementary Figure 2. Changes in the levels of phosphorylated Erk and Akt in response to increasing EGF doses with (2μM SLF'-TMP) and without (DMSO) plasma membrane recruitment of rKRas.
(A) Representative western blot showing pAkt) and pErk changes with increasing EGF dose in Wild-type MDCK cells. Tubulin and endogenous panRas expression is also shown.
(B) and (C) show the same changes in pAk and pErk as in (A), but for rWT KRas expressing cells (B) and rG12V KRas expressing cells (C) respectively, with the left images showing results in DMSO exposed cells, and results on the right showing the same for SLF'-TMP exposed cells. Samples 0'1 and 0'2 are extra baseline samples used for the positive (GTPγS-loaded) and negative (GDP-loaded) controls of the Pull Downs.
(D) shows the quantified average changes in pErk and (E) shows the quantified average changes in pAkt in WT MDCK cells (left), and in rWT KRas (middle) and rG12V KRas (right) expressing cells. Responses in DMSO are in black, while responses in SLF'-TMP are in teal. For pErk, N = 2 for WT MDCK, N = 1 for rWT KRas cells in DMSO, N = 4 for rWT KRas cells in SLF'-TMP, N = 3 for rG12V KRas cells in both DMSO and SLF'-TMP. For pAkt, N = 2 for WT MDCK, N = 3 for rWT KRas cells in DMSO, N = 4 for rWT KRas cells in SLF'-TMP, N = 3 for rG12V KRas cells in both DMSO and SLF'-TMP. Data displayed as mean ± SD for 3-point moving averaged data points normalized to the point at 80 ng/ml EGF. Least square line fitted with output as 95% confidence interval of the parameters.

11 Bibliography

1. Su J, Song Y, Zhu Z, Huang X, Fan J, Qiao J, et al. Cell–cell communication: new insights and clinical implications. Signal Transduction and Targeted Therapy. 2024;9(1):196.
2. Nair A, Chauhan P, Saha B, Kubatzky KF. Conceptual Evolution of Cell Signaling. Int J Mol Sci. 2019;20(13).
3. Farnsworth KD, Nelson J, Gershenson C. Living is Information Processing: From Molecules to Global Systems. Acta Biotheoretica. 2013;61(2):203-22.
4. Kirschner MW. The Meaning of Systems Biology. Cell. 2005;121(4):503-4.
5. Chen RE, Thorner J. Systems biology approaches in cell signaling research. Genome Biology. 2005;6(10):235.
6. Shahzad K, Loor JJ. Application of Top-Down and Bottom-up Systems Approaches in Ruminant Physiology and Metabolism. Curr Genomics. 2012;13(5):379-94.
7. Harvey JJ. An Unidentified Virus which causes the Rapid Production of Tumours in Mice. Nature. 1964;204(4963):1104-5.
8. Kirsten WH, Mayer LA. Morphologic responses to a murine erythroblastosis virus. J Natl Cancer Inst. 1967;39(2):311-35.
9. Scolnick EM, Rands E, Williams D, Parks WP. Studies on the nucleic acid sequences of Kirsten sarcoma virus: a model for formation of a mammalian RNA-containing sarcoma virus. J Virol. 1973;12(3):458-63.
10. Scolnick EM, Parks WP. Harvey sarcoma virus: a second murine type C sarcoma virus with rat genetic information. J Virol. 1974;13(6):1211-9.
11. Parks WP, Scolnick EM. In vitro translation of Harvey murine sarcoma virus RNA. J Virol. 1977;22(3):711-9.
12. Shih TY, Williams DR, Weeks MO, Maryak JM, Vass WC, Scolnick EM. Comparison of the genomic organization of Kirsten and Harvey sarcoma viruses. J Virol. 1978;27(1):45-55.
13. Shih TY, Weeks MO, Young HA, Scolnick EM. Identification of a sarcoma virus-coded phosphoprotein in nonproducer cells transformed by Kirsten or Harvey murine sarcoma virus. Virology. 1979;96(1):64-79.
14. Scolnick EM, Papageorge AG, Shih TY. Guanine nucleotide-binding activity as an assay for src protein of rat-derived murine sarcoma viruses. Proceedings of the National Academy of Sciences. 1979;76(10):5355-9.
15. Willingham MC, Pastan I, Shih TY, Scolnick EM. Localization of the src gene product of the Harvey strain of MSV to plasma membrane of transformed cells by electron microscopic immunocytochemistry. Cell. 1980;19(4):1005-14.
16. Ellis RW, DeFeo D, Shih TY, Gonda MA, Young HA, Tsuchida N, et al. The p21 src genes of Harvey and Kirsten sarcoma viruses originate from divergent members of a family of normal vertebrate genes. Nature. 1981;292(5823):506-11.
17. Chang EH, Gonda MA, Ellis RW, Scolnick EM, Lowy DR. Human genome contains four genes homologous to transforming genes of Harvey and Kirsten murine sarcoma viruses. Proceedings of the National Academy of Sciences. 1982;79(16):4848-52.
18. Chang EH, Furth ME, Scolnick EM, Lowy DR. Tumorigenic transformation of mammalian cells induced by a normal human gene homologous to the oncogene of Harvey murine sarcoma virus. Nature. 1982;297(5866):479-83.
19. Gibbs JB, Sigal IS, Poe M, Scolnick EM. Intrinsic GTPase activity distinguishes normal and oncogenic ras p21 molecules. Proceedings of the National Academy of Sciences. 1984;81(18):5704-8.
20. Santos E, Tronick SR, Aaronson SA, Pulciani S, Barbacid M. T24 human bladder carcinoma oncogene is an activated form of the normal human homologue of BALB- and Harvey-MSV transforming genes. Nature. 1982;298(5872):343-7.

21. Marshall CJ, Hall A, Weiss RA. A transforming gene present in human sarcoma cell lines. Nature. 1982;299(5879):171-3.
22. Reddy EP, Reynolds RK, Santos E, Barbacid M. A point mutation is responsible for the acquisition of transforming properties by the T24 human bladder carcinoma oncogene. Nature. 1982;300(5888):149-52.
23. Taparowsky E, Suard Y, Fasano O, Shimizu K, Goldfarb M, Wigler M. Activation of the T24 bladder carcinoma transforming gene is linked to a single amino acid change. Nature. 1982;300(5894):762-5.
24. Bos JL. ras oncogenes in human cancer: a review. Cancer Res. 1989;49(17):4682-9.
25. Der CJ, Krontiris TG, Cooper GM. Transforming genes of human bladder and lung carcinoma cell lines are homologous to the ras genes of Harvey and Kirsten sarcoma viruses. Proc Natl Acad Sci U S A. 1982;79(11):3637-40.
26. Parada LF, Tabin CJ, Shih C, Weinberg RA. Human EJ bladder carcinoma oncogene is homologue of Harvey sarcoma virus ras gene. Nature. 1982;297(5866):474-8.
27. Shimizu K, Goldfarb M, Perucho M, Wigler M. Isolation and preliminary characterization of the transforming gene of a human neuroblastoma cell line. Proc Natl Acad Sci U S A. 1983;80(2):383-7.
28. Hall A, Marshall CJ, Spurr NK, Weiss RA. Identification of transforming gene in two human sarcoma cell lines as a new member of the ras gene family located on chromosome 1. Nature. 1983;303(5916):396-400.
29. Colicelli J. Human RAS superfamily proteins and related GTPases. Sci STKE. 2004;2004(250):Re13.
30. Wennerberg K, Rossman KL, Der CJ. The Ras superfamily at a glance. J Cell Sci. 2005;118(Pt 5):843-6.
31. Capon DJ, Seeburg PH, McGrath JP, Hayflick JS, Edman U, Levinson AD, et al. Activation of Ki-ras2 gene in human colon and lung carcinomas by two different point mutations. Nature. 1983;304(5926):507-13.
32. Castellano E, Santos E. Functional specificity of ras isoforms: so similar but so different. Genes Cancer. 2011;2(3):216-31.
33. Willumsen BM, Christensen A, Hubbert NL, Papageorge AG, Lowy DR. The p21 ras C-terminus is required for transformation and membrane association. Nature. 1984;310(5978):583-6.
34. Hobbs GA, Der CJ, Rossman KL. RAS isoforms and mutations in cancer at a glance. J Cell Sci. 2016;129(7):1287-92.
35. Choy E, Chiu VK, Silletti J, Feoktistov M, Morimoto T, Michaelson D, et al. Endomembrane trafficking of ras: the CAAX motif targets proteins to the ER and Golgi. Cell. 1999;98(1):69-80.
36. Casey PJ, Solski PA, Der CJ, Buss JE. p21ras is modified by a farnesyl isoprenoid. Proc Natl Acad Sci U S A. 1989;86(21):8323-7.
37. Schaber MD, O'Hara MB, Garsky VM, Mosser SC, Bergstrom JD, Moores SL, et al. Polyisoprenylation of Ras in vitro by a farnesyl-protein transferase. Journal of Biological Chemistry. 1990;265(25):14701-4.
38. Wright LP, Philips MR. Thematic review series: Lipid Posttranslational Modifications CAAX modification and membrane targeting of Ras. Journal of Lipid Research. 2006;47(5):883-91.
39. Whyte DB, Kirschmeier P, Hockenberry TN, Nunez-Oliva I, James L, Catino JJ, et al. K- and N-Ras Are Geranylgeranylated in Cells Treated with Farnesyl Protein Transferase Inhibitors*. Journal of Biological Chemistry. 1997;272(22):14459-64.
40. Seabra MC, Reiss Y, Casey PJ, Brown MS, Goldstein JL. Protein farnesyltransferase and geranylgeranyltransferase share a common alpha subunit. Cell. 1991;65(3):429-34.
41. Boyartchuk VL, Ashby MN, Rine J. Modulation of Ras and a-factor function by carboxyl-terminal proteolysis. Science. 1997;275(5307):1796-800.
42. Dai Q, Choy E, Chiu V, Romano J, Slivka SR, Steitz SA, et al. Mammalian prenylcysteine carboxyl methyltransferase is in the endoplasmic reticulum. J Biol Chem. 1998;273(24):15030-4.

43. Hancock JF, Magee AI, Childs JE, Marshall CJ. All ras proteins are polyisoprenylated but only some are palmitoylated. Cell. 1989;57(7):1167-77.
44. Swarthout JT, Lobo S, Farh L, Croke MR, Greentree WK, Deschenes RJ, et al. DHHC9 and GCP16 constitute a human protein fatty acyltransferase with specificity for H- and N-Ras. J Biol Chem. 2005;280(35):31141-8.
45. Bivona TG, Quatela SE, Bodemann BO, Ahearn IM, Soskis MJ, Mor A, et al. PKC regulates a farnesyl-electrostatic switch on K-Ras that promotes its association with Bcl-XL on mitochondria and induces apoptosis. Mol Cell. 2006;21(4):481-93.
46. Cox AD, Der CJ, Philips MR. Targeting RAS Membrane Association: Back to the Future for Anti-RAS Drug Discovery? Clin Cancer Res. 2015;21(8):1819-27.
47. Lynch SJ, Snitkin H, Gumper I, Philips MR, Sabatini D, Pellicer A. The differential palmitoylation states of N-Ras and H-Ras determine their distinct Golgi subcompartment localizations. J Cell Physiol. 2015;230(3):610-9.
48. Lorentzen A, Kinkhabwala A, Rocks O, Vartak N, Bastiaens PI. Regulation of Ras localization by acylation enables a mode of intracellular signal propagation. Sci Signal. 2010;3(140):ra68.
49. Hancock JF, Paterson H, Marshall CJ. A polybasic domain or palmitoylation is required in addition to the CAAX motif to localize p21ras to the plasma membrane. Cell. 1990;63(1):133-9.
50. Gelabert-Baldrich M, Soriano-Castell D, Calvo M, Lu A, Viña-Vilaseca A, Rentero C, et al. Dynamics of KRas on endosomes: involvement of acidic phospholipids in its association. Faseb j. 2014;28(7):3023-37.
51. Jura N, Scotto-Lavino E, Sobczyk A, Bar-Sagi D. Differential modification of Ras proteins by ubiquitination. Mol Cell. 2006;21(5):679-87.
52. Sasaki AT, Carracedo A, Locasale JW, Anastasiou D, Takeuchi K, Kahoud ER, et al. Ubiquitination of K-Ras enhances activation and facilitates binding to select downstream effectors. Sci Signal. 2011;4(163):ra13.
53. Barceló C, Paco N, Morell M, Alvarez-Moya B, Bota-Rabassedas N, Jaumot M, et al. Phosphorylation at Ser-181 of oncogenic KRAS is required for tumor growth. Cancer Res. 2014;74(4):1190-9.
54. Alvarez-Moya B, López-Alcalá C, Drosten M, Bachs O, Agell N. K-Ras4B phosphorylation at Ser181 is inhibited by calmodulin and modulates K-Ras activity and function. Oncogene. 2010;29(44):5911-22.
55. Yang MH, Nickerson S, Kim ET, Liot C, Laurent G, Spang R, et al. Regulation of RAS oncogenicity by acetylation. Proceedings of the National Academy of Sciences. 2012;109(27):10843-8.
56. Schmick M, Vartak N, Papke B, Kovacevic M, Truxius DC, Rossmannek L, et al. KRas localizes to the plasma membrane by spatial cycles of solubilization, trapping and vesicular transport. Cell. 2014;157(2):459-71.
57. Baumdick M, Brüggemann Y, Schmick M, Xouri G, Sabet O, Davis L, et al. EGF-dependent re-routing of vesicular recycling switches spontaneous phosphorylation suppression to EGFR signaling. Elife. 2015;4.
58. Leventis R, Silvius JR. Lipid-binding characteristics of the polybasic carboxy-terminal sequence of K-ras4B. Biochemistry. 1998;37(20):7640-8.
59. Rocks O, Peyker A, Kahms M, Verveer PJ, Koerner C, Lumbierres M, et al. An acylation cycle regulates localization and activity of palmitoylated Ras isoforms. Science. 2005;307(5716):1746-52.
60. Chandra A, Grecco HE, Pisupati V, Perera D, Cassidy L, Skoulidis F, et al. The GDI-like solubilizing factor PDEδ sustains the spatial organization and signalling of Ras family proteins. Nature Cell Biology. 2012;14(2):148-58.
61. Schmick M, Kraemer A, Bastiaens PIH. Ras moves to stay in place. Trends in Cell Biology. 2015;25(4):190-7.

62. Dharmaiah S, Bindu L, Tran TH, Gillette WK, Frank PH, Ghirlando R, et al. Structural basis of recognition of farnesylated and methylated KRAS4b by PDEδ. Proc Natl Acad Sci U S A. 2016;113(44):E6766-e75.
63. Hanzal-Bayer M, Renault L, Roversi P, Wittinghofer A, Hillig RC. The complex of Arl2-GTP and PDE delta: from structure to function. Embo j. 2002;21(9):2095-106.
64. Ismail S. A GDI/GDF-like system for sorting and shuttling ciliary proteins. Small GTPases. 2017;8(4):208-11.
65. Vetter IR, Wittinghofer A. The Guanine Nucleotide-Binding Switch in Three Dimensions. Science. 2001;294(5545):1299-304.
66. Simanshu DK, Nissley DV, McCormick F. RAS Proteins and Their Regulators in Human Disease. Cell. 2017;170(1):17-33.
67. Wittinghofer F. Ras signalling. Caught in the act of the switch-on. Nature. 1998;394(6691):317, 9-20.
68. John J, Sohmen R, Feuerstein J, Linke R, Wittinghofer A, Goody RS. Kinetics of interaction of nucleotides with nucleotide-free H-ras p21. Biochemistry. 1990;29(25):6058-65.
69. Trahey M, McCormick F. A cytoplasmic protein stimulates normal N-ras p21 GTPase, but does not affect oncogenic mutants. Science. 1987;238(4826):542-5.
70. Bos JL, Rehmann H, Wittinghofer A. GEFs and GAPs: critical elements in the control of small G proteins. Cell. 2007;129(5):865-77.
71. Hunter JC, Manandhar A, Carrasco MA, Gurbani D, Gondi S, Westover KD. Biochemical and Structural Analysis of Common Cancer-Associated KRAS Mutations. Molecular Cancer Research. 2015;13(9):1325-35.
72. Traut TW. Physiological concentrations of purines and pyrimidines. Mol Cell Biochem. 1994;140(1):1-22.
73. Scheffzek K, Ahmadian MR, Kabsch W, Wiesmüller L, Lautwein A, Schmitz F, et al. The Ras-RasGAP complex: structural basis for GTPase activation and its loss in oncogenic Ras mutants. Science. 1997;277(5324):333-8.
74. Hall BE, Bar-Sagi D, Nassar N. The structural basis for the transition from Ras-GTP to Ras-GDP. Proc Natl Acad Sci U S A. 2002;99(19):12138-42.
75. Boriack-Sjodin PA, Margarit SM, Bar-Sagi D, Kuriyan J. The structural basis of the activation of Ras by Sos. Nature. 1998;394(6691):337-43.
76. Kötting C, Kallenbach A, Suveyzdis Y, Wittinghofer A, Gerwert K. The GAP arginine finger movement into the catalytic site of Ras increases the activation entropy. Proc Natl Acad Sci U S A. 2008;105(17):6260-5.
77. Gideon P, John J, Frech M, Lautwein A, Clark R, Scheffler JE, et al. Mutational and kinetic analyses of the GTPase-activating protein (GAP)-p21 interaction: the C-terminal domain of GAP is not sufficient for full activity. Mol Cell Biol. 1992;12(5):2050-6.
78. Vigil D, Cherfils J, Rossman KL, Der CJ. Ras superfamily GEFs and GAPs: validated and tractable targets for cancer therapy? Nat Rev Cancer. 2010;10(12):842-57.
79. Margarit SM, Sondermann H, Hall BE, Nagar B, Hoelz A, Pirruccello M, et al. Structural evidence for feedback activation by Ras.GTP of the Ras-specific nucleotide exchange factor SOS. Cell. 2003;112(5):685-95.
80. Bandaru P, Kondo Y, Kuriyan J. The Interdependent Activation of Son-of-Sevenless and Ras. Cold Spring Harb Perspect Med. 2019;9(2).
81. Freedman TS, Sondermann H, Friedland GD, Kortemme T, Bar-Sagi D, Marqusee S, et al. A Ras-induced conformational switch in the Ras activator Son of sevenless. Proceedings of the National Academy of Sciences. 2006;103(45):16692.
82. Liao TJ, Jang H, Fushman D, Nussinov R. Allosteric KRas4B Can Modulate SOS1 Fast and Slow Ras Activation Cycles. Biophys J. 2018;115(4):629-41.
83. Sondermann H, Soisson SM, Boykevisch S, Yang SS, Bar-Sagi D, Kuriyan J. Structural analysis of autoinhibition in the Ras activator Son of sevenless. Cell. 2004;119(3):393-405.

84. Egan SE, Giddings BW, Brooks MW, Buday L, Sizeland AM, Weinberg RA. Association of Sos Ras exchange protein with Grb2 is implicated in tyrosine kinase signal transduction and transformation. Nature. 1993;363(6424):45-51.
85. Buday L, Egan SE, Rodriguez Viciana P, Cantrell DA, Downward J. A complex of Grb2 adaptor protein, Sos exchange factor, and a 36-kDa membrane-bound tyrosine phosphoprotein is implicated in ras activation in T cells. J Biol Chem. 1994;269(12):9019-23.
86. Jun JE, Rubio I, Roose JP. Regulation of ras exchange factors and cellular localization of ras activation by lipid messengers in T cells. Front Immunol. 2013;4:239.
87. Gureasko J, Galush WJ, Boykevisch S, Sondermann H, Bar-Sagi D, Groves JT, et al. Membrane-dependent signal integration by the Ras activator Son of sevenless. Nat Struct Mol Biol. 2008;15(5):452-61.
88. Lee YK, Low-Nam ST, Chung JK, Hansen SD, Lam HYM, Alvarez S, et al. Mechanism of SOS PR-domain autoinhibition revealed by single-molecule assays on native protein from lysate. Nature Communications. 2017;8(1):15061.
89. Ren H, Lee AA, Lew LJN, DeGrandchamp JB, Groves JT. Positive feedback in Ras activation by full-length SOS arises from autoinhibition release mechanism. Biophysical Journal. 2024.
90. Scheffzek K, Shivalingaiah G. Ras-Specific GTPase-Activating Proteins-Structures, Mechanisms, and Interactions. Cold Spring Harb Perspect Med. 2019;9(3).
91. Bollag G, McCormick F. NF is enough of GAP. Nature. 1992;356(6371):663-4.
92. Stowe IB, Mercado EL, Stowe TR, Bell EL, Oses-Prieto JA, Hernández H, et al. A shared molecular mechanism underlies the human rasopathies Legius syndrome and Neurofibromatosis-1. Genes Dev. 2012;26(13):1421-6.
93. Cichowski K, Santiago S, Jardim M, Johnson BW, Jacks T. Dynamic regulation of the Ras pathway via proteolysis of the NF1 tumor suppressor. Genes Dev. 2003;17(4):449-54.
94. McGillicuddy LT, Fromm JA, Hollstein PE, Kubek S, Beroukhim R, De Raedt T, et al. Proteasomal and genetic inactivation of the NF1 tumor suppressor in gliomagenesis. Cancer Cell. 2009;16(1):44-54.
95. Hollstein PE, Cichowski K. Identifying the Ubiquitin Ligase complex that regulates the NF1 tumor suppressor and Ras. Cancer Discov. 2013;3(8):880-93.
96. Grewal T, Koese M, Tebar F, Enrich C. Differential Regulation of RasGAPs in Cancer. Genes Cancer. 2011;2(3):288-97.
97. Uings IJ, Farrow SN. Cell receptors and cell signalling. Mol Pathol. 2000;53(6):295-9.
98. Konturek JW, Bielanski W, Konturek SJ, Bogdal J, Oleksy J. Distribution and release of epidermal growth factor in man. Gut. 1989;30(9):1194-200.
99. Alvarado D, Klein DE, Lemmon MA. Structural basis for negative cooperativity in growth factor binding to an EGF receptor. Cell. 2010;142(4):568-79.
100. Joshi MS, Stanoev A, Huebinger J, Soetje B, Zorina V, Roßmannek L, et al. The EGFR phosphatase RPTP γ is a redox‐regulated suppressor of promigratory signaling. The EMBO Journal. 2023;42(10):e111806.
101. Yarden Y, Schlessinger J. Self-phosphorylation of epidermal growth factor receptor: evidence for a model of intermolecular allosteric activation. Biochemistry. 1987;26(5):1434-42.
102. Zhang X, Gureasko J, Shen K, Cole PA, Kuriyan J. An Allosteric Mechanism for Activation of the Kinase Domain of Epidermal Growth Factor Receptor. Cell. 2006;125(6):1137-49.
103. Ogiso H, Ishitani R, Nureki O, Fukai S, Yamanaka M, Kim JH, et al. Crystal structure of the complex of human epidermal growth factor and receptor extracellular domains. Cell. 2002;110(6):775-87.
104. Stallaert W, Brüggemann Y, Sabet O, Baak L, Gattiglio M, Bastiaens PIH. Contact inhibitory Eph signaling suppresses EGF-promoted cell migration by decoupling EGFR activity from vesicular recycling. Sci Signal. 2018;11(541).

105. Sigismund S, Argenzio E, Tosoni D, Cavallaro E, Polo S, Di Fiore PP. Clathrin-Mediated Internalization Is Essential for Sustained EGFR Signaling but Dispensable for Degradation. Developmental Cell. 2008;15(2):209-19.
106. Levkowitz G, Waterman H, Zamir E, Kam Z, Oved S, Langdon WY, et al. c-Cbl/Sli-1 regulates endocytic sorting and ubiquitination of the epidermal growth factor receptor. Genes Dev. 1998;12(23):3663-74.
107. Lowenstein EJ, Daly RJ, Batzer AG, Li W, Margolis B, Lammers R, et al. The SH2 and SH3 domain-containing protein GRB2 links receptor tyrosine kinases to ras signaling. Cell. 1992;70(3):431-42.
108. Batzer AG, Rotin D, Ureña JM, Skolnik EY, Schlessinger J. Hierarchy of binding sites for Grb2 and Shc on the epidermal growth factor receptor. Mol Cell Biol. 1994;14(8):5192-201.
109. Gale NW, Kaplan S, Lowenstein EJ, Schlessinger J, Bar-Sagi D. Grb2 mediates the EGF-dependent activation of guanine nucleotide exchange on Ras. Nature. 1993;363(6424):88-92.
110. Li N, Batzer A, Daly R, Yajnik V, Skolnik E, Chardin P, et al. Guanine-nucleotide-releasing factor hSos1 binds to Grb2 and links receptor tyrosine kinases to Ras signalling. Nature. 1993;363(6424):85-8.
111. Iversen L, Tu HL, Lin WC, Christensen SM, Abel SM, Iwig J, et al. Molecular kinetics. Ras activation by SOS: allosteric regulation by altered fluctuation dynamics. Science. 2014;345(6192):50-4.
112. Voice JK, Klemke RL, Le A, Jackson JH. Four human ras homologs differ in their abilities to activate Raf-1, induce transformation, and stimulate cell motility. J Biol Chem. 1999;274(24):17164-70.
113. Walsh AB, Bar-Sagi D. Differential activation of the Rac pathway by Ha-Ras and K-Ras. J Biol Chem. 2001;276(19):15609-15.
114. Chiu VK, Bivona T, Hach A, Sajous JB, Silletti J, Wiener H, et al. Ras signalling on the endoplasmic reticulum and the Golgi. Nature Cell Biology. 2002;4(5):343-50.
115. Mattingly RR, Macara IG. Phosphorylation-dependent activation of the Ras-GRF/CDC25Mm exchange factor by muscarinic receptors and G-protein beta gamma subunits. Nature. 1996;382(6588):268-72.
116. Medema RH, de Vries-Smits AM, van der Zon GC, Maassen JA, Bos JL. Ras activation by insulin and epidermal growth factor through enhanced exchange of guanine nucleotides on p21ras. Mol Cell Biol. 1993;13(1):155-62.
117. Bivona TG, Pérez De Castro I, Ahearn IM, Grana TM, Chiu VK, Lockyer PJ, et al. Phospholipase Cgamma activates Ras on the Golgi apparatus by means of RasGRP1. Nature. 2003;424(6949):694-8.
118. Zhang W, Liu HT. MAPK signal pathways in the regulation of cell proliferation in mammalian cells. Cell Research. 2002;12(1):9-18.
119. Morrison DK. MAP kinase pathways. Cold Spring Harb Perspect Biol. 2012;4(11).
120. Vara JÁF, Casado E, de Castro J, Cejas P, Belda-Iniesta C, González-Barón M. PI3K/Akt signalling pathway and cancer. Cancer Treatment Reviews. 2004;30(2):193-204.
121. Soriano O, Alcón-Pérez M, Vicente-Manzanares M, Castellano E. The Crossroads between RAS and RHO Signaling Pathways in Cellular Transformation, Motility and Contraction. Genes [Internet]. 2021; 12(6).
122. Marshall CJ. Specificity of receptor tyrosine kinase signaling: transient versus sustained extracellular signal-regulated kinase activation. Cell. 1995;80(2):179-85.
123. Moodie SA, Willumsen BM, Weber MJ, Wolfman A. Complexes of Ras.GTP with Raf-1 and mitogen-activated protein kinase kinase. Science. 1993;260(5114):1658-61.
124. Widmann C, Gibson S, Jarpe MB, Johnson GL. Mitogen-activated protein kinase: conservation of a three-kinase module from yeast to human. Physiol Rev. 1999;79(1):143-80.
125. Aktas H, Cai H, Cooper GM. Ras Links Growth Factor Signaling to the Cell Cycle Machinery via Regulation of Cyclin D1 and the Cdk Inhibitor p27KIP1. Molecular and Cellular Biology. 1997;17(7):3850-7.

126. Cargnello M, Roux PP. Activation and function of the MAPKs and their substrates, the MAPK-activated protein kinases. Microbiol Mol Biol Rev. 2011;75(1):50-83.
127. Cutler RE, Jr., Stephens RM, Saracino MR, Morrison DK. Autoregulation of the Raf-1 serine/threonine kinase. Proc Natl Acad Sci U S A. 1998;95(16):9214-9.
128. Hmitou I, Druillennec S, Valluet A, Peyssonnaux C, Eychène A. Differential regulation of B-raf isoforms by phosphorylation and autoinhibitory mechanisms. Mol Cell Biol. 2007;27(1):31-43.
129. Freeman AK, Ritt DA, Morrison DK. The importance of Raf dimerization in cell signaling. Small GTPases. 2013;4(3):180-5.
130. Adam G, Delbrück M. Reduction of dimensionality in biological diffusion processes. Structural chemistry and molecular biology. 1968;198:198-215.
131. Axelrod D, Wang MD. Reduction-of-dimensionality kinetics at reaction-limited cell surface receptors. Biophysical journal. 1994;66(3 Pt 1):588-600.
132. Zamir E. Oncogenic Signaling from the Plasma Membrane. In: Vartak N, and Bastiaens P. I. H., editor. In Y Yarden, & G Tarcic (Eds), *Vesicle Trafficking in Cancer*: New York: Springer; 2013. p. 57 - 74.
133. Freeman AK, Ritt DA, Morrison DK. Effects of Raf dimerization and its inhibition on normal and disease-associated Raf signaling. Mol Cell. 2013;49(4):751-8.
134. Hu J, Stites EC, Yu H, Germino EA, Meharena HS, Stork PJS, et al. Allosteric activation of functionally asymmetric RAF kinase dimers. Cell. 2013;154(5):1036-46.
135. Roskoski R, Jr. ERK1/2 MAP kinases: structure, function, and regulation. Pharmacol Res. 2012;66(2):105-43.
136. Roskoski R, Jr. MEK1/2 dual-specificity protein kinases: structure and regulation. Biochem Biophys Res Commun. 2012;417(1):5-10.
137. Torii S, Kusakabe M, Yamamoto T, Maekawa M, Nishida E. Sef is a spatial regulator for Ras/MAP kinase signaling. Dev Cell. 2004;7(1):33-44.
138. Chen RH, Sarnecki C, Blenis J. Nuclear localization and regulation of erk- and rsk-encoded protein kinases. Mol Cell Biol. 1992;12(3):915-27.
139. Lenormand P, Sardet C, Pagès G, L'Allemain G, Brunet A, Pouysségur J. Growth factors induce nuclear translocation of MAP kinases (p42mapk and p44mapk) but not of their activator MAP kinase kinase (p45mapkk) in fibroblasts. J Cell Biol. 1993;122(5):1079-88.
140. Brunet A, Roux D, Lenormand P, Dowd S, Keyse S, Pouysségur J. Nuclear translocation of p42/p44 mitogen-activated protein kinase is required for growth factor-induced gene expression and cell cycle entry. Embo j. 1999;18(3):664-74.
141. Lidke DS, Huang F, Post JN, Rieger B, Wilsbacher J, Thomas JL, et al. ERK nuclear translocation is dimerization-independent but controlled by the rate of phosphorylation. J Biol Chem. 2010;285(5):3092-102.
142. Garrington TP, Johnson GL. Organization and regulation of mitogen-activated protein kinase signaling pathways. Current Opinion in Cell Biology. 1999;11(2):211-8.
143. Fehrenbacher N, Bar-Sagi D, Philips M. Ras/MAPK signaling from endomembranes. Mol Oncol. 2009;3(4):297-307.
144. Markevich NI, Tsyganov MA, Hoek JB, Kholodenko BN. Long-range signaling by phosphoprotein waves arising from bistability in protein kinase cascades. Mol Syst Biol. 2006;2:61.
145. Kholodenko BN, Hancock JF, Kolch W. Signalling ballet in space and time. Nat Rev Mol Cell Biol. 2010;11(6):414-26.
146. von Kriegsheim A, Baiocchi D, Birtwistle M, Sumpton D, Bienvenut W, Morrice N, et al. Cell fate decisions are specified by the dynamic ERK interactome. Nat Cell Biol. 2009;11(12):1458-64.
147. Santos SDM, Verveer PJ, Bastiaens PIH. Growth factor-induced MAPK network topology shapes Erk response determining PC-12 cell fate. Nature Cell Biology. 2007;9(3):324-30.
148. Luttrell LM. Composition and function of G protein-coupled receptor signalsomes controlling mitogen-activated protein kinase activity. Journal of Molecular Neuroscience. 2005;26(2):253-64.

149. Sjölander A, Yamamoto K, Huber BE, Lapetina EG. Association of p21ras with phosphatidylinositol 3-kinase. Proc Natl Acad Sci U S A. 1991;88(18):7908-12.
150. Rodriguez-Viciana P, Warne PH, Dhand R, Vanhaesebroeck B, Gout I, Fry MJ, et al. Phosphatidylinositol-3-OH kinase direct target of Ras. Nature. 1994;370(6490):527-32.
151. Yan J, Roy S, Apolloni A, Lane A, Hancock JF. Ras isoforms vary in their ability to activate Raf-1 and phosphoinositide 3-kinase. J Biol Chem. 1998;273(37):24052-6.
152. Castellano E, Sheridan C, Thin MZ, Nye E, Spencer-Dene B, Diefenbacher ME, et al. Requirement for interaction of PI3-kinase p110α with RAS in lung tumor maintenance. Cancer Cell. 2013;24(5):617-30.
153. Alessi DR, Andjelkovic M, Caudwell B, Cron P, Morrice N, Cohen P, et al. Mechanism of activation of protein kinase B by insulin and IGF-1. Embo j. 1996;15(23):6541-51.
154. He Y, Sun MM, Zhang GG, Yang J, Chen KS, Xu WW, et al. Targeting PI3K/Akt signal transduction for cancer therapy. Signal Transduction and Targeted Therapy. 2021;6(1):425.
155. Dan HC, Ebbs A, Pasparakis M, Van Dyke T, Basseres DS, Baldwin AS. Akt-dependent activation of mTORC1 complex involves phosphorylation of mTOR (mammalian target of rapamycin) by IκB kinase α (IKKα). J Biol Chem. 2014;289(36):25227-40.
156. Glaviano A, Foo ASC, Lam HY, Yap KCH, Jacot W, Jones RH, et al. PI3K/AKT/mTOR signaling transduction pathway and targeted therapies in cancer. Molecular Cancer. 2023;22(1):138.
157. Collisson EA, Trejo CL, Silva JM, Gu S, Korkola JE, Heiser LM, et al. A central role for RAF→MEK→ERK signaling in the genesis of pancreatic ductal adenocarcinoma. Cancer Discov. 2012;2(8):685-93.
158. Soares HP, Ming M, Mellon M, Young SH, Han L, Sinnet-Smith J, et al. Dual PI3K/mTOR Inhibitors Induce Rapid Overactivation of the MEK/ERK Pathway in Human Pancreatic Cancer Cells through Suppression of mTORC2. Mol Cancer Ther. 2015;14(4):1014-23.
159. Sos ML, Fischer S, Ullrich R, Peifer M, Heuckmann JM, Koker M, et al. Identifying genotype-dependent efficacy of single and combined PI3K- and MAPK-pathway inhibition in cancer. Proc Natl Acad Sci U S A. 2009;106(43):18351-6.
160. Gillies TE, Pargett M, Silva JM, Teragawa CK, McCormick F, Albeck JG. Oncogenic mutant RAS signaling activity is rescaled by the ERK/MAPK pathway. Mol Syst Biol. 2020;16(10):e9518.
161. Manning BD, Toker A. AKT/PKB Signaling: Navigating the Network. Cell. 2017;169(3):381-405.
162. Carracedo A, Ma L, Teruya-Feldstein J, Rojo F, Salmena L, Alimonti A, et al. Inhibition of mTORC1 leads to MAPK pathway activation through a PI3K-dependent feedback loop in human cancer. J Clin Invest. 2008;118(9):3065-74.
163. Shaul YD, Seger R. The MEK/ERK cascade: From signaling specificity to diverse functions. Biochimica et Biophysica Acta (BBA) - Molecular Cell Research. 2007;1773(8):1213-26.
164. Tyson JJ, Chen KC, Novak B. Sniffers, buzzers, toggles and blinkers: dynamics of regulatory and signaling pathways in the cell. Current Opinion in Cell Biology. 2003;15(2):221-31.
165. Kolch W, Berta D, Rosta E. Dynamic regulation of RAS and RAS signaling. Biochemical Journal. 2023;480(1):1-23.
166. Boykevisch S, Zhao C, Sondermann H, Philippidou P, Halegoua S, Kuriyan J, et al. Regulation of ras signaling dynamics by Sos-mediated positive feedback. Curr Biol. 2006;16(21):2173-9.
167. Huang CY, Ferrell JE. Ultrasensitivity in the mitogen-activated protein kinase cascade. Proceedings of the National Academy of Sciences. 1996;93(19):10078-83.
168. Xiong W, Ferrell JE. A positive-feedback-based bistable 'memory module' that governs a cell fate decision. Nature. 2003;426(6965):460-5.
169. Ferrell JE. Self-perpetuating states in signal transduction: positive feedback, double-negative feedback and bistability. Current Opinion in Cell Biology. 2002;14(2):140-8.
170. Lake D, Corrêa SA, Müller J. Negative feedback regulation of the ERK1/2 MAPK pathway. Cell Mol Life Sci. 2016;73(23):4397-413.

171. Li X, Huang Y, Jiang J, Frank SJ. ERK-dependent threonine phosphorylation of EGF receptor modulates receptor downregulation and signaling. Cellular Signalling. 2008;20(11):2145-55.
172. Porfiri E, McCormick F. Regulation of epidermal growth factor receptor signaling by phosphorylation of the ras exchange factor hSOS1. J Biol Chem. 1996;271(10):5871-7.
173. Dong C, Waters SB, Holt KH, Pessin JE. SOS phosphorylation and disassociation of the Grb2-SOS complex by the ERK and JNK signaling pathways. J Biol Chem. 1996;271(11):6328-32.
174. Kamioka Y, Yasuda S, Fujita Y, Aoki K, Matsuda M. Multiple decisive phosphorylation sites for the negative feedback regulation of SOS1 via ERK. J Biol Chem. 2010;285(43):33540-8.
175. Dougherty MK, Müller J, Ritt DA, Zhou M, Zhou XZ, Copeland TD, et al. Regulation of Raf-1 by direct feedback phosphorylation. Mol Cell. 2005;17(2):215-24.
176. Kidger AM, Keyse SM. The regulation of oncogenic Ras/ERK signalling by dual-specificity mitogen activated protein kinase phosphatases (MKPs). Semin Cell Dev Biol. 2016;50:125-32.
177. Hanafusa H, Torii S, Yasunaga T, Nishida E. Sprouty1 and Sprouty2 provide a control mechanism for the Ras/MAPK signalling pathway. Nat Cell Biol. 2002;4(11):850-8.
178. Kim HJ, Bar-Sagi D. Modulation of signalling by Sprouty: a developing story. Nature Reviews Molecular Cell Biology. 2004;5(6):441-50.
179. Wakioka T, Sasaki A, Kato R, Shouda T, Matsumoto A, Miyoshi K, et al. Spred is a Sprouty-related suppressor of Ras signalling. Nature. 2001;412(6847):647-51.
180. Stanoev A, Mhamane A, Schuermann KC, Grecco HE, Stallaert W, Baumdick M, et al. Interdependence between EGFR and Phosphatases Spatially Established by Vesicular Dynamics Generates a Growth Factor Sensing and Responding Network. Cell Systems. 2018;7(3):295-309.e11.
181. Shin SY, Rath O, Choo SM, Fee F, McFerran B, Kolch W, et al. Positive- and negative-feedback regulations coordinate the dynamic behavior of the Ras-Raf-MEK-ERK signal transduction pathway. J Cell Sci. 2009;122(Pt 3):425-35.
182. Shankaran H, Ippolito DL, Chrisler WB, Resat H, Bollinger N, Opresko LK, et al. Rapid and sustained nuclear-cytoplasmic ERK oscillations induced by epidermal growth factor. Mol Syst Biol. 2009;5:332.
183. Zhang H, Zhao Y, Tian T, Paton AW, Paton JC, Kitamura M. Oscillation of mitogen-activated protein kinases in response to endoplasmic reticulum stress. Analytical Biochemistry. 2011;417(2):292-4.
184. Arkun Y, Yasemi M. Dynamics and control of the ERK signaling pathway: Sensitivity, bistability, and oscillations. PLoS One. 2018;13(4):e0195513.
185. Albeck JG, Mills GB, Brugge JS. Frequency-modulated pulses of ERK activity transmit quantitative proliferation signals. Mol Cell. 2013;49(2):249-61.
186. Gao T, Furnari F, Newton AC. PHLPP: a phosphatase that directly dephosphorylates Akt, promotes apoptosis, and suppresses tumor growth. Mol Cell. 2005;18(1):13-24.
187. Ihle NT, Byers LA, Kim ES, Saintigny P, Lee JJ, Blumenschein GR, et al. Effect of KRAS Oncogene Substitutions on Protein Behavior: Implications for Signaling and Clinical Outcome. JNCI: Journal of the National Cancer Institute. 2012;104(3):228-39.
188. Tidyman WE, Rauen KA. The RASopathies: developmental syndromes of Ras/MAPK pathway dysregulation. Current Opinion in Genetics & Development. 2009;19(3):230-6.
189. Rauen KA. The RASopathies. Annu Rev Genomics Hum Genet. 2013;14:355-69.
190. Schubbert S, Zenker M, Rowe SL, Böll S, Klein C, Bollag G, et al. Germline KRAS mutations cause Noonan syndrome. Nat Genet. 2006;38(3):331-6.
191. Razzaque MA, Nishizawa T, Komoike Y, Yagi H, Furutani M, Amo R, et al. Germline gain-of-function mutations in RAF1 cause Noonan syndrome. Nat Genet. 2007;39(8):1013-7.
192. Pandit B, Sarkozy A, Pennacchio LA, Carta C, Oishi K, Martinelli S, et al. Gain-of-function RAF1 mutations cause Noonan and LEOPARD syndromes with hypertrophic cardiomyopathy. Nat Genet. 2007;39(8):1007-12.
193. Beukers W, Hercegovac A, Zwarthoff EC. HRAS mutations in bladder cancer at an early age and the possible association with the Costello Syndrome. Eur J Hum Genet. 2014;22(6):837-9.

194. Prior IA, Hood FE, Hartley JL. The Frequency of Ras Mutations in Cancer. Cancer Research. 2020;80(14):2969-74.
195. Foulds L. The experimental study of tumor progression: a review. Cancer Res. 1954;14(5):327-39.
196. Kinzler KW, Vogelstein B. Lessons from Hereditary Colorectal Cancer. Cell. 1996;87(2):159-70.
197. Drews RM, Hernando B, Tarabichi M, Haase K, Lesluyes T, Smith PS, et al. A pan-cancer compendium of chromosomal instability. Nature. 2022;606(7916):976-83.
198. Sandoval J, Esteller M. Cancer epigenomics: beyond genomics. Current Opinion in Genetics & Development. 2012;22(1):50-5.
199. Widschwendter M, Jones A, Evans I, Reisel D, Dillner J, Sundström K, et al. Epigenome-based cancer risk prediction: rationale, opportunities and challenges. Nature Reviews Clinical Oncology. 2018;15(5):292-309.
200. Hanahan D, Weinberg RA. The Hallmarks of Cancer. Cell. 2000;100(1):57-70.
201. Yuan S, Almagro J, Fuchs E. Beyond genetics: driving cancer with the tumour microenvironment behind the wheel. Nature Reviews Cancer. 2024;24(4):274-86.
202. Weinberg RA. Oncogenes and tumor suppressor genes. CA Cancer J Clin. 1994;44(3):160-70.
203. Li Y, Zhang Y, Li X, Yi S, Xu J. Gain-of-Function Mutations: An Emerging Advantage for Cancer Biology. Trends Biochem Sci. 2019;44(8):659-74.
204. Wang LH, Wu CF, Rajasekaran N, Shin YK. Loss of Tumor Suppressor Gene Function in Human Cancer: An Overview. Cell Physiol Biochem. 2018;51(6):2647-93.
205. Weinstein IB, Joe AK. Mechanisms of Disease: oncogene addiction—a rationale for molecular targeting in cancer therapy. Nature Clinical Practice Oncology. 2006;3(8):448-57.
206. Weinstein IB, Joe A. Oncogene Addiction. Cancer Research. 2008;68(9):3077.
207. Lim K-H, Counter CM. Reduction in the requirement of oncogenic Ras signaling to activation of PI3K/AKT pathway during tumor maintenance. Cancer Cell. 2005;8(5):381-92.
208. Gupta S, Ramjaun AR, Haiko P, Wang Y, Warne PH, Nicke B, et al. Binding of ras to phosphoinositide 3-kinase p110alpha is required for ras-driven tumorigenesis in mice. Cell. 2007;129(5):957-68.
209. Hoshino R, Chatani Y, Yamori T, Tsuruo T, Oka H, Yoshida O, et al. Constitutive activation of the 41-/43-kDa mitogen-activated protein kinase signaling pathway in human tumors. Oncogene. 1999;18(3):813-22.
210. Wagner PL, Perner S, Rickman DS, LaFargue CJ, Kitabayashi N, Johnstone SF, et al. In situ evidence of KRAS amplification and association with increased p21 levels in non-small cell lung carcinoma. Am J Clin Pathol. 2009;132(4):500-5.
211. Sasaki H, Hikosaka Y, Kawano O, Moriyama S, Yano M, Fujii Y. Evaluation of Kras gene mutation and copy number gain in non-small cell lung cancer. J Thorac Oncol. 2011;6(1):15-20.
212. Birkeland E, Wik E, Mjøs S, Hoivik EA, Trovik J, Werner HM, et al. KRAS gene amplification and overexpression but not mutation associates with aggressive and metastatic endometrial cancer. Br J Cancer. 2012;107(12):1997-2004.
213. Zhou JD, Yao DM, Li XX, Zhang TJ, Zhang W, Ma JC, et al. KRAS overexpression independent of RAS mutations confers an adverse prognosis in cytogenetically normal acute myeloid leukemia. Oncotarget. 2017;8(39):66087-97.
214. Land H, Parada LF, Weinberg RA. Tumorigenic conversion of primary embryo fibroblasts requires at least two cooperating oncogenes. Nature. 1983;304(5927):596-602.
215. Willecke K, Schäfer R. Human oncogenes. Human Genetics. 1984;66(2):132-42.
216. Prior IA, Lewis PD, Mattos C. A comprehensive survey of Ras mutations in cancer. Cancer Res. 2012;72(10):2457-67.
217. Vatansever S, Erman B, Gümüş ZH. Comparative effects of oncogenic mutations G12C, G12V, G13D, and Q61H on local conformations and dynamics of K-Ras. Computational and Structural Biotechnology Journal. 2020;18:1000-11.

218. De Roock W, Jonker DJ, Di Nicolantonio F, Sartore-Bianchi A, Tu D, Siena S, et al. Association of KRAS p.G13D mutation with outcome in patients with chemotherapy-refractory metastatic colorectal cancer treated with cetuximab. Jama. 2010;304(16):1812-20.
219. Blasco RB, Francoz S, Santamaría D, Cañamero M, Dubus P, Charron J, et al. c-Raf, but not B-Raf, is essential for development of K-Ras oncogene-driven non-small cell lung carcinoma. Cancer Cell. 2011;19(5):652-63.
220. Rubio II, Wetzker R. A permissive function of phosphoinositide 3-kinase in ras activation mediated by inhibition of GTPase-activating proteins. Curr Biol. 2000;10(23):R883.
221. Eser S, Reiff N, Messer M, Seidler B, Gottschalk K, Dobler M, et al. Selective requirement of PI3K/PDK1 signaling for Kras oncogene-driven pancreatic cell plasticity and cancer. Cancer Cell. 2013;23(3):406-20.
222. Hamilton M, Wolfman A. Ha-ras and N-ras regulate MAPK activity by distinct mechanisms in vivo. Oncogene. 1998;16(11):1417-28.
223. Najumudeen AK, Fey SK, Millett LM, Ford CA, Gilroy K, Gunduz N, et al. KRAS allelic imbalance drives tumour initiation yet suppresses metastasis in colorectal cancer in vivo. Nature Communications. 2024;15(1):100.
224. Waters AM, Der CJ. KRAS: The Critical Driver and Therapeutic Target for Pancreatic Cancer. Cold Spring Harb Perspect Med. 2018;8(9).
225. Brummelkamp TR, Bernards R, Agami R. Stable suppression of tumorigenicity by virus-mediated RNA interference. Cancer Cell. 2002;2(3):243-7.
226. Aoki K, Yoshida T, Matsumoto N, Ide H, Sugimura T, Terada M. Suppression of Ki-ras p21 levels leading to growth inhibition of pancreatic cancer cell lines with Ki-ras mutation but not those without Ki-ras mutation. Mol Carcinog. 1997;20(2):251-8.
227. Sung H, Ferlay J, Siegel RL, Laversanne M, Soerjomataram I, Jemal A, et al. Global Cancer Statistics 2020: GLOBOCAN Estimates of Incidence and Mortality Worldwide for 36 Cancers in 185 Countries. CA Cancer J Clin. 2021;71(3):209-49.
228. Fearon ER, Vogelstein B. A genetic model for colorectal tumorigenesis. Cell. 1990;61(5):759-67.
229. Zhang L, Shay JW. Multiple Roles of APC and its Therapeutic Implications in Colorectal Cancer. J Natl Cancer Inst. 2017;109(8).
230. Imamura Y, Morikawa T, Liao X, Lochhead P, Kuchiba A, Yamauchi M, et al. Specific mutations in KRAS codons 12 and 13, and patient prognosis in 1075 BRAF wild-type colorectal cancers. Clin Cancer Res. 2012;18(17):4753-63.
231. Jones RP, Sutton PA, Evans JP, Clifford R, McAvoy A, Lewis J, et al. Specific mutations in KRAS codon 12 are associated with worse overall survival in patients with advanced and recurrent colorectal cancer. Br J Cancer. 2017;116(7):923-9.
232. Lièvre A, Bachet JB, Le Corre D, Boige V, Landi B, Emile JF, et al. KRAS mutation status is predictive of response to cetuximab therapy in colorectal cancer. Cancer Res. 2006;66(8):3992-5.
233. Peeters M, Oliner KS, Price TJ, Cervantes A, Sobrero AF, Ducreux M, et al. Analysis of KRAS/NRAS Mutations in a Phase III Study of Panitumumab with FOLFIRI Compared with FOLFIRI Alone as Second-line Treatment for Metastatic Colorectal Cancer. Clinical Cancer Research. 2015;21(24):5469-79.
234. Till JE, Bucheit LA, Zhang N, Clemens KM, Carpenter EL. Association of KRAS G12D vs. G12V circulating tumor DNA variant allele fraction and real-world overall survival in metastatic non-small cell lung and colorectal cancers. Journal of Clinical Oncology. 2024;42(16_suppl):3041-.
235. Korf BR. Malignancy in neurofibromatosis type 1. Oncologist. 2000;5(6):477-85.
236. Landry JP, Schertz KL, Chiang Y-J, Bhalla AD, Yi M, Keung EZ, et al. Comparison of Cancer Prevalence in Patients With Neurofibromatosis Type 1 at an Academic Cancer Center vs in the General Population From 1985 to 2020. JAMA Network Open. 2021;4(3):e210945-e.
237. Ksionda O, Limnander A, Roose JP. RasGRP Ras guanine nucleotide exchange factors in cancer. Front Biol (Beijing). 2013;8(5):508-32.

238. Serrano M, Lin AW, McCurrach ME, Beach D, Lowe SW. Oncogenic ras Provokes Premature Cell Senescence Associated with Accumulation of p53 and p16INK4a. Cell. 1997;88(5):593-602.
239. Ferbeyre G, de Stanchina E, Lin AW, Querido E, McCurrach ME, Hannon GJ, et al. Oncogenic ras and p53 cooperate to induce cellular senescence. Mol Cell Biol. 2002;22(10):3497-508.
240. Collado M, Serrano M. Senescence in tumours: evidence from mice and humans. Nat Rev Cancer. 2010;10(1):51-7.
241. Tuveson DA, Shaw AT, Willis NA, Silver DP, Jackson EL, Chang S, et al. Endogenous oncogenic K-ras(G12D) stimulates proliferation and widespread neoplastic and developmental defects. Cancer Cell. 2004;5(4):375-87.
242. Guerra C, Mijimolle N, Dhawahir A, Dubus P, Barradas M, Serrano M, et al. Tumor induction by an endogenous K-ras oncogene is highly dependent on cellular context. Cancer Cell. 2003;4(2):111-20.
243. Hindul NL, Abbott LR, Adan SMD, Straatman KR, Fry AM, Hirota K, et al. Endogenous oncogenic KRAS expression increases cell proliferation and motility in near-diploid hTERT RPE-1 cells. J Biol Chem. 2024;300(6):107409.
244. Lin AW, Barradas M, Stone JC, van Aelst L, Serrano M, Lowe SW. Premature senescence involving p53 and p16 is activated in response to constitutive MEK/MAPK mitogenic signaling. Genes Dev. 1998;12(19):3008-19.
245. Courtois-Cox S, Genther Williams SM, Reczek EE, Johnson BW, McGillicuddy LT, Johannessen CM, et al. A negative feedback signaling network underlies oncogene-induced senescence. Cancer Cell. 2006;10(6):459-72.
246. Sarkisian CJ, Keister BA, Stairs DB, Boxer RB, Moody SE, Chodosh LA. Dose-dependent oncogene-induced senescence in vivo and its evasion during mammary tumorigenesis. Nature Cell Biology. 2007;9(5):493-505.
247. Kamijo T, Zindy F, Roussel MF, Quelle DE, Downing JR, Ashmun RA, et al. Tumor suppression at the mouse INK4a locus mediated by the alternative reading frame product p19ARF. Cell. 1997;91(5):649-59.
248. Qiu W, Sahin F, Iacobuzio-Donahue CA, Garcia-Carracedo D, Wang WM, Kuo CY, et al. Disruption of p16 and activation of Kras in pancreas increase ductal adenocarcinoma formation and metastasis in vivo. Oncotarget. 2011;2(11):862-73.
249. Ito RE, Oneyama C, Aoki K. Oncogenic mutation or overexpression of oncogenic KRAS or BRAF is not sufficient to confer oncogene addiction. PLoS One. 2021;16(4):e0249388.
250. Young A, Lou D, McCormick F. Oncogenic and wild-type Ras play divergent roles in the regulation of mitogen-activated protein kinase signaling. Cancer Discov. 2013;3(1):112-23.
251. Keller JW, Haigis KM, Franklin JL, Whitehead RH, Jacks T, Coffey RJ. Oncogenic K-RAS subverts the antiapoptotic role of N-RAS and alters modulation of the N-RAS:gelsolin complex. Oncogene. 2007;26(21):3051-9.
252. Ikonomou G, Kostourou V, Shirasawa S, Sasazuki T, Samiotaki M, Panayotou G. Interplay between oncogenic K-Ras and wild-type H-Ras in Caco2 cell transformation. J Proteomics. 2012;75(17):5356-69.
253. Jeng HH, Taylor LJ, Bar-Sagi D. Sos-mediated cross-activation of wild-type Ras by oncogenic Ras is essential for tumorigenesis. Nat Commun. 2012;3:1168.
254. Moghadamchargari Z, Shirzadeh M, Liu C, Schrecke S, Packianathan C, Russell DH, et al. Molecular assemblies of the catalytic domain of SOS with KRas and oncogenic mutants. Proceedings of the National Academy of Sciences. 2021;118(12):e2022403118.
255. Cheng DK, Oni TE, Thalappillil JS, Park Y, Ting HC, Alagesan B, et al. Oncogenic KRAS engages an RSK1/NF1 pathway to inhibit wild-type RAS signaling in pancreatic cancer. Proc Natl Acad Sci U S A. 2021;118(21).
256. Lim KH, Ancrile BB, Kashatus DF, Counter CM. Tumour maintenance is mediated by eNOS. Nature. 2008;452(7187):646-9.

257. To MD, Rosario RD, Westcott PM, Banta KL, Balmain A. Interactions between wild-type and mutant Ras genes in lung and skin carcinogenesis. Oncogene. 2013;32(34):4028-33.
258. Zhang Z, Wang Y, Vikis HG, Johnson L, Liu G, Li J, et al. Wildtype Kras2 can inhibit lung carcinogenesis in mice. Nat Genet. 2001;29(1):25-33.
259. Bremner R, Balmain A. Genetic changes in skin tumor progression: correlation between presence of a mutant ras gene and loss of heterozygosity on mouse chromosome 7. Cell. 1990;61(3):407-17.
260. Guerrero I, Villasante A, Corces V, Pellicer A. Loss of the normal N-ras allele in a mouse thymic lymphoma induced by a chemical carcinogen. Proc Natl Acad Sci U S A. 1985;82(23):7810-4.
261. Li J, Zhang Z, Dai Z, Plass C, Morrison C, Wang Y, et al. LOH of chromosome 12p correlates with Kras2 mutation in non-small cell lung cancer. Oncogene. 2003;22(8):1243-6.
262. Estep AL, Tidyman WE, Teitell MA, Cotter PD, Rauen KA. HRAS mutations in Costello syndrome: detection of constitutional activating mutations in codon 12 and 13 and loss of wild-type allele in malignancy. Am J Med Genet A. 2006;140(1):8-16.
263. Spandidos A, Wilkie NM. The normal human H-ras1 gene can act as an onco-suppressor. Br J Cancer Suppl. 1988;9:67-71.
264. Diaz R, Ahn D, Lopez-Barcons L, Malumbres M, Perez de Castro I, Lue J, et al. The N-ras proto-oncogene can suppress the malignant phenotype in the presence or absence of its oncogene. Cancer Res. 2002;62(15):4514-8.
265. Grabocka E, Pylayeva-Gupta Y, Jones MJ, Lubkov V, Yemanaberhan E, Taylor L, et al. Wild-type H- and N-Ras promote mutant K-Ras-driven tumorigenesis by modulating the DNA damage response. Cancer Cell. 2014;25(2):243-56.
266. Matallanas D, Romano D, Al-Mulla F, O'Neill E, Al-Ali W, Crespo P, et al. Mutant K-Ras activation of the proapoptotic MST2 pathway is antagonized by wild-type K-Ras. Mol Cell. 2011;44(6):893-906.
267. Xu J, Haigis KM, Firestone AJ, McNerney ME, Li Q, Davis E, et al. Dominant role of oncogene dosage and absence of tumor suppressor activity in Nras-driven hematopoietic transformation. Cancer Discov. 2013;3(9):993-1001.
268. Bentley C, Jurinka SS, Kljavin NM, Vartanian S, Ramani SR, Gonzalez LC, et al. A requirement for wild-type Ras isoforms in mutant KRas-driven signalling and transformation. Biochem J. 2013;452(2):313-20.
269. To MD, Wong CE, Karnezis AN, Del Rosario R, Di Lauro R, Balmain A. Kras regulatory elements and exon 4A determine mutation specificity in lung cancer. Nat Genet. 2008;40(10):1240-4.
270. Sheffels E, Kortum RL. The Role of Wild-Type RAS in Oncogenic RAS Transformation. Genes (Basel). 2021;12(5).
271. Maruyama C, Tomisawa M, Wakana S, Yamazaki H, Kijima H, Suemizu H, et al. Overexpression of human H-ras transgene is responsible for tumors induced by chemical carcinogens in mice. Oncol Rep. 2001;8(2):233-7.
272. Tsunematsu S, Saito H, Kagawa T, Morizane T, Hata J, Nakamura T, et al. Hepatic tumors induced by carbon tetrachloride in transgenic mice carrying a human c-H-ras proto-oncogene without mutations. Int J Cancer. 1994;59(4):554-9.
273. Integrated genomic analyses of ovarian carcinoma. Nature. 2011;474(7353):609-15.
274. Comprehensive molecular profiling of lung adenocarcinoma. Nature. 2014;511(7511):543-50.
275. Zhang Z, Kobayashi S, Borczuk AC, Leidner RS, Laframboise T, Levine AD, et al. Dual specificity phosphatase 6 (DUSP6) is an ETS-regulated negative feedback mediator of oncogenic ERK signaling in lung cancer cells. Carcinogenesis. 2010;31(4):577-86.
276. Swanson KD, Winter JM, Reis M, Bentires-Alj M, Greulich H, Grewal R, et al. SOS1 mutations are rare in human malignancies: implications for Noonan Syndrome patients. Genes Chromosomes Cancer. 2008;47(3):253-9.

277. Spencer DM, Wandless TJ, Schreiber SL, Crabtree GR. Controlling Signal Transduction with Synthetic Ligands. Science. 1993;262(5136):1019-24.
278. Rivera VM, Clackson T, Natesan S, Pollock R, Amara JF, Keenan T, et al. A humanized system for pharmacologic control of gene expression. Nature Medicine. 1996;2(9):1028-32.
279. Dang DT. Molecular Approaches to Protein Dimerization: Opportunities for Supramolecular Chemistry. Front Chem. 2022;10:829312.
280. Nanda S, Calderon A, Sachan A, Duong T-T, Koch J, Xin X, et al. Rho GTPase activity crosstalk mediated by Arhgef11 and Arhgef12 coordinates cell protrusion-retraction cycles. Nature Communications. 2023;14(1):8356.
281. Putyrski M, Schultz C. Protein translocation as a tool: The current rapamycin story. FEBS Lett. 2012;586(15):2097-105.
282. Banaszynski LA, Wandless TJ. Conditional Control of Protein Function. Chemistry & Biology. 2006;13(1):11-21.
283. Wayne Schultz L, Clardy J. Chemical inducers of dimerization: The atomic structure of FKBP12-FK1012A-FKBP12. Bioorganic & Medicinal Chemistry Letters. 1998;8(1):1-6.
284. Ho SN, Biggar SR, Spencer DM, Schreiber SL, Crabtree GR. Dimeric ligands define a role for transcriptional activation domains in reinitiation. Nature. 1996;382(6594):822-6.
285. Liu P, Calderon A, Konstantinidis G, Hou J, Voss S, Chen X, et al. A bioorthogonal small-molecule-switch system for controlling protein function in live cells. Angew Chem Int Ed Engl. 2014;53(38):10049-55.
286. Chen X, Wu Y-W. Tunable and Photoswitchable Chemically Induced Dimerization for Chemo-optogenetic Control of Protein and Organelle Positioning. Angewandte Chemie International Edition. 2018;57(23):6796-9.
287. Klewer L, Wu Y-W. Light-Induced Dimerization Approaches to Control Cellular Processes. Chemistry – A European Journal. 2019;25(54):12452-63.
288. Ballister ER, Aonbangkhen C, Mayo AM, Lampson MA, Chenoweth DM. Localized light-induced protein dimerization in living cells using a photocaged dimerizer. Nature Communications. 2014;5(1):5475.
289. Strickland D, Lin Y, Wagner E, Hope CM, Zayner J, Antoniou C, et al. TULIPs: tunable, light-controlled interacting protein tags for cell biology. Nat Methods. 2012;9(4):379-84.
290. Wu YI, Frey D, Lungu OI, Jaehrig A, Schlichting I, Kuhlman B, et al. A genetically encoded photoactivatable Rac controls the motility of living cells. Nature. 2009;461(7260):104-8.
291. Chen X, Venkatachalapathy M, Dehmelt L, Wu YW. Multidirectional Activity Control of Cellular Processes by a Versatile Chemo-optogenetic Approach. Angew Chem Int Ed Engl. 2018;57(37):11993-7.
292. Vogel H. Controlling Ras activity by manipulating its localization: Technische Universität Dortmund; 2018.
293. Schindelin J, Arganda-Carreras I, Frise E, Kaynig V, Longair M, Pietzsch T, et al. Fiji: an open-source platform for biological-image analysis. Nature Methods. 2012;9(7):676-82.
294. Schneider CA, Rasband WS, Eliceiri KW. NIH Image to ImageJ: 25 years of image analysis. Nat Methods. 2012;9(7):671-5.
295. Ting PY, Johnson CW, Fang C, Cao X, Graeber TG, Mattos C, et al. Tyrosine phosphorylation of RAS by ABL allosterically enhances effector binding. Faseb j. 2015;29(9):3750-61.
296. Ballester R, Furth ME, Rosen OM. Phorbol ester- and protein kinase C-mediated phosphorylation of the cellular Kirsten ras gene product. J Biol Chem. 1987;262(6):2688-95.
297. FPbase. mTFP1 [Available from: https://www.fpbase.org/protein/mtfp1/.
298. Harding MW, Galat A, Uehling DE, Schreiber SL. A receptor for the immunosuppressant FK506 is a cis-trans peptidyl-prolyl isomerase. Nature. 1989;341(6244):758-60.
299. Siekierka JJ, Hung SHY, Poe M, Lin CS, Sigal NH. A cytosolic binding protein for the immunosuppressant FK506 has peptidyl-prolyl isomerase activity but is distinct from cyclophilin. Nature. 1989;341(6244):755-7.

300. Brüggemann Y, Karajannis LS, Stanoev A, Stallaert W, Bastiaens PIH. Growth factor–dependent ErbB vesicular dynamics couple receptor signaling to spatially and functionally distinct Erk pools. Science Signaling. 2021;14(683):eabd9943.
301. Kholodenko BN. Negative feedback and ultrasensitivity can bring about oscillations in the mitogen-activated protein kinase cascades. Eur J Biochem. 2000;267(6):1583-8.
302. Bhalla US, Ram PT, Iyengar R. MAP kinase phosphatase as a locus of flexibility in a mitogen-activated protein kinase signaling network. Science. 2002;297(5583):1018-23.
303. de Ménorval M-A, Mir LM, Fernández ML, Reigada R. Effects of Dimethyl Sulfoxide in Cholesterol-Containing Lipid Membranes: A Comparative Study of Experiments In Silico and with Cells. PLOS ONE. 2012;7(7):e41733.
304. Verheijen M, Lienhard M, Schrooders Y, Clayton O, Nudischer R, Boerno S, et al. DMSO induces drastic changes in human cellular processes and epigenetic landscape in vitro. Scientific Reports. 2019;9(1):4641.
305. Singh AB, Tsukada T, Zent R, Harris RC. Membrane-associated HB-EGF modulates HGF-induced cellular responses in MDCK cells. J Cell Sci. 2004;117(Pt 8):1365-79.
306. Nakagawa T, Hayase Y, Sasahara M, Haneda M, Kikkawa R, Higashiyama S, et al. Distribution of heparin-binding EGF-like growth factor protein and mRNA in the normal rat kidneys. Kidney International. 1997;51(6):1774-9.
307. Singh AB, Harris RC. Autocrine, paracrine and juxtacrine signaling by EGFR ligands. Cellular Signalling. 2005;17(10):1183-93.
308. Roose JP, Mollenauer M, Ho M, Kurosaki T, Weiss A. Unusual interplay of two types of Ras activators, RasGRP and SOS, establishes sensitive and robust Ras activation in lymphocytes. Molecular and cellular biology. 2007;27(7):2732-45.
309. Cohen-Saidon C, Cohen AA, Sigal A, Liron Y, Alon U. Dynamics and Variability of ERK2 Response to EGF in Individual Living Cells. Molecular Cell. 2009;36(5):885-93.
310. Adler M, Alon U. Fold-change detection in biological systems. Current Opinion in Systems Biology. 2018;8:81-9.
311. Hood FE, Klinger B, Newlaczyl AU, Sieber A, Dorel M, Oliver SP, et al. Isoform-specific Ras signaling is growth factor dependent. Mol Biol Cell. 2019;30(9):1108-17.

12 Aids Used

I acknowledge the use of DeepL (https://www.deepl.com/en/translator) for translating and refining the German abstract (Zusammenfassung) of my thesis. Parts of the text were translated from English to German using DeepL's AI-based translation service.

Additional help to translate the abstract into German was received from 3 colleagues, Dr. Birga Sötje, Dr. Hans Seidel, and Sabrina Seidler.

13 Acknowledgements

I would like to thank the following people for their unwavering support through prayers, encouragement, and acts of service. Without them, I would not have been able to complete my Ph.D.

I am grateful for the opportunity offered to me by my supervisor, Prof. Dr. Philippe Bastiaens to conduct my PhD studies in his department and under his guidance and supervision. It was indeed challenging, but I have learned a lot through the process and grown both as a person and as a scientist. I am grateful to my Thesis Advisory Committee members, Dr. Peter Bieling and Dr. Christian Schröter for their guidance and feedback regarding my project.

I am also thankful to Dr. Astrid Krämer who helped me with scientific matters and onboarding me into the department when I first arrived here, and Tanja Forck who has helped with organizational matters throughout my time in the department. I extend sincere appreciation towards various members of Department II, who have taught me so much scientifically in terms of knowledge and skills, or indeed helped me when I could not do certain tasks on my own. Without them, I would not have developed the way I did. My thanks go to current members of the department – Dr. Luis Muñoz-Nava, Dr. Birga Sötje, Dr. Mario Caracci Oporto, Sabrina Seidler, Dr. Hans Seidel, Dr. Mike Armstrong, Hendrike Schütz, Samrajni Ghosh, Kirsten Michel, Manuela Grygier, Dr. Sven Müller, and to past members alike – Dr. Maitreyi S. Joshi, Dr. Sarah Imtiaz, Dr. Manuel A. Campos Medina, Dr. Bruno Scocozza, Dr. Christian Klein, Lisaweta Roßmannek, Dr. Marina Gattiglio, Michael Reichl, Dr. Yannick Brueggemann and Dr. Holger Vogel. I am also grateful towards other members of the department, for their continuous support through conversations and feedback during group meetings.

I would also like to express my appreciation towards the IMPRS coordinators, Christa Hornemann and Dr. Lucia Sironi, who have shown unparalleled support for me since receiving my PhD. offer. I am grateful for my PhD buddies from the IMPRS community who offered a sense of support and comradery – Dr. Sheila Mainye, Dr. Benjamin Buchmuller, and Dr. Suchet Nanda. Special thanks go to those with whom I started this journey in July 2018 when we had our interviews - Dr. Manuel A. Campos Medina, Dr. Stella Polido, and Dr. Anson Shek; we were in this together.

Daniel Schmalz, Heiner Walter, Nico Streeck, Matteo Carnielo, Paul Stahl, Maphisa Maphisa, and Walid Talasch – you helped me not only survive but also overcome the challenges I had during COVID lockdowns.

My special and heartfelt gratitude goes to my friends, who have been there for me in more ways than I can express. Thapelo Masunge, Dr. Leone Buckle, Dr. Andrea Cordaro, Dr. Richard P. Biggers, Dr. Yuuki Yanagisawa, Dr. Mpho D. Molosiwa, Dr. Sheila Mainye, Maria Marera, Dr. Peter Nganga, Dr. Moses Ikpeme, Dr. Femi Omotoyinbo, Ncumisa and Christian Schnapp, Keitumetse Mogoase, Dr. Victor Manisa, Dr. Kagiso Bikane, Jan Gehm, Kagiso O'niel Kgetse, Timothy Ricardo Aaron, Masa Martina Jansen, Paul Beckbailey, Herb, Will, and Ronny, Noah Hessami, Solomon and Madeline Kalu, Johannes Brejora, Mustafa, Simon B. Johannson and Timur Sahi – you all have been a blessing in so many ways. You are all very special and dear to me. I am grateful to my small groups from Hillsong Düsseldorf and Kensington Temple LCC, as well as my Barnie group, who have stood by me spiritually during my PhD. You guys are awesome. Special thanks to Dr. Yaw Adansi-Pipim who has been a mentor and a brother.

I am immensely grateful for my family; my parents Pulane, Mogotsa and Elsie, my siblings especially Mpho and Loruo, and my cousins Kagiso, Thabile, Bonile, and Itseng. Your steadfast love and support have been invaluable through this PhD process. La bofelo, ke leboga Modimo, ka gonne ke ene a mphileng matla, thata le bokgoni jwa go fetsa. Tsotlhe tse ke di dirileng ke ka ntateng ya gagwe.